Diffuse X-ray Scattering from Disordered Crystals

T. R. Welberry*

Research School of Chemistry, Australian National University, Canberra ACT 0200, Australia

B. D. Butler

National Institute of Standards and Technology, 325 Broadway, Boulder, Colorado 80303

Received January 17, 1995 (Revised Manuscript Received July 17, 1995)

Contents

1. Introduction 2369
2. Theory and Its Application to Alloy Systems 2370
2.1. The Diffuse Intensity 2370
2.2. Two Simple Examples 2371
2.3. Diffuse Scattering in Metallic Alloys 2373
3. Experimental Aspects 2376
3.1. X-ray Sources 2377
3.2. X-ray Detectors 2377
3.3. Sources of Background Scattering 2378
3.4. Data Corrections 2378
3.5. Measurement of the Diffuse Intensity 2379
4. Nonstoichiometric Oxides and Halides 2380
4.1. Cubic Stabilized Zirconias (CSZ's) 2380
4.2. Wüstite, $Fe_{1-x}O$ 2382
4.3. Mullite, $Al_2(Al_{2+2x}Si_{2-2x})O_{10-x}$ 2382
4.4. Anion-Excess Fluorite, $(Ca_{1-x}Y_x)F_{2+x}$ 2384
4.5. Superconducting Oxides 2385
4.6. Solid Electrolytes—β-Aluminas, α-AgI 2386
4.7. Summary 2386
5. Low-Dimensional Conductors 2386
5.1. Peierls Instability 2386
5.2. Charge-Transfer Salts 2387
5.3. Pinning of Charge Density Waves 2387
5.4. Two-Dimensional Conductors 2388
6. Inclusion Compounds (Guest-Host Systems) 2389
6.1. Urea Inclusion Compounds 2389
6.2. Triiodide Chain Compounds 2390
6.3. Hollandite 2391
6.4. Graphite Intercalation Compounds 2392
7. Diffuse Scattering from Molecular Crystals 2392
7.1. Substitutional Disorder in Anthracene and Benzene Derivatives 2392
7.2. Disorder Involving Atomic Displacements 2393
7.3. Disorder in Polyphenyls 2394
7.4. Orientational Disorder in Solid C_{60} 2394
8. Diffuse Scattering from Macromolecular Crystals 2394
9. Diffuse Scattering from Quasi-Crystals 2397
9.1. Penrose Tiling 2397
9.2. Disordered Growth Tiling 2399
9.3. Examples of Real Quasi-Crystals Exhibiting Disorder 2399
10. Conclusion 2400

1. Introduction

Over the 80 years since the first discovery of the diffraction of X-rays by crystals, crystallography has grown into a very precise, widely applicable, and definitive tool. The undoubted success of this *conventional* crystallography (crystal structure determination) is due, to a very large extent, to the fact that the same basic method may be applied to materials as diverse as a simple salt which contains only a few atoms per cell to macromolecular crystals which may contain thousands of atoms per cell. The assumption in all cases is that the crystal consists of a three-dimensional array of identical units, and this gives rise to a diffraction pattern consisting of discrete diffraction peaks (called Bragg reflections). The measurement and analysis of such discrete diffraction data has become routine for all but the most complex of examples.

Real materials, however, only approximate this ideal, and the diffraction patterns of most materials contain, in addition to sharp Bragg peaks, a weak continuous background known as diffuse scattering. This scattering necessarily arises whenever there are departures of any kind from the ideal of a perfectly regular array of identical units. Such departures from ideality may arise in a whole variety of different ways and to different extents, but all of these effects may be brought together under a common name: *disorder*. Although much of present day knowledge of the solid state has been derived from crystallographic studies using Bragg diffraction, the properties of many important materials are dependent not simply on the *average* crystal structure but are often crucially dependent on the departures from ideality that are present. For example, the useful mechanical properties of many alloys and ceramics, the optoelectronic properties of many materials, and many electrical properties of semiconductors and high-temperature superconductivity depend upon the presence of various types of disorder.

The basic scattering event of an X-ray photon interacting with a crystal lattice occurs on a time scale of $\sim 10^{-16}$ s. This is several orders of magnitude faster than typical thermal vibration frequencies so, to a good approximation, the X-ray diffraction experiment sees atoms or molecules statistically displaced from their average positions as a result of such thermal motion. This may be termed thermal disorder and the scattering associated with it as thermal diffuse scattering or TDS. Disorder may also arise as a result of mixing different atomic or molecular species (solid solutions) or where a molecular species can pack into the basic crystal lattice in two (or more) different orientations. This may result from the presence of isolated substitutional defects, clusters

0009-2665/95/0795-2369$15.50/0 © 1995 American Chemical Society

Richard Welberry was an undergraduate at St. John's College, Cambridge, from 1964 to 1967, and subsequently obtained his Ph.D. in 1970 at the Chemical Crystallography Department, University College, London. He was for five years a Postdoctoral Fellow at the University College Cardiff Physics Department, following which he was appointed Fellow/Senior Fellow in the Research School of Chemistry, Australian National University.

Brent Butler received B.S. and M.S. degrees in Mechanical Engineering from the University of Missouri—Columbia and a Ph.D. in the field of materials science from Northwestern University (1991). From 1991 to 1993 he was at the Research School of Chemistry, Australian National University, on a postdoctoral appointment. He is currently at the National Institute of Standards and Technology, Boulder, CO, on a National Research Council Fellowship.

of such defects, or interstitials where the defects reside on sites not normally occupied in the average lattice. The scattering associated with this chemical disorder is often termed short-range order (SRO) diffuse scattering. Chemical disorder will normally be accompanied by (static) atomic distortions that help alleviate local stresses, and these distortions also give rise to diffuse scattering. In most real materials, thermal, substitutional, and static displacement diffuse scattering will be present to varying degrees, and instances can be found where any one of these dominates the diffraction pattern.

Whereas the conventional analysis of Bragg peaks provides information about the average crystal structure (information such as atomic coordinates, site occupancies, or mean-squared atomic displacements—all properties of *single* atom sites), diffuse scattering contains information about how *pairs* of atoms behave and is thus potentially a rich source of information on how atoms and molecules interact. Crystallographers have been aware of such scattering since the earliest times, but development of techniques for recording and analyzing it have lagged well behind the advances made in conventional crystallography. Typical diffuse intensities are several orders of magnitude below Bragg peak intensities, and this was clearly a major impediment to earlier generations of researchers. With advances in X-ray sources (rotating anodes, synchrotron radiation) and in methods of detection (linear detectors, area detectors, image plates, etc.) good quality diffuse diffraction data are now more readily accessible. The one major impediment to the utilization of this rich source of information is the diversity of different effects that arise in nature and the fact that no one formulation of theory appears capable of usefully describing all of them.

The quantitative treatment of X-ray diffuse scattering was pioneered by B. E. Warren and his students (see, for example, his book on X-ray diffraction[1]). Since that time, much progress has been made and several other reviews of different aspects of diffuse X-ray scattering and disorder have been published.[2-11] Our concern is predominantly with disordered crystals and we omit any discussion of the phonon theory of thermal diffuse scattering (TDS), except where this impinges on a particular static disorder problem. For a review of thermal diffuse scattering see Willis.[12] In this paper we attempt to present the subject of diffuse scattering from disordered crystals extending from those areas for which the most quantitative treatments are viable to those where, for a variety of experimental or theoretical reasons, only rudimentary discussions are feasible. The aim in taking this approach is to give a broad overview of the sort of information that may be obtained from diffuse scattering, the range of experimental and theoretical techniques that may be used, and the detail that might be expected in many different circumstances.

In a few cases, examples of the complementary techniques of neutron and electron diffraction are mentioned, but, in order to limit the scope of this review, we confine our attention mainly to those systems where X-ray scattering has been used. Neutron diffuse scattering studies do, however, employ many of the same analysis methods outlined in this paper, and despite the relative scarcity of neutron sources and the large single crystals required, neutrons have been used successfully to probe disorder in a wide range of materials. Electron diffraction is also widely applicable, provided that the material is "beam-stable" and is ideally suited to revealing the presence of diffuse scattering in a short time. Multiple scattering in electron diffraction precludes the possibility of quantitative measurements of diffuse scattering, and the method also has the disadvantage that only sections of reciprocal space passing through the origin are accessible.

2. Theory and Its Application to Alloy Systems

2.1. The Diffuse Intensity

There are many ways to describe mathematically the diffuse intensity from crystalline materials. For instance, a disordered crystal can be described as the sum of an average structure plus a set of periodic

modulations in concentration and atomic displacement away from this average. Such an approach leads to a description of the diffuse scattering grounded in Fourier transform (reciprocal) space[13-16] and so is particularly useful when investigating disordered crystals that display relatively sharp diffuse features in their measured diffraction data. Reciprocal space methods are thus well suited to describe longer ranged correlations in a disordered crystal and can be powerfully applied even to systems containing short- or intermediate-range correlations.[17] More widely used (and more amenable to the construction of physical models), however, is a description of the diffuse intensity based on short range chemical and displacement correlations associated with (real-space) interatomic distances.[18-25] Here the emphasis is on "short range" because it is hoped that a relatively small number of correlation parameters can adequately describe the disorder. Because it directly includes the occupations and displacements of individual atoms, this real-space description is also useful for demonstrating more clearly how disorder manifests itself in the diffraction pattern. We therefore present a discussion of this approach here.

In the kinematic limit the total scattered intensity I_T can be computed as a simple Fourier summation over the positions $\mathbf{r}_n$ of each atom n in the crystal multiplied by its complex conjugate:

$$I_T(\mathbf{s}) = (\sum_n f_n \exp\{2\pi i\mathbf{s}\cdot\mathbf{r}_n\})(\sum_{n'} f_{n'}^* \exp\{-2\pi i\mathbf{s}\cdot\mathbf{r}_{n'}\}) \quad (1)$$

Here the Fourier coefficients f_n are the (complex) atomic scattering factors, and $\mathbf{s}$ is the scattered wave vector of magnitude $|\mathbf{s}| = 2\sin(\theta)/\lambda$. 2θ is the scattering angle, and λ is the X-ray wavelength. All information regarding the absolute atomic positions is lost to the scattered intensity because it is formed from this product. Instead, the intensity depends only on the relative positions of pairs of atoms in the crystal. For this reason, and because there will generally be several pairs of atoms with similar separations (i.e. the atoms are distributed on a crystal lattice), it is more convenient to write the scattered intensity as a sum over the average scattering properties associated with all vectors $\mathbf{R}_{lmn}$ that separate crystallographic sites of the average structure. That is,

$$I_T(\mathbf{s}) = \sum_{\mathbf{R}_{lmn}} N_{lmn}\langle f_0 f_{lmn}^* \exp\{2\pi i\mathbf{s}\cdot\mathbf{r}_{lmn}\}\rangle \quad (2)$$

where N_{lmn} is the total number of atom pairs associated with the vector $\mathbf{R}_{lmn}$. $\mathbf{r}_{lmn}$ is the actual separation of an atom pair associated with $\mathbf{R}_{lmn}$ and is conveniently expressed as $\mathbf{r}_{lmn} = \mathbf{R}_{lmn} + \mathbf{u}_{lmn}$, where $\mathbf{u}_{lmn}$ corrects for the instantaneous thermal and static displacement contributions to the atom positions. The subscripts indicate the scattering factors are to be associated with the atom at the origin o and terminus lmn of the interatomic vector $\mathbf{r}_{lmn}$. Here we intend lmn to only label distinct crystallographic site separations. Integers can, however, be assigned to them when indexing a primitive lattice with a single crystallographic site, but, in general, they will label noninteger site−site distances. Introducing atomic species to eq 2 we obtain

$$I_T(\mathbf{s}) = \sum_{\mathbf{R}_{lmn}}\sum_{ij} N_{lmn} c_i f_i P_{lmn}^{ij} f_j^* \langle\exp\{2\pi i\mathbf{s}\cdot\mathbf{u}_{lmn}^{ij}\}\rangle \times \exp\{2\pi i\mathbf{s}\cdot\mathbf{R}_{lmn}\} \quad (3)$$

For convenience the indices i and j label both an atom type and the crystallographic sublattice upon which that atom type resides and c_i is the sublattice concentration of species i. The P_{lmn}^{ij} are conditional probabilities describing the likelihood that there exists an atom of type j at the end of an interatomic vector $\mathbf{r}_{lmn}$ given that there is an atom of type i at the origin of this vector.

From this equation it is now a simple matter to define the scattering from a hypothetical average lattice, that is, one in which all local properties are replaced by global averages. The conditional probability P_{lmn}^{ij} is thus replaced by the concentration c_j and $\langle\exp\{2\pi i\mathbf{s}\cdot\mathbf{u}_{lmn}^{ij}\}\rangle$ by $\langle\exp\{2\pi i\mathbf{s}\cdot\mathbf{u}^{ij}\}\rangle$. By dropping the subscript lmn from the $\mathbf{u}^{ij}$, we indicate that the average of the exponent is to be taken over the displacements of *all* valid interatomic vectors, not just those indicated by the triplet lmn. The resulting coefficients thus no longer depend on lmn and the average scattering can be written

$$I_{ave}(\mathbf{s}) = \sum_{\mathbf{R}_{lmn}}\sum_{ij} N_{lmn} c_i c_j f_i f_j^* \langle\exp\{2\pi i\mathbf{s}\cdot\mathbf{u}^{ij}\}\rangle \exp\{2\pi i\mathbf{s}\cdot\mathbf{R}_{lmn}\} \quad (4)$$

The average intensity defined this way has constant Fourier coefficients, so the summation over all $\mathbf{R}_{lmn}$ will produce sharp δ-function like peaks at each of the reciprocal lattice points—that is, this expression describes the location and intensity of the Bragg peaks. Since $I_T(\mathbf{s}) = I_{ave}(\mathbf{s}) + I_{diffuse}(\mathbf{s})$, an expression for the diffuse intensity can be obtained by simply taking the difference between the total intensity (eq 3) and the average scattered intensity (eq 4):

$$I_{diffuse}(\mathbf{s}) = \sum_{\mathbf{R}_{lmn}}\sum_{ij} N_{lmn} c_i c_j f_i f_j^* \left[\frac{P_{lmn}^{ij}}{c_j}\langle\exp\{2\pi i\mathbf{s}\cdot\mathbf{u}_{lmn}^{ij}\}\rangle - \langle\exp\{2\pi i\mathbf{s}\cdot\mathbf{u}^{ij}\}\rangle\right] \times \exp\{2\pi i\mathbf{s}\cdot\mathbf{R}_{lmn}\} \quad (5)$$

By definition, the expressions enclosed in large brackets vanishes at large interatomic vectors (only local deviations are allowed from the average structure). Equation 5 therefore represents a summation with relatively few terms and so does not contain any sharp Bragg-like features. It describes a broadly distributed, smoothly varying, intensity component. Since only vectors $\mathbf{R}_{lmn}$ that are small relative to the crystal dimensions contribute to this sum $N_{lmn} \approx N_p$, the number of primitive unit cells in the crystal, so N_p can be factored to the front of eq 5 to simplify the expression further.

2.2. Two Simple Examples

It is instructive at this stage to show how eq 5 can be applied. We consider two simple limiting cases,

one involving thermal displacement disorder and the other substitutional disorder. For a one-component crystal in which the atoms vibrate *independently* about their average lattice sites the term in large bracket in eq 5 is zero for all vectors except $\mathbf{R}_{lmn} = 0$. For this term $\mathbf{u}_{lmn} = 0$ (an atom has no deviation in displacement with respect to itself). If we further assume that the thermal displacements are normally distributed with mean-squared vibrational amplitude $\langle\delta^2\rangle$ (the Einstein model), then

$$\langle\exp\{2\pi i\mathbf{s}\cdot\mathbf{u}\}\rangle = \langle\exp\{2\pi i\mathbf{s}\cdot\boldsymbol{\delta}\}\rangle\langle\exp\{-2\pi i\mathbf{s}\cdot\boldsymbol{\delta}'\}\rangle = \exp\{-16\pi^2([\sin^2(\theta)]/\lambda^2)\langle\delta^2\rangle\} = \exp\{-2M\} \quad (6)$$

where $\boldsymbol{\delta}$ is a vector representing the thermal displacement of an atom from its lattice site ($\boldsymbol{\delta}$ is normally distributed) and $\exp\{-2M\}$ is the usual Debye temperature factor.[26] The diffuse intensity is therefore

$$I_{\text{diffuse}}(\mathbf{s}) = Nf^2(1 - \exp\{-2M\}) \quad (7)$$

where N is the total number of atoms in the crystal. The scattering from the average structure using eq 4 becomes

$$I_{\text{ave}}(\mathbf{s}) = f^2 e^{-2M} \sum_{\mathbf{R}_{lmn}} N_{lmn} \exp\{2\pi i\mathbf{s}\cdot\mathbf{R}_{lmn}\} \quad (8)$$

which describes sharp Bragg peaks depressed by the Debye temperature factor—a result well known to crystallographers. In real crystals the thermal motion will be correlated for neighboring atoms. In this case the first term in the expression for the diffuse intensity will be given by eq 7, but there will also be several other contributing terms. These additional terms are all sinusoidal and so *will not change the total amount* of diffuse scattering obtained by integrating eq 7, but will instead tend to modulate and redistribute the intensity of eq 7. In real materials this thermal diffuse scattering is generally redistributed such that it is concentrated near the Bragg peak locations. (Some care must, therefore, be taken when evaluating $\exp\{-2M\}$ from Bragg reflection data to avoid underestimating its value.) The expression for the average scattering (eq 8) in this case remains unchanged.

Note should be taken here of the likely relative magnitudes of the diffuse vs Bragg scattering. Near the reciprocal space origin the thermal diffuse intensity approaches 0 so only the Bragg scattering is important, but, at very large scattering angles the thermal effects tend to depress the Bragg peaks while the thermal diffuse intensity grows. Under normal circumstances (moderate diffraction angles and average thermal motion) the Bragg peak intensities will be several orders of magnitude larger than the diffuse background. This results largely from the fact that the diffuse intensity is distributed more broadly throughout the reciprocal space volume, whereas the Bragg scattering is highly concentrated about the reciprocal lattice positions. The *integrated* thermal diffuse intensity can, in principle, be of the same order as the integrated Bragg intensities far from the reciprocal space origin.

A second instructive limiting case is the diffuse scattering from a system containing random substitutional disorder but where thermal and static atomic displacements can be neglected. Random substitution implies that in eq 5 $P^{ij}_{lmn} = c_j$ for all lmn except $\mathbf{R}_{lmn} = 0$, where instead P^{ij}_{ooo} is 1 when $i = j$ and 0 otherwise. Like the situation with random thermal motion only one term (in $\mathbf{R}_{lmn}$) contributes to the diffuse intensity

$$I_{\text{diffuse}}(\mathbf{s}) = N_p \sum_{ij} c_i c_j f_i f_j^* [(P^{ij}_{ooo}/c_j) - 1] \quad (9)$$

For a binary substitutional system of components labeled A and B, eq 9 simplifies (after some algebraic manipulation) to

$$I_{\text{diffuse}}(\mathbf{s}) = Nc_A c_B (f_A - f_B)^2 \quad (10)$$

The diffuse intensity described by eqs 9 and 10 is called the Laue monotonic diffuse scattering and is present in all materials that contain substitutional disorder. Analogous to the situation with thermal diffuse scattering outlined above, if the substitution is not random but correlated over short ranges, then there will be several more (sinusoidal) terms in eqs 9 and 10. These terms only *redistribute* the Laue monotonic intensity. The resulting diffuse scattering is termed the short-range order (SRO) diffuse intensity and is often written in the form

$$I_{\text{SRO}}(\mathbf{s}) = -N_p \sum_{\mathbf{R}_{lmn}} \sum_{ij} c_i c_j f_i f_j^* \alpha^{ij}_{lmn} \cos(2\pi\mathbf{s}\cdot\mathbf{R}_{lmn}) \quad (11)$$

where

$$\alpha^{ij}_{lmn} = 1 - (P^{ij}_{lmn}/c_j) \quad (12)$$

are the Warren–Cowley short-range order parameters. As a general rule, this SRO intensity appears around and beneath the Bragg diffraction peaks in systems where like atoms cluster, but, in systems where the atom species tend to alternate on neighboring sites, the SRO intensity peaks near superstructure positions in the diffraction pattern. Like the situation with thermal motion, these correlations would not affect the average scattering because it contains information only about the average occupancies of the crystallographic sites and the set of $\mathbf{R}_{lmn}$ which defines the average crystal lattice.

It should be clear from the above discussion that measurement of the Bragg peak intensities cannot provide information regarding either the local chemical or displacement correlations, because this intensity component is independent of such structural details. It is the diffuse part of the diffraction pattern that is altered by the presence of these correlations, and it is here that we must look for clues to the nature of the disorder. Measurements of the diffuse intensity in real materials can therefore provide great insight into the disorder present in a crystal that cannot be obtained using normal crystallographic analysis techniques and which may be difficult or impossible to obtain using other experimental methods.

2.3. Diffuse Scattering in Metallic Alloys

The first direct application of equations like those presented above was by Cowley[27] for the case of short-range order diffuse scattering from single crystals of the alloy Cu_3Au above its ordering temperature. Cowley neglected the effects due to atomic displacements and so expressed his diffuse intensity as resulting solely from short-range chemical ordering. The diffuse intensity for this case can be derived from eq 11 by explicitly expanding the summation over atom species ij, noting that

$$c_A P^{AB}_{lmn} = c_B P^{BA}_{lmn} \qquad P^{AB}_{lmn} + P^{AA}_{lmn} = 1$$
$$P^{BA}_{lmn} + P^{BB}_{lmn} = 1 \tag{13}$$

and combining like algebraic terms:

$$I_{SRO}(h_1,h_2,h_3) = N_p(f_A - f_B)^2 \sum_{lmn} \alpha^{AB}_{lmn} \cos\{2\pi(h_1 l + h_2 m + h_3 n)\} \tag{14}$$

Here, the continuous reciprocal space coordinates, h_1, h_2, and h_3, have been introduced, and l, m, and n are half-integers representing the interatomic distances in this fcc structure and so satisfy the condition $l + m + n =$ integer.

The SRO diffuse intensity is thus simply a three dimensional cosine Fourier sum with coefficients α^{AB}_{lmn}. Cowley recognized that a measurement of the SRO diffuse scattering taken throughout the reciprocal space volume could be Fourier-inverted to yield the atomic pair correlations directly. The alloy Cu_3Au has a high symmetry cubic structure so the measurement needed only to include a scattering volume $^1/_{32}$ of a complete reciprocal cell. He measured the diffuse intensity at 450 points inside this "minimum repeat volume", interpolated from these values to uniformly cover that volume, and then applied the appropriate symmetry relationships to fill the reciprocal unit cell. The diffuse intensity he measured on the h_1h_20 reciprocal plane is shown in Figure 1. The ordering is such in this alloy that the

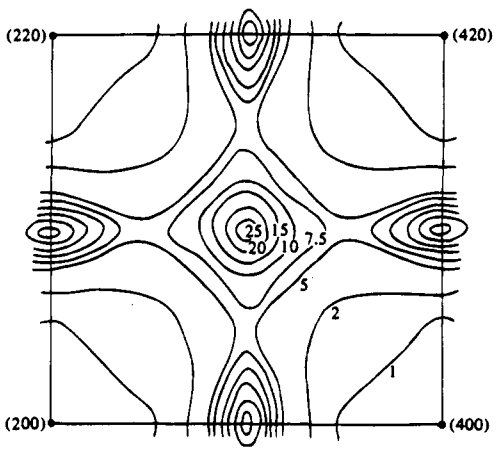

Figure 1. Cowley's original measurement of the SRO diffuse intensity from a single crystal of Cu_3Au above the critical temperature for ordering. Shown here is the h_1h_20 reciprocal plane. (Reproduced from ref 27 with kind permission of Professor J. M. Cowley. Copyright 1950 American Institute of Physics.)

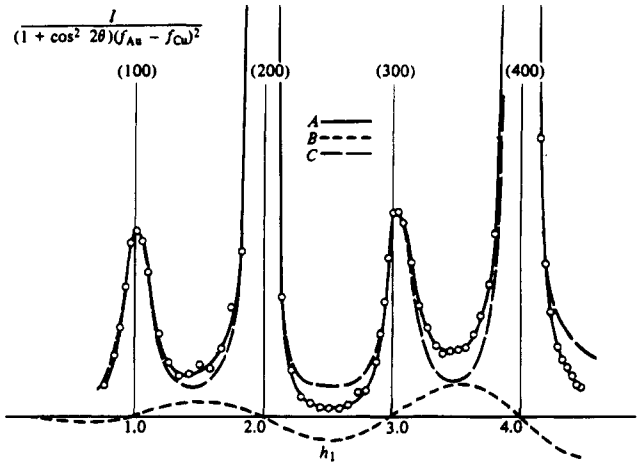

Figure 2. The measured diffuse intensity along the line h_100 from a single crystal of Cu_3Au quenched from above the ordering temperature (see ref 32). A (—) is the measured intensity, B (- - -) is the predicted modulation due to the atomic size effect, and C (— —) is the difference between curves A and B, i.e., the SRO diffuse intensity. (Reproduced from ref 32 with permission of the *Journal of Applied Physics*. Copyright 1951 American Institute of Physics.)

diffuse intensity is peaked at the superstructure locations corresponding to the long-range ordered state of this alloy below the critical temperature. The disk-like shape of the diffuse scattering maxima result from details of the local ordering.

The short-range order coefficients, obtained by inversion of the measured diffuse intensity, were normalized so that $\alpha^{AB}_{000} = 1$ as required by definition (that is, the probability that atoms of type A and B both share the same site is 0). The resulting analysis demonstrated that the structure of Cu_3Au above the critical temperature qualitatively resembles the long-range ordered state with the exception that the chemical correlations fall off rapidly with distance. The actual magnitudes of the correlations can be used to test theories of ordering in alloys.[28-31]

Since this seminal work by Cowley, many improvements have been made to his basic method. The most important of these has been the inclusion of effects on the diffuse scattering due to static atomic displacements. In a disordered alloy these displacements result from the fact that distinct atom species tend to differ in size. Warren, Averbach, and Roberts[32] were the first to publish a theory describing this *atomic size effect* and showed that these displacements (to first order) cause an asymmetry in the diffuse intensity across integer reciprocal space positions. This asymmetry is shown for the case of diffuse scattering from a single crystal of Cu_3Au along a reciprocal space line in Figure 2. This figure shows that the effect is approximately sinusoidal, is smallest at low diffraction angles, and becomes increasingly pronounced at larger angles.

The most widely used methods for analyzing diffuse intensities that include the effects of static displacements are based on ideas originally presented by Borie[18] and Borie and Sparks[21] which were subsequently improved upon by Tibballs[22] and Georgopoulos and Cohen.[24] These methods are based on a Taylor series expansion of the complex exponentials

of eq 5 to terms harmonic in the displacements $\mathbf{u}^{ij}_{lmn}$ and $\mathbf{u}^{ij}$. That is, the approximation

$$\langle \exp\{2\pi i \mathbf{s}\cdot\mathbf{u}\}\rangle \approx 1 + \langle 2\pi i \mathbf{s}\cdot\mathbf{u}\rangle + {}^1/_2\langle (2\pi i \mathbf{s}\cdot\mathbf{u})^2\rangle \quad (15)$$

is made. Substituting eq 15 for the exponential terms of eq 5 yields an expression for the diffuse intensity composed of three parts,

$$I_{\text{diffuse}} = I_{\text{SRO}} + I_1 + I_2 \quad (16)$$

where

$$I_{\text{SRO}}(h_1h_2h_3) = -\sum_{lmn}\sum_{ij} c_i c_j f_i f_j^* \alpha^{ij}_{lmn} \cos\{2\pi(h_1 l + h_2 m + h_3 n)\} \quad (17)$$

$$I_1(h_1h_2h_3) = -2\pi \sum_{lmn}\sum_{ij} c_i c_j f_i f_j^* (1 - \alpha^{ij}_{lmn})[h_1\langle X^{ij}_{lmn}\rangle + h_2\langle Y^{ij}_{lmn}\rangle + h_3\langle Z^{ij}_{lmn}\rangle]\sin\{2\pi(h_1 l + h_2 m + h_3 n)\} \quad (18)$$

$$\begin{aligned} I_2(h_1h_2h_3) = & -2\pi^2 \sum_{lmn}\sum_{ij} c_i c_j f_i f_j^* [h_1{}^2\{(1 - \alpha^{ij}_{lmn})\langle (X^{ij}_{lmn})^2\rangle - \langle (X^{ij})^2\rangle\} + h_2{}^2\{(1 - \alpha^{ij}_{lmn})\langle (Y^{ij}_{lmn})^2\rangle - \langle (Y^{ij})^2\rangle\} + \\ & h_3{}^2\{(1 - \alpha^{ij}_{lmn})\langle (Z^{ij}_{lmn})^2\rangle - \langle (Z^{ij})^2\rangle\} + \\ & 2(1 - \alpha^{ij}_{lmn})\{h_1h_2\langle (X^{ij}_{lmn}Y^{ij}_{lmn})\rangle + h_1h_3\langle (X^{ij}_{lmn}Z^{ij}_{lmn})\rangle + \\ & h_2h_3\langle (Y^{ij}_{lmn}Z^{ij}_{lmn})\rangle\}]\cos\{2\pi(h_1 l + h_2 m + h_3 n)\} \end{aligned} \quad (19)$$

Here, X, Y, and Z are the three components of the vectors $\mathbf{u}$ and the sub/superscripts convey the meanings outlined in the previous section. In eqs 17–19 the component intensities are expressed in "electron units" per primitive unit cell where an electron unit refers to the scattered intensity, as given by the Thomson formula,[33] that would result if the crystal were to be replaced by a single classical electron.

The effect of random thermal motion can be accounted for by simply multiplying each of the atomic scattering factors f by the Debye temperature factor e^{-M_i}. From the perspective of an X-ray photon, the thermal motion is frozen so the Debye factor should only be applied to terms with nonzero interatomic length. A simple correction for this can be included by adding and subtracting Debye corrected terms corresponding to the zero length interatomic vector. For example, the SRO order intensity can be corrected by adding the additional term[34]

$$-[\sum_{ij} c_i c_j f_i f_j^* \{1 - \exp\{-(M_i + M_j)\}\}] \quad (20)$$

to eq 17 and applying the Debye correction to all of the atomic scattering factors in the diffuse intensity summations. A similar term for I_2 (and all other even intensity components) should also be included. First-order thermal diffuse scattering (TDS) which results from simple correlations in displacement between pairs of atoms will be accounted for in the term I_2 and so it is not necessary to correct for this. Higher-order terms in the TDS are not included in eqs 17–19 and so must either be neglected or calculated and then subtracted from the measurement.

The benefit of expressing the scattering using eqs 17–19 is that the diffuse intensity now consists of a sum of several intensity components, each of which contains a function periodic with the reciprocal lattice but with unique leading coefficients. For example, in a binary cubic alloy one of these component intensities (derived from eq 19) is

$$I^{\text{AB}}_{XY} = -8\pi^2 c_{\text{A}} c_{\text{B}} \mathscr{Re}\{f_{\text{A}} f_{\text{B}}^*\} h_1 h_2 \sum_{lmn} (1 - \alpha^{\text{AB}}_{lmn})\langle (X^{\text{AB}}_{lmn} Y^{\text{AB}}_{lmn})\rangle \sin(2\pi h_1 l)\sin(2\pi h_2 m)\cos(2\pi h_3 n) \quad (21)$$

Here $\mathscr{Re}$ signifies the real part. The summation in eq 21 represents a periodic function in reciprocal space which is modified by a leading coefficient that consists of a function of the atomic scattering factors and the reciprocal space coordinates. In binary systems there will be 25 such component intensities, one SRO intensity (already derived in eq 14), six components associated with the term I_1, and 18 components associated with the term I_2. (Note that the nine terms implicit in eq 18 can be reduced to six by adding the constraint that the weighted average displacements of the AA, AB, and BB pairs must sum to zero.) The important point is that every one of these 25 intensity components is a product of a periodic function (the Fourier summations) and a unique coefficient that is a function of both the scattering factors and reciprocal space coordinates. *A collection of 25 intensity measurements made at reciprocal space locations related by the crystal symmetry thus constitute a linear system of equations* in which the quantities expressed by the summations can be solved for. A full reciprocal cell can be filled with any of the 25 periodic functions by repeating this procedure at every point in the minimum repeat volume (the same repeat volume Cowley used in his measurements of SRO). Fourier inversion then yields the real-space quantities of interest. Inversion of the intensity components associated with I_1, for example, provides the average displacement of atom pairs from their respective sites, whereas the term I_2 provides parameters describing the degree to which the atomic displacements are correlated.

A classic example of the application of this analysis method is the study by Matsubara and Cohen[35–37] of diffuse scattering in Al–2% Cu alloys. When these alloys are quenched from a high-temperature solid solution phase and later aged at moderate temperatures, small coherent precipitates called Guinier–Preston (G.P.) zones form. These zones are the primary strengthening mechanism of Al alloys so there is a great deal of interest in the details of their structure. The measured diffuse intensity from a single crystal of this alloy on the plane $h_3 = 0$ is displayed in Figure 3. Unlike the situation of ordering in Cu_3Au, the diffuse scattering from this material is concentrated near the Bragg peak locations, not the superstructure locations, indicating that Cu atoms cluster. The shape of the diffuse scattering is rodlike and indicates that these Cu clusters have a platelet morphology and that the orientation of these plates are parallel to the cube axes.

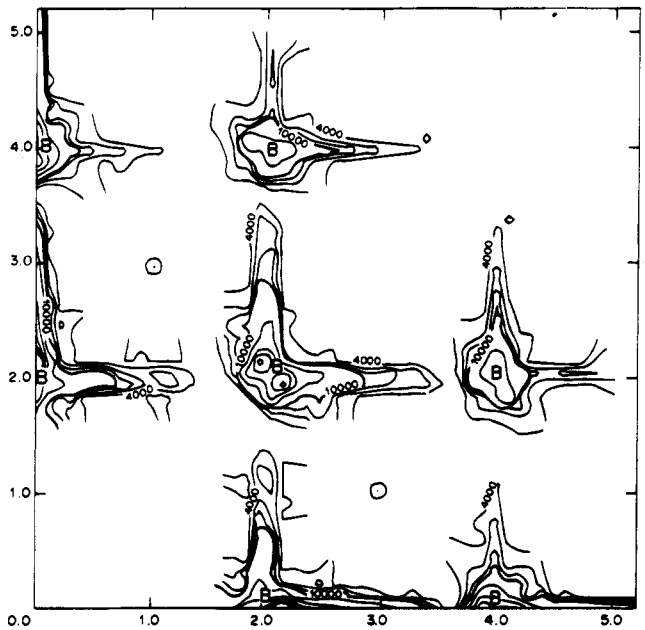

Figure 3. Matsubara and Cohen's (1985) measurement of the diffuse intensity on the h_1h_20 reciprocal plane from a single crystal of an Al–2% Cu alloy. The crystal was quenched from the solid solution region and then aged to form G.P. zones. In this clustering alloy the diffuse intensity is centered about the Bragg peak locations. The asymmetry in the measured intensity results from large sizde effect distortions. (Reproduced from ref 36 with kind permission of Professor J.B. Cohen. Copyright 1985 Elsevier.)

The diffuse scattering is stronger on the high angle side of the Bragg peaks. This pronounced asymmetry results from the atomic size effect and so a quantitative analysis of this diffraction pattern required the use of the analysis method outlined above.

Matsubara and Cohen[36] normalized the measured diffuse intensity to the scattering from Al powder and polystyrene standards thus placing the measurements on an absolute scale. The advantage gained by taking this extra care in the measurement is that the calculated Compton incoherent scattering could be subtracted and that there was no need to normalize the intensities so that $\alpha_{000}^{AB} = 1$ as Cowley did. Instead, the value obtained for α_{000}^{AB} from the analysis can be compared to its theoretical value as a check on the accuracy of the method. They obtained a value $\alpha_{000}^{AB} = 1$, within experimental uncertainty, indicating that the 24 atomic displacement intensity components had been properly separated from the SRO diffuse intensity. Detailed discussion of how absolute intensity measurements are made and corrections due to incoherent scattering, detector dead-time, polarization, surface roughness, and TDS can be found in Schwartz and Cohen[7] and Epperson, Anderson, and Chen.[4]

Once the Warren–Cowley short-range order parameters have been determined, a structural model consistent with these parameters needs to be found. Gehlen and Cohen[38] have developed a technique whereby a large computer model of the ordering is adjusted using Monte Carlo techniques until the SRO parameters of the model match the measured values. While it is not possible to determine a single unique structure this way (there are many models which can reproduce a given set of ordering parameters) Gragg, Bardhan, and Cohen[39] have pointed out that a particular choice of SRO (pair correlation) parameters places considerable constraints on the multibody correlations. Atomic configurations generated using this simulation technique can therefore be thought of as representative of the actual structure with high probability. From such an analysis Matsubara and Cohen showed that not all of the Cu precipitates (G.P. zones) form single atomic layers, but that a significant fraction of the zones have multiple layers. A detailed discussion of the current state of this computer technique can be found in the recent review by Epperson, Anderson, and Chen.[4]

The method outlined above has also been extended to include ternary systems. Because of the large number of separate intensity components that a ternary system requires, this has been done by varying the scattering contrast of the atomic species present and combining several measurements. In this way systems of equations no more complex than those derived for the binary alloy can be used. This was first done using isotopic replacement techniques and neutron diffraction on an Fe–Cr–Ni alloy.[40] Recently, anomalous dispersion methods at synchrotron radiation sources have been employed to investigate ordering in Al–Cu–Zn[41] and Hg–Cd–Te[42] crystals.

In nearly all studies where a direct separation of the diffuse intensity has been made, the focus has been primarily on the SRO component. Recently, however, this emphasis is shifting to the size–effect terms which can provide additional interesting information about the structure of disordered materials. One recent study of an Fe–Ni–C austenite single crystal by Butler and Cohen[43] used anomalous dispersion (to make the Ni and Fe scattering powers to be nearly the same) and were thus able to solve for the intensity component due to (Fe,Ni)–C pair displacements. The resulting displacement parameters are directly related to the distance of separation of Fe and C atoms. The atomic displacements surrounding the interstitial carbon atom could therefore be determined, and these measured displacements used to test empirically derived Fe–C interaction potentials. In an Fe–Cr alloy, Reinhard et al.,[44] investigated the atomic displacement parameters using a related least-squares analysis method. They discovered that both the Fe–Fe and Cr–Cr near-neighbor pairs contract toward each other contrary to what would be expected since Cr atoms are "larger" than Fe atoms. This was explained as resulting from species-dependent solution–lattice couplings—an important result which helps explain stress–strain relationships in Fe–Cr alloys. Techniques, like those used to generate atomic configurations consistent with the SRO parameters, are beginning to be applied to generate models of the displacements based on the size–effect parameters contained in I_1.[45] A recent study of the atomic size effect employing computer simulation[46] has shown that the term I_2 can also lead to interesting diffraction effects whereby the diffuse intensity tends to be "absent" on certain symmetry planes of the reciprocal space.

It is difficult to test the validity of truncating the Taylor series expansion at the harmonic term as in eq 15. This is because a binary system would have 55 intensity components if the expansion is taken to third order—more than twice the number of components needed for the normal analysis—making a full comparison of the two methods using experimental data impractical. Computer simulation was recently used, however, to make this test for an oxide system.[47] Here it is possible to compare the exact diffuse intensity with an expansion of eq 5 to arbitrary order in atomic displacement. For the particular example chosen, which contained relatively large (3% rms) atomic displacements, a Taylor expansion to second order was found to fit the exact scattering reasonably well out to a reciprocal coordinate $h \approx 2$. Beyond this, however, higher order terms in the expansion must be included. An experimental measurement of the diffuse intensity in a cubic stabilized zirconia (the system to which the computer simulation related) showed clear evidence of diffraction effects due to intensity components associated with the third-order term of the Taylor expansion. Care should therefore be exercised when applying these methods to systems where the atomic distortions are large.

As an attempt to minimize the number of intensity components to solve for and thus perhaps improve on the accuracy of the diffuse scattering analysis method outlined above, several investigators have begun to analyze diffuse scattering data from alloys using the "null Laue" method.[48,49] This method recognizes that in a binary alloy all even-order terms in the Taylor expansion of eq 5 vary as $|c_A f_A + c_B f_B|^2$, whereas I_{SRO} and I_1 vary as $(f_A - f_B)^2$ and $\mathcal{R}e\{f_{A,B}(f_A - f_B)\}$, respectively. The measured diffuse scattering from a crystal tuned to a wavelength in which $(f_A - f_B) \approx 0$ (the null Laue condition) can be subtracted directly from a measurement made at a different wavelength where $(f_A - f_B) \neq 0$ by simply scaling the earlier measurement to account for this change in scattering contrast. After subtraction only the diffuse scattering from I_{SRO} and I_1 remain so there are only seven instead of the usual 25 intensity components left to solve for. This considerably simplifies the resulting analysis. In practice it is difficult to exactly satisfy the "null Laue" condition so the diffuse scattering is measured at three different wavelengths and the null Laue diffuse scattering is obtained by iteration. This method has been used to study short-range chemical and displacement disorder in Fe–Cr,[44] Fe–Ni,[50] and Ni–Cr[51] alloys.

An alternative to using a Taylor expansion has been presented by Dietrich and Fenzl.[25] They propose that a cumulant expansion of the exponential is more appropriate as it is guaranteed to converge and should do so more rapidly than a simple Taylor expansion. Expanded in cumulants to second order, eq 15 can be written

$$\langle \exp\{2\pi i \mathbf{s}\cdot\mathbf{u}\}\rangle \approx \exp\{2\pi i[\langle \mathbf{s}\cdot\mathbf{u}\rangle + {}^1/_2\langle(\mathbf{s}\cdot\mathbf{u})^2\rangle - \langle \mathbf{s}\cdot\mathbf{u}\rangle^2]\} \quad (22)$$

Equation 22 is exact when the displacements $\mathbf{u}$ are normally distributed and will, in general, be more accurate than eq 15. The practical difficulty of using eq 22 for diffuse scattering analysis is that it does not permit the diffuse intensity to be expressed as a summation of component intensities as is possible when using the Taylor expansion. The correlation parameters α^{ij}_{lmn}, $\langle X^{ij}_{lmn}\rangle$, $\langle(X^{ij}_{lmn})^2\rangle$, etc. must instead be solved for simultaneously using least-squares techniques. This can be accomplished by expanding the summation explicitly over the interatomic vectors lmn and solving for the correlation parameters. This has the distinct disadvantage that you must choose in advance which lmn to include in the analysis. In three dimensions the number of such vectors will be large even if only modest interatomic distances are to be considered. With the Taylor expansion method the separated intensity components are Fourier inverted to obtain the correlation parameters, and thus all correlation parameters within limits set by the resolution of the measurement can be determined. Such methods may play a significant role in the future in the application to materials where large atomic distortions are present and the Taylor expansion is of questionable accuracy.

3. Experimental Aspects

The measurement of X-ray diffuse diffraction patterns poses special challenges that are not normally encountered when measuring Bragg peak intensities. These challenges arise from two facts: (1) Diffuse intensities are generally several orders of magnitude weaker than the Bragg peaks, and (2) the diffuse intensity is not composed of a set of discrete reflections but is instead a continuous function of the reciprocal space coordinates.

The fact that the diffuse intensities are much weaker creates the obvious difficulty that the time necessary to acquire measurement statistics approaching those routinely obtained from a Bragg reflection increases dramatically. Unfortunately, this is not the only difficulty encountered when measuring a weak diffuse signal. Diffraction of the Bremsstrahlung X-rays, Compton inelastic scattering, X-ray fluorescence from the various atom species in the sample (excited either by the fundamental X-ray frequency or harmonics that pass through the monochromator), scattering from air molecules near the sample, and scattering from the sample holder and/or container can all give contributions to the total measured intensity that are comparable in magnitude to the desired diffuse signal. These effects are regarded as only minor nuisances in the measurement of Bragg intensities but can make the collection of diffuse scattering data difficult, particularly if a quantitative analysis of the data is desired.

Furthermore, because the diffuse intensity is continuous throughout the reciprocal space, any complete diffuse scattering measurement must sample numerous points in order to approximate accurately the scattered intensity. For instance, while in a simple metallic alloy the integrated intensity under just a few dozen Bragg peaks is sufficient to determine the average structure to very high accuracy, a diffuse scattering measurement of a disordered alloy crystal with the same average structure might require several thousand individual measurements to sample (only coarsely) the full 3D diffraction volume.

Ideally, a general purpose X-ray diffuse scattering measurement apparatus would thus consist of (1) an intense source of X-rays to overcome the inherently weak diffuse scattering, (2) an evacuated sample chamber and sample holder that will not scatter X-rays in order to minimize sources of background scattering, (3) a high-resolution energy dispersive detector that can distinguish between the coherently diffracted X-rays and the incoherent and fluorescent backgrounds, and (4) a detector that can integrate intensities from many reciprocal space locations simultaneously. It is difficult to satisfy all of these demands so all experimental arrangements reflect compromises made to obtain the best diffraction data, within a practical period of time, from a particular class of crystals and using readily available equipment. Below, the types of X-ray sources and detectors currently in use, sources of background scattering, and corrections that might be applied to diffuse scattering data are outlined. This is followed by a description of some of the experimental configurations in current use. The list is not meant to be exhaustive. It is intended only to illustrate the technical difficulties likely to be encountered when making a diffuse scattering measurement and to present some examples of how various components can be used to make these measurements.

3.1. X-ray Sources

Standard laboratory X-ray sources (sealed-tube and rotating anode) are still widely used for diffuse X-ray scattering studies. A monochromator, set to select one of the characteristic emission lines of the anode, is essential because the coherent scattering from the Bremsstrahlung background might overwhelm the diffuse signal. Typically, a singly or doubly bent mosaic crystal monochromator is employed (most often pyrolytic graphite) to maximize the total X-ray flux. Some angular resolution can be sacrificed for this purpose, because diffuse scattering measurements do not generally require high resolution unless there is a need to work close to the Bragg reflections or highly anisotropic diffuse phenomena are being studied.[52] With laboratory sources it may take several weeks to collect data on a single sample. Incident beam monitors are thus often employed to correct long time fluctuations in the incident intensity (caused by barometric pressure changes, X-ray tube decay, etc.).[7]

The availability of synchrotron radiation sources, which have X-ray fluxes several orders above that of a sealed tube or rotating anode, has created great opportunities for diffuse scattering investigations.[53,54] Many crystals that would have been impractical to study because of the weak scattered intensities can now be probed using synchrotrons. The possibilities will increase dramatically in the coming few years when the next generation of synchrotron radiation sources (the ESRF in Europe, the APS in the United States, and SPRING-8 in Japan) will be available for general use.

Besides this enormous increase in flux, synchrotrons also allow the incident X-ray energy to be tunable instead of limited to the few emission lines that standard laboratory sources are capable of providing. An X-ray wavelength might be conveniently chosen to avoid unwanted fluorescence or even tuned to just below an X-ray absorption edge to take advantage of anomalous dispersion. With anomalous dispersion the scattering power of a single atomic species can be adjusted so that its effect on the diffraction pattern is enhanced or diminished. Additional structural information may be obtained by monitoring the changes in diffuse intensity resulting from changes in incident energy. This has proven to be a powerful tool in neutron scattering where a similar effect can be obtained through isotopic substitution[55] and is being increasingly used for diffuse scattering studies (it makes the "null Laue" method experimentally possible, for instance[48,51]).

3.2. X-ray Detectors

The electronic "point" counters typically used in the measurement of Bragg peaks are also used for diffuse scattering measurements. These include gas proportional counters, scintillation counters, and solid-state detectors. The relatively inexpensive gas and scintillation counters have energy resolutions of about 20% and 50%, respectively, and so can be used only to discriminate against fluorescent photons of energy far from the characteristic radiation and the various harmonics ($\lambda/2$, $\lambda/3$, etc.) that may pass through the monochromator. Solid-state detectors[56] (based on intrinsic semiconductor crystals of pure Ge or Li-doped Si or Ge) have much better energy resolution, about 3%, and are thus useful when the need to discriminate the coherent radiation from a nearby fluorescent line arises. These detectors are more expensive and cumbersome because they need to be cooled to eliminate thermal noise.

Position-sensitive detectors (PSDs) are particularly useful for the collection of diffuse scattering data as many points in the reciprocal volume can be integrated simultaneously speeding up the measurement considerably. Wire detectors (both 1D, which are often employed for powder diffraction, and 2D, which are increasingly used by macromolecular crystallographers) are convenient to use because each X-ray photon detected is electronically recorded. The data can therefore be displayed in real time without having to resort to a development step as is necessary with photographic emulsions.

X-ray film is still widely used because large areas can be covered and recorded with much higher spatial resolution than with any other detector. It is also inexpensive and can be cut to shape and bent to fit into a variety of X-ray cameras. Imaging plates[57] are also flexible but with the advantage that they are more sensitive than X-ray film (by about a factor of 60). These detectors contain a photostimulable storage phosphor (typically, $BaFBr:Eu^{2+}$ or $CaSO_4:Dy^{3+}$) that is read by scanning a laser across its surface and recording the stimulated luminescence. Currently, the spatial resolution[58] of image plate X-ray detectors is of the order of 100 μm—significantly worse than can be obtained with film but this should not be a problem for most diffuse scattering measurements. Charge-coupled devices (CCD) also offer the possibility to be used as 1D and 2D detectors in X-ray diffuse scattering studies.[59] These can be used

as fast integrating detectors that either directly detect the X-ray photons or detect the emission of light from a phosphor exposed to the scattered X-rays. Unfortunately, CCD detectors are small (about 10 mm on edge) so it is difficult to cover large angular ranges and this limits their usefulness. Advances in the application of this technology are, however, rapid so the use of CCD-based X-ray detectors may soon become much more common.

With the exception of wire detectors, the PSDs mentioned above have no useful energy resolution and so cannot be used in situations where a large fluorescent background is created unless some other means of eliminating this unwanted background (such as using preferentially absorbing filters) is provided. Wire detectors can be connected to pulse-height analysis electronics thus becoming position-sensitive proportional counters (PSPC)[60] and so obtain an energy resolution similar to gas proportional counters, but this is often not done in practice.

3.3. Sources of Background Scattering

Because a diffuse scattering signal is potentially extremely weak, sources of background scattering that might normally be ignored may need to be carefully monitored. Fluorescent radiation, characteristic of the atom species present in the sample, often causes the greatest difficulty. It is excited when the incident X-ray energy is above (or just slightly below[61]) a K or L absorption edge and might also be excited by harmonics of the fundamental energy which can be passed by the monochromator.

Because low-energy X-rays (less than about 5 keV) are highly absorbed by air the K fluorescence from elements with atomic number less than about 22 (Ti) and L fluorescence from elements of atomic number below about 52 (Te) can generally be ignored. If the fluorescent X-ray photons have an energy much smaller than the coherent X-rays, but above 5 keV, then a filter (such as Al foil) may be placed in the path to preferentially absorb the fluorescence. When the fluorescent energy differs from the incident energy by less than about 30% a detector with energy discrimination will need to be employed to remove it. A solid-state detector can discriminate fluorescence within about 200 eV of the incident energy, which is sufficient for most studies that do not involve anomalous dispersion. When working very close to an absorption edge, however, even a solid-state detector does not have the resolution necessary to eliminate fluorescence entirely. This is best handled by employing a monochromator on the diffracted beam[62] which, depending on the optical arrangement, can provide an energy resolution of several electron-volts. An alternative is to monitor, for instance, the K_α fluorescence which will be well separated from the absorption edge, estimated the K_β contribution from this, and then subtract it from the measured intensity.[41]

X-rays scattered due to the Compton effect are also a source of background. The Compton incoherent X-rays differ in wavelength from the coherent X-rays by a factor

$$\Delta\lambda = 0.02426[1 - \cos(2\theta)] \qquad (23)$$

where 2θ is the scattering angle. This relation is independent of the incident energy and corresponds to a difference of about 10−400 eV in the energy and angular ranges generally employed in diffuse scattering measurements. It is thus very difficult to discriminate from the coherent X-rays. An estimate of the magnitude of the Compton scattering from a particular element in the sample can be obtained from the relation[63]

$$I_{\text{inc}} = I_{\text{e}}[Z - \sum_{n=1}^{Z} f_n^{\,2}] \qquad (24)$$

where Z is the atomic number, $f_n^{\,2}$ is the square of the scattering power of an individual electron of the element being considered, and $I_{\text{e}} = I_{\text{coh}} + I_{\text{inc}}$ is the classical Thomson scattering associated with a single electron. At small angles $\sum_{n=1}^{Z} f_n^{\,2} \approx Z$ so the incoherent scattering is small, but at large angles $\sum_{n=1}^{Z} f_n^{\,2} \rightarrow 0$ and the Compton scattering dominates. The term $\sum_{n=1}^{Z} f_n^{\,2}$ is tabulated for each element[64,65] so it is possible to compute the Compton component at each diffraction angle and then subtract this from experimental data that has been measured in absolute scattering units (i.e., normalized to I_{e}).

It is difficult to block the scattering from air molecules in the incident beam path near the sample with scatter slits, so it is helpful to eliminate it by housing the sample in an evacuated chamber. To avoid excessive absorption of the incident beam this housing is typically made of Be and mechanical vacuum is sufficient to eliminate essentially all air scattering. Alternatively, the housing can be filled with a low-density gas (such as He) that will not scatter as strongly as air. It is, of course, desirable to minimize scattering from the sample holder as well. If this is not possible, as will likely be the case with many macromolecular crystal samples that are grown in a glass capillary, it is important to recognize that the sample holder will contribute substantially to the background. It is possible to measure (and correct for) this background contribution by translating the capillary along its axis until the sample is out of the beam.

3.4. Data Corrections

As with Bragg scattering data, standard corrections to account for absorption, polarization, and detector efficiency, must be applied before a quantitative analysis of the diffuse scattering data can begin. Absorption corrections for many standard shapes (cylinders, spheres, etc.) have been derived for use in crystal structure determination and these are equally applicable for diffuse scattering. It is difficult to compute an accurate absorption correction for large, oddly shaped, crystals so it helps to employ a reflection geometry in which the incident and scattered beams are at the same angle with respect to a large flat surface of the crystal. Absorption will then be constant for all angles. If this method is used it is important for the crystal face to be polished smooth or there might be some additional absorption at low angles that can result from a rough surface.

Standard laboratory monochromated X-ray sources are only partially polarized, whereas synchrotron

radiation tends to be polarized nearly completely along one direction. It is important, therefore, to be aware of the degree of polarization of the source and to make appropriate corrections to the data. Although the diffuse diffraction intensities are usually weak, the data often cover a wide dynamic range. Electronic detectors may thus need to have their reported counts adjusted to account for deadtime.[66] It is also prudent to measure the detector's dark current and make an appropriate correction to the data.

When a direct numerical inversion of the corrected data is to be made, for example, in the metallic alloy examples of the previous section, the corrected data need to be placed on an absolute scale. This is done by normalizing the measured intensity to that from a suitable standard sample such as polystyrene, or Al or Ni powder standards. Details on how to make this conversion can be found in Schwartz and Cohen[7] and in Epperson, Anderson, and Chen.[4]

3.5. Measurement of the Diffuse Intensity

The type of experimental arrangement employed to perform a diffuse scattering measurement depends largely on the volume of the diffraction space that is to be measured and the type of detector that will be used. For instance, if a full reciprocal space volume is to be measured and a point-counting detector is used, then some means of rotating the crystal through all angles relative to the incident beam and rotating the detector to various diffraction angles will be required. This is most conveniently done by employing a standard four-circle X-ray diffractometer and is the arrangement typically used for the measurement of diffuse scattering in alloys.[7]

The standard experimental configuration for alloy measurement consists of a sealed-tube or rotating anode X-ray source that is monochromated using doubly bent pyrolytic graphite. A single crystal with a large polished face (several millimeters on edge) is placed on a goniostat which is then mounted inside an evacuated Be hemisphere. A scintillation or solid-state detector (depending on the energy resolution required) is mounted on the detector arm and the slits are set to accept a relatively large angular range to maximize the number of detected photons at each position (high angular resolution is generally not required). A monitor detector (typically a spare scintillation counter) is used to measure the scattering from a thin polymer placed in the incident beam so that fluctuations in the X-ray beam power can be corrected.

A similar arrangement is used at synchrotron radiation sources except a Si(111) double-crystal monochromator is normally used and the X-rays are focused by a cylindrical (sometimes toroidally bent) glancing angle Pt-coated mirror. This mirror also serves to eliminate the intense $\lambda/3$ harmonic that is passed by the Si monochromator. An incident beam monitor is also essential for synchrotron measurements as the X-ray intensity decays with the current in the storage ring which can vary by a factor of 2 or more during a several hour measurement. For working very close to an absorption edge, Ice and Sparks[62] have developed a spectrometer consisting of a graphite diffracted beam monochromator that is set to scatter onto a linear position sensitive detector. The energy resolution of this device is such that, at most angles, both the resonant Raman[61] (fluorescence) and the Compton incoherent scattering can be separated from the coherent signal. The Compton scattering cannot be separated easily at low angles because of the small energy difference, but, fortunately the correction is small at these angles.

The advantage of using an experimental arrangement like this is that very accurate quantitative diffuse X-ray scattering measurements can be made which can easily be converted to absolute scattering units. The disadvantage is that collecting data from large reciprocal space volumes will be slow (even if the X-ray source is intense) because the detector/sample must be moved to each point in the measuremenmt volume. Position-sensitive detectors, which are capable of integrating the scattering from several points simultaneously, are useful for overcoming this difficulty.

Osborn and Welberry[67] have designed a diffuse scattering measurement system based on a 1D position sensitive detector that allows rapid collection of diffuse scattering data using a sealed tube X-ray source. This experimental design is an electronic implementation of a standard Weissenberg camera set to collect data in the "flat cone" geometry.[68] Here the (curved-wire) PSD is mounted vertically on one circle of the diffractometer which is set at an angle ζ from the main horizontal monochromatic X-ray beam. The sample is mounted about a horizontal axis on a second circle. For any one setting of ζ, a full 360° rotation of the crystal allows the measurement of the diffuse scattering in a complete reciprocal plane normal to the crystal rotation axis. A reciprocal space volume can be measured by collecting data on successive planes.

This diffraction geometry has been used successfully to collect data from several molecular crystal and oxide samples (see sections 4 and 7). The PSD does not have any energy discrimination capability, so the samples are limited to those that have little fluorescence or in which the fluorescence is of low enough energy with respect to the main beam that it can be filtered. Also, if highly absorbing materials are used, small crystals will need to be employed to minimize the effects of absorption. Examples of diffraction data taken with this instrument are shown in Figures 5, 6, 8, 19, and 20. It should be noted that the problem of fluorescence can be minimized if synchrotron radiation is used since the most suitable wavelength for a particular problem can be chosen.

Standard X-ray film techniques such as rotation, oscillation, and Laue (fixed-crystal/fixed-film monochromatic radiation) photographs[8] are also used because they can, in principle, measure the largest diffraction volumes in the shortest period of time. Laue photographs record a spherical 2D section of the scattering and require considerably less complicated equipment to produce than other photographs. This is the preferred method in situations where crystal maneuverability is limited (for example, the low-temperature measurements of 1D conductors, see

section 5). Oscillation photographs can also be used to survey large regions of reciprocal space. They provide an integrated measurement over a range of spherical sections through the scattering and project this onto a single photographic plate. Because of the integration they are less able to resolve fine detail compared to the Laue method. They are the most frequently used technique for the measurement of diffuse intensities in large molecule crystals (see section 8). Moving film methods such as precession and Weissenberg photographs provide data in complete planar 2D sections of the reciprocal space, but are less efficient than the rotation, oscillation, or Laue methods since a large fraction of the scattered intensity is eliminated by the layer screens at any one time. Precession photographs have the advantage that they provide immediately an undistorted view of the reciprocal section, but have a more complex mechanical operation than the Weissenberg. Full reciprocal space volumes can be recorded by taking a series of either of these types of photograph at different crystal settings.

Quantitative data can be extracted from these photographic exposures by reading the optical density with a microdensitometer. Alternatively, the more sensitive, but lower resolution, image plates or 2D wire detectors can be used instead of X-ray film. Samples that fluoresce need to be avoided.

Many other experimental configurations for the measurement of diffuse scattering are possible. For instance a white beam could be used and the scattering measured with an energy dispersive detector.[69] A radial scan in reciprocal space can thus be recorded with a single crystal/detector orientation. A linear PSD could be mounted on the detector arm of a diffractometer to record a range of scattering angles to the same effect.[70] With the renewed interest in diffuse scattering measurement that has resulted from the availability of synchrotron radiation sources, many other useful ways to record the diffuse intensity are bound to be developed.

4. Nonstoichiometric Oxides and Halides

After the alloy systems, simple nonstoichiometric inorganic systems such as simple mixed oxides or halides potentially offer the next best prospect for quantitative analysis of diffuse scattering. For these systems, the number of parameters inherent in the formalism described in the section 2 (based on Taylor expansion of the diffraction equation to second order) is still within the bounds of what is practically feasible. Several such systems have been studied in some detail. Notable early studies were carried out on the systems TiO_x[71] and VO_x[72] but here we concentrate on systems in which there has been more recent activity.

4.1. Cubic Stabilized Zirconias (CSZ's)

The "stabilization" of the high-temperature cubic polymorph of ZrO_2 by the addition of a relatively large amount (~5−50 mol %) of the oxides of a variety of lower valent metals—such as CaO, MgO, Y_2O_3, or the lanthanide sesquioxides Ln_2O_3—and subsequent quenching from high enough temperatures (~1600 °C) leads to anion-deficient materials with important ceramic and superionic conduction properties. Although the average structure of these materials, as revealed by analysis of the Bragg reflections, is extremely simple (fluorite-type, space group $Fm3m$, see Figure 4), details of the exact nature of disordered structure have occupied scientists for many years.[73−82] Despite extensive investigations there still appears to be a lack of consensus among workers regarding the nature of the structural disorder.

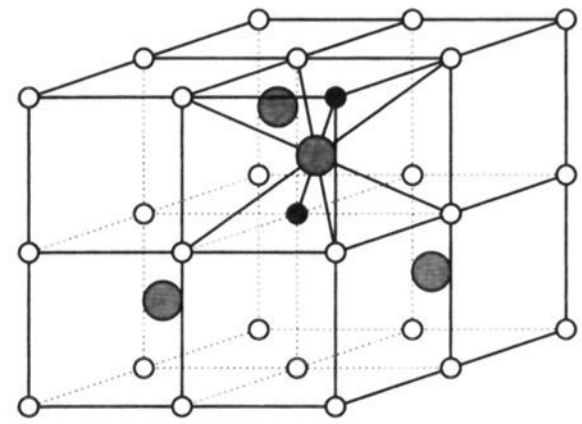

Figure 4. Schematic diagram of the structure of CSZ's. The oxygen atoms (open circles) lie on a simple cubic lattice, while the cations (large shaded circles) occupy alternate cubes consisting of eight oxygen atoms to form an fcc lattice. A defect consisting of a pair of vacancies (black circles) separated by $^1/_2\langle 111\rangle$ is depicted in one of the cubes.

Morinaga et al.[78] carried out a quantitative comparative study of the diffuse scattering from two cubic zirconias of compositions $Ca_{0.150}Zr_{0.850}O_{1.850}$ and $Y_{0.214}Zr_{0.786}O_{1.893}$. They used expressions derived from the Taylor expansion to second order of the basic diffraction equation (see theory section) and fitted these to the observed scattering. They concluded that the diffuse scattering, which is similar for the two materials, is largely due to ionic displacements from the average structure, principally oxygens displaced locally in the ⟨100⟩ directions. Moreover, the short-range order parameters that were determined indicated that the stabilizing ion (Ca/Y) tends to be a second neighbor to an oxygen ion vacancy. These results are at variance with the model of the structure proposed by Rossell and co-workers,[74,83,84] in which it is the Zr atoms that are associated with the oxygen vacancies and the stabilizing ions are found in domains of the so-called ϕ_1 structure ($CaZr_4O_9$) and have a full complement of eight coordinating oxygens.

Neder, Frey, and co-workers[82,85−87] have made extensive studies of the diffuse scattering (neutron) in calcia-stabilized zirconias of various compositions and at ambient and elevated temperatures (up to 1750 K). These workers developed a theoretical framework for interpreting the diffuse scattering which was quite different from the formalism used by Faber et al., and followed earlier theories proposed by Hashimoto.[88] These workers consider that the crystal consists of correlated microdomains. Each microdomain is described by the deviation of its structure factor from the structure factor of the average structure, and the correlation between the microdomains is described by a discontinuous distribution function. This formulation allowed rapid calculation of the diffraction pattern, so least-squares fitting to the observed data could be made for a

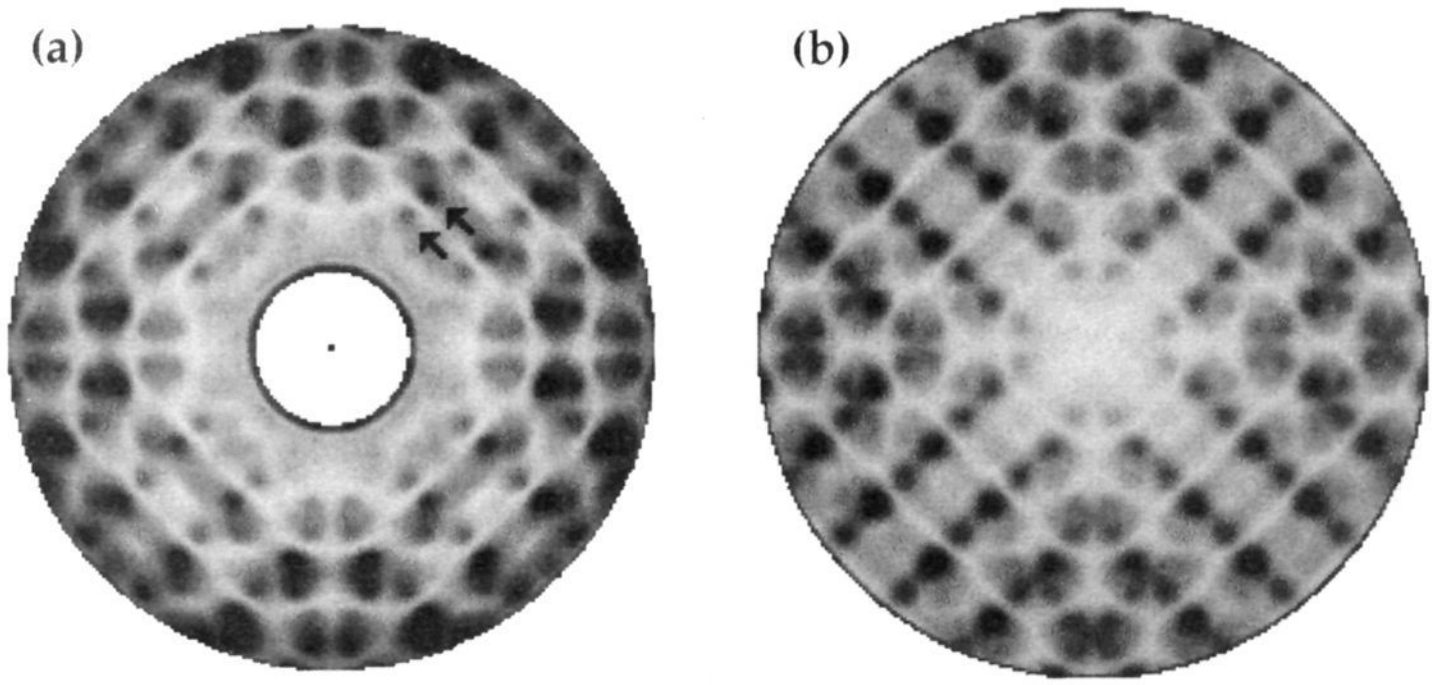

Figure 5. (a) Observed diffraction pattern of the (h k $^1/_2$) section of Y-CSZ. Arrows indicate a pair of asymmetric peaks mentioned in the text. (b) Pattern calculated for the same section from a Monte Carlo simulation of a model system.

variety of different models consisting of different types of microdomains. For each model the parameters refined included positional parameters describing the relaxation of the ions away from the position of the ideal fluorite structure.

From these studies it was concluded that the defect structure consists of two types of detects: microdomains based on a single oxygen vacancy with relaxed neighboring ions, and microdomains based on a pair of oxygen vacancies separated by $^1/_2$ ⟨111⟩. In both types of microdomain it was concluded that the calcium ion is associated with the vacancy.

Welberry et al.[5,89,90] using a position sensitive X-ray detector system, recorded a more comprehensive and detailed set of diffraction patterns than had hitherto been available for an yttria-stabilized zirconia, $Y_{0.39}Zr_{61}O_{1.805}$. Rather than attempting to analyze the scattering directly in terms of the mathematical formalism given in the theory section, they used this formalism instead to guide a Monte Carlo simulation model. These data, an example section of which is shown in Figure 5a, reveal a number of distinctive qualitative features which, these authors argue, must be reproduced by any viable model of the system. In particular: sets of planes (lines in the 2D section) of very low intensity are visible normal to each ⟨110⟩ direction; pairs of diffuse peaks which span these lines are seen to be systematically more intense on the high-angle side of the line than on the low-angle side; there are also distinctive triangular regions of scattering either side of the (0 4 $^1/_2$) reciprocal position, making a feature somewhat reminiscent of a "bow-tie".

A model which was able to account for these features was developed (see Figure 5b). It consisted of two stages: a model for the ordering of the oxygen vacancies, followed by a relaxation of the cations around these vacancies. The model which best fitted the observed patterns was one in which the vacancies were ordered in such a way that nearest- and second-nearest neighboring pairs were avoided, as well as third neighbors along the diagonal of empty cubes of oxygens. Vacancy pairs along the diagonals of cubes containing the cations were favored. The cations were relaxed in such a way that if either of the two oxygen sites which span a given cation-cation vector were vacant, then the cations tended to move apart, while if both were occupied then the cations moved relatively closer together. The particular vacancy ordering scheme gave rise to the pairs of spots and the relaxation scheme resulted in the occurrence of the planes of low intensity caused by the correlated motion of cations along the ⟨110⟩ rows of closest contact, away from the defect sites. The asymmetry of the intensity of each pair of diffuse peaks occurred when the magnitude of the distortion was ~3%. For small distortions the asymmetry was negligible. In this work it was assumed, in contrast to the earlier work of Morinaga et al.,[78] that the cations provide the major contribution to the scattering. This was justified on the grounds that, although the average structure reveals that the oxygens have mean-squared displacements perhaps twice as large as the cations, the much greater scattering factors of the cations still dominate. Further evidence for the fact that the scattering is mainly due to the cations is given by the fact that the low-intensity planes are much less visible in Ca-CSZ's where additional contributions to the intensity arise from the direct contrast between the scattering factors of the two types of cation.

An important observation coming from this study is the fact that for Y-CSZ the first two terms in the Taylor expansion, that is, the SRO term and the size−effect term, eqs 17 and 18, are 0. The scattering must largely arise from scattering terms I_2, eq 19, and higher. However, since I_2 is a sum of *cosines*, the asymmetry in the intensity of the pairs of peaks must arise from the higher order I_3 term which like all odd-numbered terms involves a sum of *sines*. This means that analyzing the data in terms of a Taylor expansion truncated at second order cannot be justified—the magnitude of the displacements are too large in this system. In the case of the analysis of the Ca-CSZ's carried out by Morinaga et al.,[78] scattering due to the size−effect term I_1 is present, so an asymmetry in the intensities of the pairs of peaks can be obtained without the need to invoke I_3. However, I_1 is of opposite sign to I_3 and consequently, if displacement parameters are refined on the as-

sumption that they are due to I_1 when in fact they are due to I_3, spurious results might be expected. This may provide an explanation why Morinaga et al.[78] found the Ca ions to be the ones associated with the vacancies, which is counter to all the chemical arguments of Rossel and co-workers that the Zr and not the Ca or Y should be 6-fold coordinated.

A more recent study[91] approached the problem from a different point of view in order to reconcile the view of the diffuse scattering derived from these X-ray studies with observations using electron diffraction. In electron diffraction patterns, for which multiple scattering tends to modify the azimuthal variation of intensity that is characteristic of displacement scattering, the diffraction patterns of CSZ's are dominated by the presence of characteristic circles of diffuse scattering which occur centered at the $\frac{1}{2}\{111\}$ reciprocal positions and in planes normal to the $\{111\}^*$ reciprocal directions. A computer model of the distribution of oxygen vacancies was directly synthesized by applying modulation waves, of wave vectors corresponding to these circles, to the fluorite-type average structure. The derived oxygen distribution was then used in conjunction with the same cation relaxation method as before. When the quantity modulated was taken as the occupancy of individual oxygen sites, the calculated diffraction patterns were unsatisfactory, but when the modulations were applied to $\frac{1}{2}\langle 111\rangle$ pairs of sites the calculated patterns showed good agreement with the observed X-ray patterns.

4.2. Wüstite, $Fe_{1-x}O$

The crystal structure of wüstite, $Fe_{1-x}O$, is a defective variant of the rocksalt structure. The phase is stable to lowest temperature (576 °C) for the eutectoid composition $x = 0.055$, but at higher temperatures and pressures the composition range is extended. Below 576 °C the thermodynamically stable state is a mixture of metallic Fe and magnetite, Fe_3O_4. Quenched samples of wüstite can be studied under ambient conditions. A number of different subphases have been reported and these are designated by P′, P″, and P‴ (see Manenc[92]). Fe^{2+}, Fe^{3+}, and vacancies do not form a simple solid solution on the rocksalt cation sublattice. Average structure determinations reveal the presence of some Fe on interstitial tetrahedral sites.

Diffraction patterns of P′ wüstite show satellite peaks at reciprocal points $h \pm n_1\delta$, $k \pm n_2\delta$, and $l \pm n_3\delta$ where n_1, n_2, and n_3 are integers (0,1,2) and $\delta = 1/(R \times a_0)$ where a_0 is the cell parameter and $R \approx 2.5$. R varies with x and is generally incommensurate with the rocksalt parent lattice. The peaks are sharp for higher values of x but tend to be more diffuse for small x. It is generally accepted in the literature that the structure consists of a primitive array of defects arranged on a cell $\sim Ra_0 \times Ra_0 \times Ra_0$. Much discussion has centered on trying to establish the exact arrangement of ions in the detect and the relaxation of the surrounding rocksalt lattice. The simplest defect considered is one involving a single tetrahedron of four vacancies containing one interstitial cation (a 4:1 cluster), but various other larger defect clusters obtained by combining the simple tetrahedral cluster in corner- or edge-sharing arrangements have been postulated (see, for example, the review by Hazen and Jeanloz[93]).

The satellite peak intensities have been used to obtain structural information on a quenched wüstite with composition $x = 0.082$ by Koch and Cohen[94] by assuming a commensurate supercell, and by Yamamoto[95] by treating the satellite peaks as due to a truly incommensurate modulation. Koch and Cohen reported that the model that best fitted their observations was one in which the defect clusters consisted of 13 vacancies and four tetrahedral interstitial ions (13:4 cluster). Cations around this cluster tended to move in toward the cluster while anions tended to move away. Yamamoto's analysis of the same data showed that the problem could be treated as a three-dimensionally modulated structure but gave very similar results for the local arrangement of the ions. In a recent powder neutron diffraction study Radler et al.[96] reported that for wüstites that are relatively oxidized ($x = 0.08-0.10$), a range of defect clusters (7:2), (10:3), as well as the Koch and Cohen (13:4) cluster appear to be present.

An early study of diffuse scattering in wüstite was carried out by Hayakawa et al.[97] for various compositions at 1113 K. This study, in agreement with the previous analyses of the peak intensities of the quenched samples, found a local contraction of the lattice around the defects. A full diffuse scattering analysis has more recently been carried out on a wüstite of composition $x = 0.07$ at 1173 K by Garstein et al.[98] and subsequently discussed in a number of papers.[99,100] The diffraction data that were obtained were separated into scattering due to ionic displacements and that due to the defect arrangement. The resulting local order parameters that were extracted indicated vacancy-clustering similar to that reported for the P′ quenched phase. However, the order that existed between the clusters was similar to that for P″ and quite different from that of the P′ subphase.

Recently, Welberry and Christy[101] have recorded diffuse scattering data from a quenched wüstite of composition close to the eutectoid ($x = 0.057$). This had typical P′ arrangement of satellite peaks but these were diffuse, anisotropically elongated, and were interconnected by weaker continuous streaks (Figure 6). In addition there were broader regions of scattering extending over larger regions of reciprocal space. This study showed how the basic features of the scattering could be understood in terms of a paracrystal-like distribution of vacancy clusters, together with local relaxation around the clusters. The study did not attempt to address the question of which types of cluster were present—the simplest (4:1) cluster was assumed, pending more detailed investigations.

4.3. Mullite, $Al_2(Al_{2+2x}Si_{2-2x})O_{10-x}$

Because of the fundamental importance of mullite to ceramic science and the recent interest in incommensurate phases generally, numerous workers have attempted to understand the structure and stability range of mullite.[102-112] Like the CSZ's described above, mullite is an anion-deficient material. The inherent disorder again involves short-range ordering

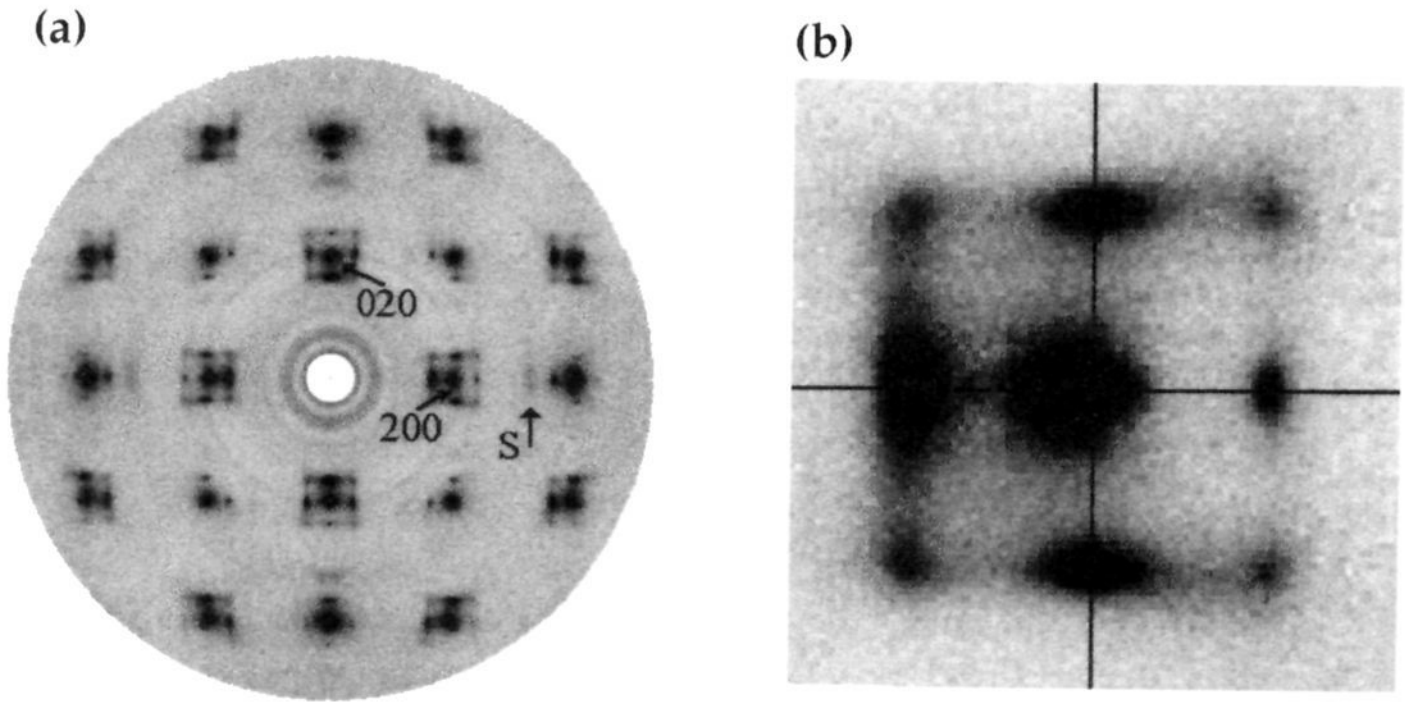

Figure 6. (a) Observed diffraction pattern of the ($hk0$) section of wüstite recorded using Mo Kα. "S" indicates a second-order satellite peak. (b) Magnified view of the region around the (200) reflection, showing the paracrystal-like streaking and the relaxation-induced asymmetry (After Welberry and Christy, ref 101).

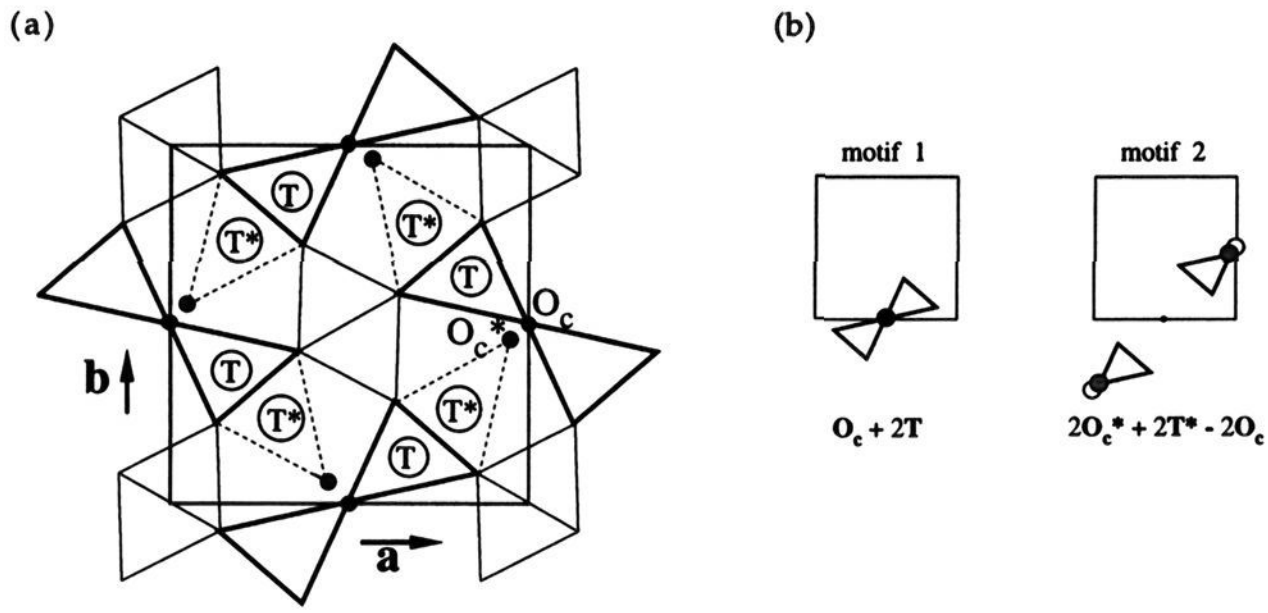

Figure 7. The average structure of mullite (a) and the two chemical motifs used in the analysis (b).

of the oxygen vacancies and associated cation shifts. Diffraction patterns of mullite (see Figure 8) show incommensurate diffraction maxima in the $^1/_2\mathbf{c}^*$ section, but, in addition to these incommensurate peaks, there is strong diffuse scattering over the whole 3D volume of reciprocal space.

Details of the average structure of mullite of composition $Al_2(Al_{2+2x}Si_{2-2x})O_{10-x}$ where $x = 0.4$, as revealed by the Bragg scattering, are shown in Figure 7a. The structure is similar to that of sillimanite, $Al(AlSi)O_5$. Chains of edge-sharing AlO_6 octahedra, running parallel to the crystallographic **c** axis, are cross-linked by (Al,Si) tetrahedra. In sillimanite the tetrahedrally coordinated cations are bridged by a single oxygen atom and are ordered in such a way that the bridging anion always connects a Si-containing tetrahedron with an Al-containing tetrahedron. In mullite some fraction x of these bridging oxygen sites are vacant. To preserve charge balance, each of the O^{2-} vacancies are accommodated by the exchange of $2Al^{3+}$ for $2Si^{4+}$. Because the tetrahedrally coordinated Al and Si are no longer present in the ratio of 1:1 these sites necessarily become chemically disordered. Furthermore, crystal structure analysis has identified the presence of a second tetrahedral site—displaced from the original by approximately 1.3 Å—that is presumably occupied by cations which have lost bridging oxygen atoms. The bridging oxygen atom was also found to occasionally occupy a site displaced 0.5 Å from its normal position and appears to be associated with the displaced tetrahedral site. In Figure 7a the (Al,Si) tetrahedral sites are labeled **T** and **T*** and the bridging anion sites are labeled $\mathbf{O_c}$ and $\mathbf{O_c}^*$ where the asterisk indicates the displaced positions mentioned above.

Following the average structure determination, McConnell and Heine[107] used a symmetry argument to characterize the form of the incommensurate modulation in terms of two ordering patterns. Subsequently the presence of these two ordering schemes was confirmed by an X-ray study of the satellite intensities.[109] These two ordering patterns represent component structures, which are, however, still averages taken over a (100) plane.

The presence of more general diffuse scattering was evident at an early stage,[102] but progress in understanding the origins of the scattering was slow until full 3D data of much higher quality became available.[110] These data were analyzed by Welberry and co-workers, first using Monte Carlo simulation and optical transform methods to compare a model with the observed patterns,[110,111] but subsequently by

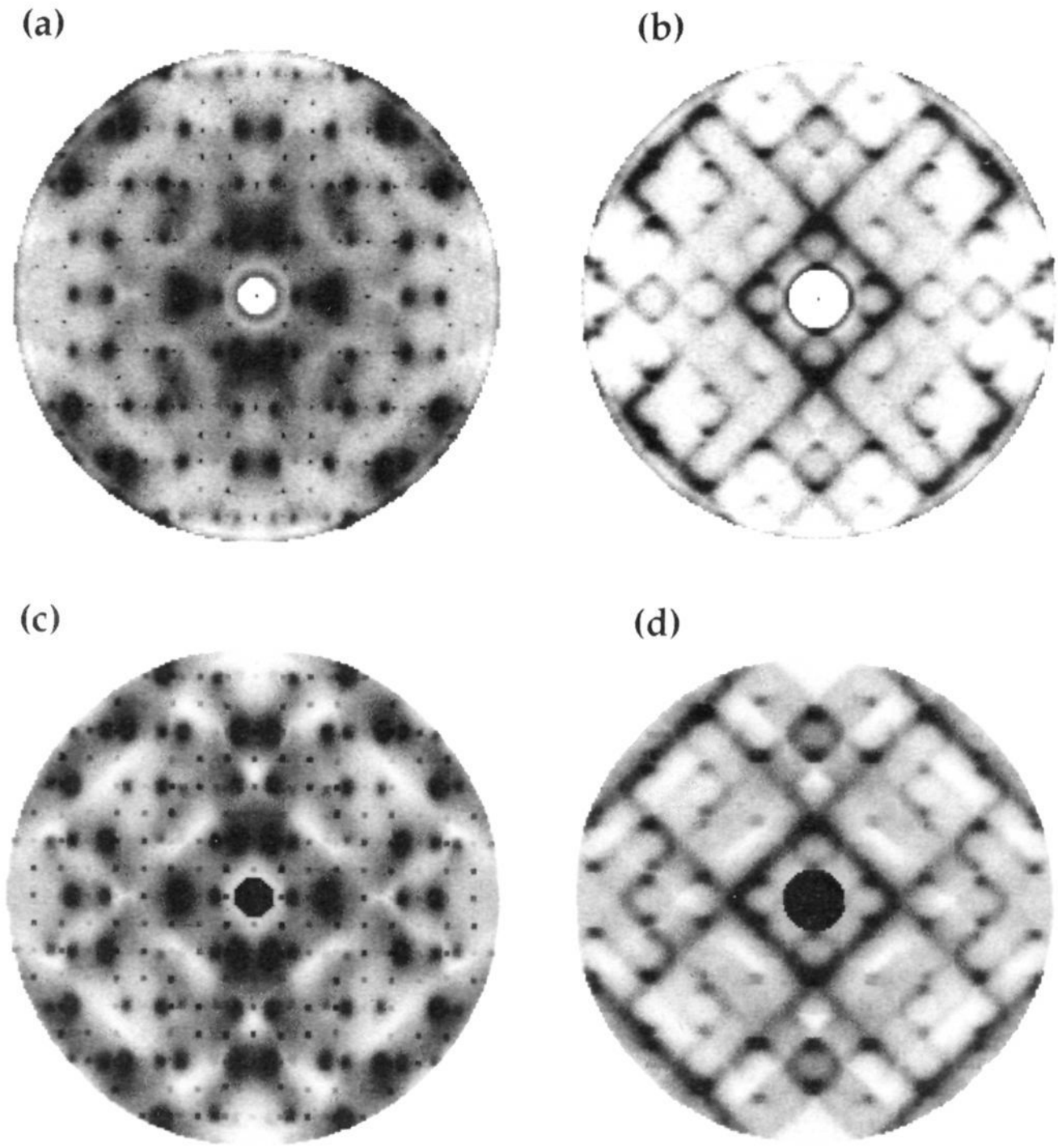

Figure 8. Example 2D sections of the 3D diffuse diffraction patterns of mullite: (a) Observed ($hk0$) section; (b) observed ($hk0.8$) section; (c), (d) calculated patterns corresponding to a and b, respectively.

directly fitting the general diffuse intensity expression obtained from the Taylor expansion to the observed intensity distribution.[112] We here give a brief summary of this later work.

With the large number of atom sites and atom types involved in the problem, it is not feasible to apply the alloy methods outlined in section 2 directly to the mullite problem. To make progress some assumptions must be made. Instead of assuming that an $\mathbf{O_c}$ oxygen site is vacant or occupied and then allowing surrounding cations to relax around these sites, it is assumed instead that there are two different chemical motifs which decorate the lattice. These are shown in Figure 7b. When a given $\mathbf{O_c}$ oxygen site is occupied, there is also associated with it two occupied **T** sites (motif 1). On the other hand if the given $\mathbf{O_c}$ oxygen site is vacant there is also associated with it two occupied **T*** sites and also the neighboring $\mathbf{O_c}$ oxygens shift to the $\mathbf{O_c}$* position (motif 2). *If these two motifs are used instead of individual atoms*, the atomic scattering factors in the diffraction equations can be replaced by *motif* scattering factors. Then, *only the SRO term I_0 need be used to explain the scattering* and the higher terms I_1, I_2, etc. can, to a good approximation, be neglected. That is, the two different motifs entirely account for the atomic displacements that result from the vacancies.

An analysis was carried out in which the SRO term defined in this way was fitted to the observed data in 3D, and short-range order parameters were determined. These α^{ij}_{lmn} now refer to the probability of finding defects of different kinds at the ends of a given vector.

To demonstrate the effectiveness of the analysis, diffraction patterns calculated from this fitted model, using only the I_0 term, are shown in Figure 8, parts c and d.

4.4. Anion-Excess Fluorite, $(Ca_{1-x}Y_x)F_{2+x}$

Halide compounds with the fluorite crystal structure, with general formula $M^{2+}X_2^-$, have a remarkable ability to accommodate large concentrations of R^{3+} dopant ions substitutionally on the M^{2+} cation sites. The addition of R^{3+} ions dramatically reduces the transition temperature T_c, above which ionic conductivity is observed, and technological interest in solid electrolytes has led to considerable research effort aimed at understanding this effect and elucidating the structural changes which accompany doping. The detailed topology of the defect clusters

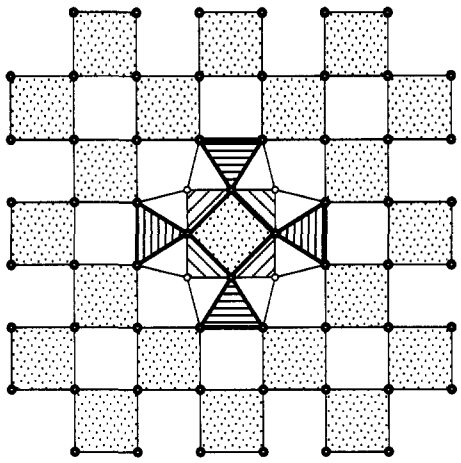

Figure 9. Schematic diagram showing how a cubeoctahedral cluster fits into the fluorite structure. Each of the faces of one of the original fluorite cubes of anions is rotated through 45° to make room for additional anions (light circles).

formed in anion-excess fluorites is still the subject of some controversy, however, even in the most widely studied system, $(Ca_{1-x}Y_x)F_{2+x}$.

Most diffraction work on these systems has involved single-crystal Bragg scattering or even powder diffraction, but recently Hull and Wilson[113] have measured and analyzed diffuse neutron diffraction data for $(Ca_{1-x}Y_x)F_{2+x}$, where $x = 0.06$. Although we are not primarily concerned with neutron scattering in this review, the method of analysis employed in this study is equally applicable to X-ray scattering. The method consists essentially of assuming the defects are isolated, and, hence, the total diffuse scattering is obtained by summing the scattering from each of the N_d defects incoherently. The structure factor for a single defect cluster is given as

$$F_D(\mathbf{Q}) = \sum_{k=1}^{n_c} P_k b_k \exp(i\mathbf{Q}\cdot\mathbf{R_k}) \exp(-W_k\mathbf{Q}) \quad (25)$$

and the total diffuse intensity as

$$I_{D,calc}(\mathbf{Q}) = C + (S_D/N_0)\sum_{i=1}^{N_0}|F_D(\mathbf{Q})|^2 \quad (26)$$

Here n_c is the number of defective ions (including vacancies) in a single defect cluster; P_k is -1 for a lattice site vacancy and $+1$ for an interstitial atom at the real-space vector $\mathbf{R_k}$; $\mathbf{Q}$ is the scattering vector; b_k is the neutron scattering length of the ion; N_0 is the number of possible orientations of the defect; S_D is a fitted scale factor; the term $\exp(-W_k\mathbf{Q})$ is the usual Debye–Waller temperature factor for atom k, and C is a fitted constant (independent of $\mathbf{Q}$) included to account for scattering due to instrumental background, multiple scattering, and incoherent scattering. Since the defect clusters often possess lower symmetry than the host fluorite lattice the summation in eq 26 averages over the N_0 possible orientations of the defect.

Testing various models for the cluster geometry showed that the model which gave the best fit to the observed scattering was a cubeoctahedral anion polyhedron formed by conversion of six edge-sharing $(Ca,Y)F_8$ fluorite cubes into corner sharing square antiprisms (see Figure 9).

4.5. Superconducting Oxides

Soon after their discovery the average crystal structures of the high Tc superconducting oxides were determined, but efforts to understand details about the nature of both the substitutional disorder and various displacive modulations observed in these materials has just begun. Most studies along these lines have employed transmission electron microscopy and powder diffraction methods because the large single crystals necessary to perform X-ray diffuse scattering studies are rare. The complex average structure of these materials also makes quantitative analysis of the diffuse scattering quite difficult even when experimental data are available. Nevertheless, a few studies demonstrate the range of diffuse scattering features are quite rich and can be used to extract useful qualitative as well as quantitative information about the structure of these technologically important compounds.

Moret et al.[114] measured the diffuse X-ray scattering from single crystals of $Tl_2Ba_2CaCu_2O_8$[Tl(2212)], $Tl_2Ba_2Ca_2Cu_3O_{10}$[Tl(2223)], and $TlBa_2Ca_2Cu_3O_9$[Tl(1223)] superconductors using a monochromated Mo Kα X-ray source in a transmission geometry that produces diffuse X-ray diffraction images (as projections of the Ewald sphere) on photographic film. Measurements of all three compounds were made with the X-ray beam approximately parallel to the crystallographic c-axis (the axis along which the Cu–O layers are stacked). All three compounds displayed an array of apparently incommensurate satellite spots. In the Tl(2212) and Tl(2223) samples the spots were observed at wave vectors of the form $q = (\pm z,0,\pm 1)$ and $q = (0,\pm z,\pm 1)$ where $z = 0.17$ (not known to an accuracy which could rule out a $^1/_6$ repeat). Related to these satellite reflections was an array of complex diffuse streaks along (110) that form arcs connecting the satellite reflections. No direct quantitative analysis or structural models reproducing these diffraction phenomena were presented but the authors suggest that the diffuse scattering and satellite reflections are related and likely result from short-range substitutional ordering of Ca on the Tl sublattice and associated static atomic displacements. The Tl(1223) sample also gave (much broader) satellite reflections and associated diffuse streaking but with different symmetry and repeat distances from the other two samples.

Jiang, Wochner, Moss, and Zschack[115] have measured the diffuse X-ray scattering from a single crystal of $YBa_2(Cu_{0.955}Al_{0.045})_3O_7$. These measurements were made using a synchrotron radiation source with an energy tuned just below the yttrium absorption edge to eliminate Y fluorescence. The diffuse scattering (normalized to absolute scattering units) was mapped around the (040), (240), and (220) fundamental reflections. Diffuse streaks were observed along the [110] directions which the authors attribute to $\langle 110\rangle$:$\langle 1\bar{1}0\rangle$ shear displacements. A calculation of the static–displacement diffuse scattering (assuming a random distribution of oxygen on the

Cu(1)−O planes) and the thermal diffuse scattering from their model are in quantitative agreement with the measured intensities. Cai, Zhu, and Welch[116] relaxed the constraint of random oxygen distributions by employing a lattice−gas model upon which an associated displacement field was applied and obtained better agreement with this data.

Recently, X-ray diffuse scattering measurements have also been made in $La_{2-x}Sr_xNiO_4$, and $La_{2-x}Sr_xCuO_4$ compounds[117] with the hope of better understanding the arrangement of charge carriers (introduced by the Sr doping) through the atomic displacements they induce. This study employed a synchrotron radiation source which was tuned to just below the Sr K-edge where fluorescence was minimized and the scattering contribution of the Sr could be altered by small changes in the incident X-ray energy. Strong diffuse scattering was observed which did not change as the wavelength was adjusted indicating the diffuse scattering does not originate from the Sr acceptors and is more likely associated with holes residing in the $(Ni/Cu)O_2$ layers.

4.6. Solid Electrolytes—β-Aluminas, α-AgI

Diffuse scattering has been used to study a number of other oxide or halide materials which are of interest because of their ionic conduction properties. In β- and β″-alumina diffuse scattering has been observed as a series of continuous diffuse rods normal to the planes containing the conduction ions.[118] The rods are continuous in intensity indicating the complete independence of each conduction plane. Measurement of the coherence length for the disorder from the width of the rods and its variation with temperature enabled the authors to deduce a model for both materials which accounts for their conductivities.[119] The relationship between the ionic conduction properties and the diffuse scattering has also been studied in α-AgI. Sakuma[120] has given an extensive theoretical treatment and applied this to the analysis of observed diffuse scattering from a powder sample. O'Sullivan et al.[121] have carried out a computer simulation study on α-AgI and compared their results to earlier X-ray measurements.[122] More recently Keen et al.[123] have recorded diffuse neutron scattering from an *in situ* grown single crystal of α-AgI at 770 K and used reverse Monte Carlo (RMC) simulation[124] to interpret their results.

4.7. Summary

The examples presented in this section demonstrate that quite different approaches may be needed to analyze the diffuse scattering data of seemingly quite similar materials. Whereas, for example, the average structure of CSZs are simple, the scattering is complex and an understanding of the diffraction patterns requires terms in the basic diffraction equation out to at least third order. Mullite, on the other hand, has a more complex average structure, but although the diffraction patterns appear equally complex they may be almost completely accounted for in terms of the first term in the diffraction equation if a suitable (very good) approximation is made. The analysis of the anion excess fluorite made a more drastic assumption that the defects were independent.

5. Low-Dimensional Conductors

Diffuse X-ray scattering has played and continues to play an important role in the development and understanding of low-dimensional conductors, insulators, and super-conductors. Early work in this area was reviewed by Comés.[125] Since most observations of the effects are carried out at very low temperatures (10−50 K), obtaining diffuse scattering data is difficult and the quality and extent of the X-ray pattern that can be obtained is severely limited. Practically all work has used the fixed-film/fixed-crystal method (Laue photograph) and monochromatic radiation. Because of the experimental difficulties, quantitative measurements of complete diffuse scattering distributions are not feasible. Nonetheless, much can be still learned from qualitative or semiquantitative studies. In addition, quantitative measurements of relative intensities as a function of temperature can provide valuable links with electronic measurements.

5.1. Peierls Instability

A characteristic feature of the diffraction patterns of 1D conductors is the presence of diffuse planes that occur, normal to the 1D conducting direction, at wave vectors $\mathbf{q} = \pm 2k_F$ from the layers of Bragg reflections. These planes can be directly attributed to a Peierls distortion[126] which occurs in a 1D metal. When observed in a fixed-film/fixed-crystal exposure, the diffuse planes appear as a set of diffuse lines, caused by the intersection of the diffuse planes with the Ewald sphere. These occur on either side of rows of Bragg reflections. Example diffraction patterns can be seen in Figure 12.

In simple terms, a 1D metal with an electron gas filling all conduction band orbitals out to a wave vector k_F at 0 K (i.e. to the Fermi surface) is unstable with respect to a static charge density wave (CDW) and accompanying periodic lattice distortion (PLD) of wavevector $\mathbf{q} = 2k_F$ (a wave vector that clearly couples occupied electronic states near one section of the Fermi surface with unoccupied states near another section). The periodic lattice distortion creates an energy gap at the Fermi surface (see Figure 10), thereby lowering the energy of the electrons below the energy gap.[127,128] The distortion proceeds until limited by the increase of elastic energy. The CDW/PLD are stable below a temperature T_P, the Peierls transition temperature, but even above T_P, pretransitional fluctuations can be observed. A detailed study of the diffuse scattering can give

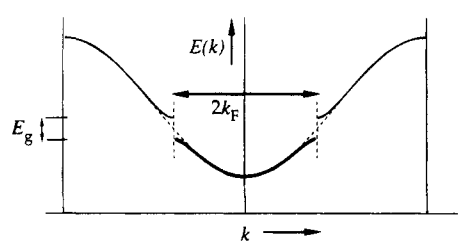

Figure 10. The simple 1D case of electronic stabilization in a "Peierls" distortion.

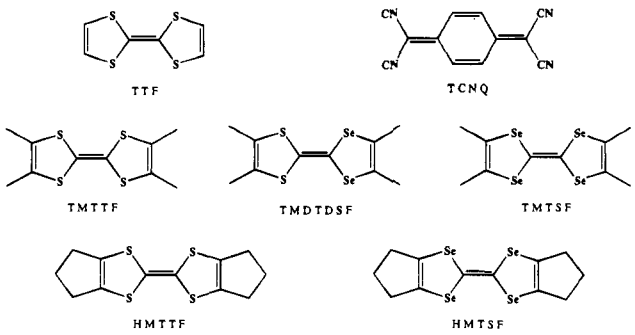

Figure 11. Some organic molecules used in charge-transfer salts that are referred to in the text.

information on the in-chain correlation length of the lattice fluctuations and on the susceptibility of the coupled electron–phonon system. Since both variations in charge density and in the atomic positions are involved, understanding the details of the diffuse scattering requires knowledge of the hierarchy of terms that occur in the diffraction equations given in section 2.

5.2. Charge-Transfer Salts

The first experimental evidence for a Peierls instability in a real system was obtained for the 1D conductor $K_2Pt(CN)_4Br_{0.3-x}H_2O$ (KCP).[129,130] With its single chains of Pt atoms, this system has remained the closest case to the early theories of the effect, but since then, the search for higher conductivities has driven the interest toward organic charge-transfer salts of which TTF–TCNQ is the prototype material.[131] A whole range of systems related to TTF–TCNQ has been studied including materials in which one or other of the acceptor (TCNQ) or donor (TTF) molecules has been replaced. Molecular drawings of some of these molecules are shown in Figure 11 for reference.

The organic charge-transfer salts have progressively complicated the original picture of the Peierls distortion of a single metallic chain. These salts are composed of segregated one-dimensional (1D) chains of donor molecules (i.e., TTF, HMTTF, HMTSF) and acceptor molecules (e.g. TCNQ) on which electrons are delocalized. Whereas KCP shows continuous diffuse planes of scattering, in the organic systems these planes are interrupted because of variations due to the molecular form factor. The extension of the molecules perpendicular to the stacking direction and, more importantly, the fact that they are often tilted away from the plane perpendicular to the stacking direction, allows transverse as well as the simple longitudinal distortions of a chain to modify the overlap of electronic orbitals and so contribute to the Peierls distortion. When these different distortions are in competition, phase transitions can occur. Another important difference is that these materials often contain two different types of metallic stack which may exhibit a Peierls transition at the same or a different temperature, further complicating the phase diagram.[125]

5.3. Pinning of Charge Density Waves

In addition to the diffuse scattering features that derive from the basic 1D instability some systems of interest display substitutional or orientational disorder of the constituent molecular species. The pinning of charge-density waves (CDW) to defects was shown to be essential for the understanding of the electronic properties of quasi-one-dimensional conducting materials,[132–134] even for low concentrations of defects such as those induced by irradiation. Consequently there has been interest in investigating the role of structural disorder in low-dimensional systems.[135,136]

Liu et al.[137] have performed extensive studies of the orientational ordering of the TMDTDSF molecule in a series of organic conductors $(TMDTDSF)_2X$ where X is a monovalent anion (PF_6, AsF_6, ReO_4, BF_4, and ClO_4). The crystals of these materials have the same average structures as their analogs $(TMTSF)_2X$ and $(TMTTF)_2X$ indicating that the asymmetric TMDTDSF molecules are disordered. In addition to the diffuse planes which arise from the Peierls distortion, the diffraction patterns contain broad regions of diffuse scattering corresponding to the Laue monotonic scattering resulting from the two different molecular orientations. These broad bands are modulated in a number of different ways and the authors have investigated this by calculating the expected diffuse intensity in the (curved) section of reciprocal space corresponding to the observed patterns, for a number of models of the local order. These models took into account the possibility of short-range order (SRO) in the orientation of the molecules both along the chains and transverse to them, static displacements of the molecules due to their environment (size-effect displacements), and the contribution of thermal diffuse scattering (TDS). In all the crystals investigated the authors found that there was no significant SRO (of molecular orientation) along the 1D chain direction but there was significant intrachain size effect. This could be attributed to the difference in size of the Se and S atoms which were in close contact along the chains. Size-effect displacements were estimated to be ~0.1 Å for first neighbors and ~0.03 Å for second neighbors. A further study of these and related systems[138] included investigations of mixed crystals $[(TMTSF)_{1-x}(TMTTF)_x]_2ClO_4$ and $(TMTSF)_2[(ReO_4)_{1-x}(ClO_4)_{1-x}]$.

The most dramatic demonstration of the pinning of the basic Peierls modulations by defects is given in a study of the effects of disorder in the solid solutions $(TTF)_x(TSF)_{1-x}TCNQ$ and $(HMTTF)_x(HMTSF)_{1-x}TCNQ$, where selenium- and sulfur-based donor molecules are alloyed.[139,140] In Figure 12 we show the X-ray patterns (taken from ref 131) of the pure HMTSF-TCNQ system and of the solid solution $(HMTTF)_{0.05}(HMTSF)_{0.95}TCNQ$. For the pure material, (a) the $\pm 2k_F$ diffuse lines are visible and there are no broad regions of scattering due to substitutional disorder. For the mixed crystal, (b) broad regions of diffuse scattering due to the substitutional disorder overlay the regions where the diffuse lines should be. On close inspection, however, the diffuse lines are visible but there is a marked asymmetry between the $+2k_F$ and $-2k_F$ lines. Now, at $+2k_F$ the lines have an intensity minimum visible at the expense of the diffuse background (white arrows) and at $-2k_F$ an intensity maximum (black arrows).

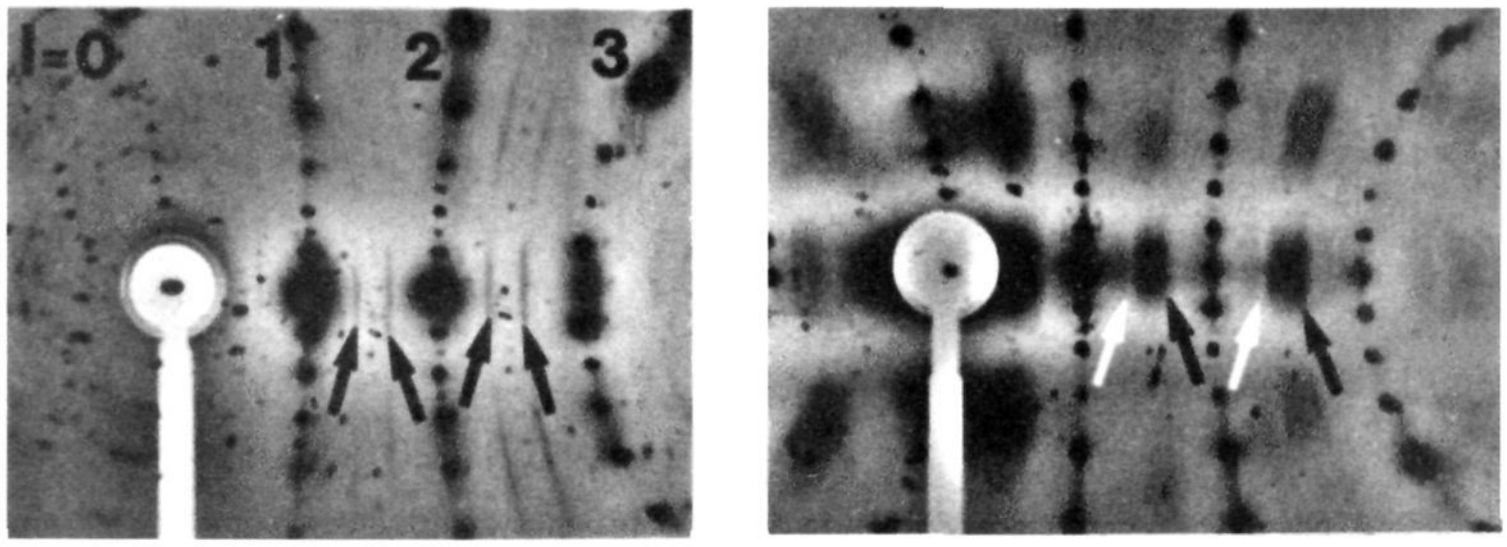

(a) (b)

Figure 12. (a) X-ray pattern from HMTSF-TCNQ at 25K showing $2k_F$ diffuse lines (black arrows). (b) X-ray pattern from the solid solution $(HMTTF)_{0.05}(HMTSF)_{0.95}TCNQ$ at 20 K showing the white diffuse lines at $+2k_F$ (white arrows) and the black diffuse lines at $-2k_F$ (black arrows) for $l > 0$. Both X-ray patterns have been taken with about the same crystal orientation, with the **c**-axis horizontal and the **b**-axis vertical. The wavelength used was $\lambda_{Cu\ K\alpha} = 1.542$ Å. (Reproduced from ref 140 with kind permission of Professor J.P. Pouget. Copyright 1994 Elsevier.)

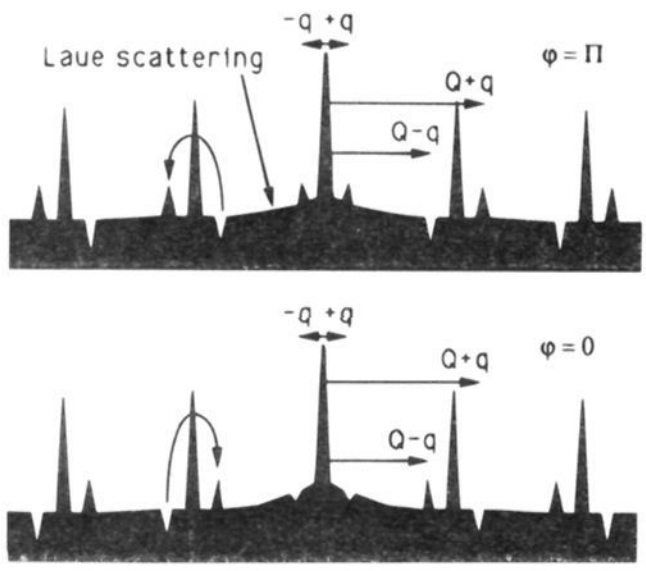

Figure 13. Schematic representation of the intensity scattered by a chain in which an impurity pins a lattice distortion of wave vector **q**. In the case where $f_A > f_B$ two extreme situations corresponding to the relative phases $\phi = \pi$ and $\phi = 0$ are shown on top and bottom, respectively. (Reproduced from ref 140 with kind permission of Professor J.P. Pouget. Copyright 1992 Editions de Physique.)

The explanation for this effect is that the white $+2k_F$ lines originate from a subtraction of a diffuse intensity term, due to lattice fluctuations, from the so-called Laue "monotonic" scattering due to the HMTTF/HMTSF disorder, while the dark $-2k_F$ lines originate from an addition. Such negative and positive interferences, which are shown schematically in Figure 13, were found to result from phase coherence between the position of the impurities and the lattice distortions.

To obtain this result the authors studied a model system consisting of a 1D chain of two species of scatterer, A and B (atoms or molecules), of concentration x_A and x_B. It is assumed that the A species are the impurities and that around each impurity, located at position $k\mathbf{a}$, a displacement wave is pinned. This wave is characterized by its wave vector **q** and its correlation length ξ. The displacement of the nth atom due to the kth impurity is written

$$\mathbf{u}_n^k = \sum_{\mathbf{q}'} \mathbf{u}_{\mathbf{q}'} \sin\{2\pi\mathbf{q}'(n-k)\mathbf{a} + \phi\} \qquad (27)$$

where $\mathbf{q}'$ belongs to the first Brillouin zone and $\mathbf{u}_{\mathbf{q}'}$ is a function of $\mathbf{q}'$ centered around **q**. For this system the authors found after much algebra that the diffuse scattering is given by

$$Y_{\mathrm{Diff}}(\mathbf{s}) = Y_{\mathrm{SRO}}(\mathbf{s}) + Y_{\mathrm{WL}}(\mathbf{s}) \qquad (28)$$

where

$$Y_{\mathrm{SRO}}(\mathbf{s}) = x_A x_B (F_A - F_B)^2 \sum_m \alpha(m) \exp(2\pi i \mathbf{s}\cdot m\mathbf{a})$$

and

$$Y_{\mathrm{WL}}(\mathbf{Q} + \mathbf{q}') = -2x_A x_B F_B (F_A - F_B)\pi \cos(\phi \mathbf{s}\cdot\mathbf{u}_{\mathbf{q}'}) \sum_k \alpha(k) \exp(2\pi i \mathbf{q}'\cdot k\mathbf{a})$$

$$Y_{\mathrm{WL}}(\mathbf{Q} - \mathbf{q}') = +2x_A x_B F_B (F_A - F_B)\pi \cos(\phi \mathbf{s}\cdot\mathbf{u}_{\mathbf{q}'}) \sum_k \alpha(k) \exp(2\pi i \mathbf{q}'\cdot k\mathbf{a})$$

Here Y_{WL} is the contribution to the intensity causing the "white-line" effect. If the quantity $F_B(F_A - F_B)\pi \cos(\phi\mathbf{s}\cdot\mathbf{u}_{\mathbf{q}'})$ is positive (negative) the white lines will appear for wave vectors larger (smaller) than those of the Bragg reflections.

Another large class of organic conductors has been synthesized by the oxidation of organic donors by various halogens. When iodine is used as an oxidizing agent, it generally leads to compounds containing the triiodide anion I_3^-. In some of these systems the triiodide anions occur as disordered chains contained in an organic matrix which is basically crystalline.[141] In this respect these materials have much in common with urea inclusion compounds and are discussed in the next section.

5.4. Two-Dimensional Conductors

In two dimensions, effects analogous to the simple 1D Peierls instability can occur, but detailed band-structure calculations are needed to determine the specific low-energy phonon modes that are involved.[142,143] Unlike many of the 1D conductors

which usually form needle-shaped crystals, many 2D conductors, such as TaS_2,[144] have a 2D layer structure with very easy (mica-like) cleavages, making them difficult to obtain in a form suitable for diffuse X-ray scattering studies. Much of the diffraction work on these 2D materials has therefore been in electron diffraction,[145-147] for which the plate-like habit is more suited.

Recent diffuse X-ray scattering work on a series of monophosphate tungsten bronzes, $(PO_2)_4(WO_3)_{2m}$ exhibited two-dimensional electronic properties.[148] Because of their structural anisotropy, the transition metal oxides and bronzes form an important class of low dimensional conductors. The blue bronze $K_{0.3}MoO_3$ is a quasi-one-dimensional conductor, and CDW instabilities have also been reported in the Mo oxides and bronzes such as γ- and η-Mo_4O_{11}, KMo_6O_{17}.[149] However, although these materials are 2D conductors, the CDW instability is basically due to the nesting of flat 1D portions of their Fermi surface built on infinite chains of MoO_6 or WO_6 octahedra.[150-152]

6. Inclusion Compounds (Guest–Host Systems)

6.1. Urea Inclusion Compounds

Unlike the case of zeolite or clathrate inclusion structures in which weakly bound guests can reside in a practically unaltered host, the urea inclusion compounds involve remarkable interaction forces between host and guest that stabilize the urea framework in a structure much different from that of pure urea. Although urea inclusion compounds have been known for a long time,[153] there is still considerable interest in attempting to relate the details of their complex diffraction patterns to basic intermolecular interactions.[154,155] The compounds consist of a hexagonal (in the high-symmetry phase) hydrogen-bonded framework of urea molecules, with open channels along a unique **c**-axis, exhibiting a honeycomb-like cross section. Within these channels, chains consisting of long chain molecules are embedded (see Figure 14). Inclusion of *n*-alkane molecules

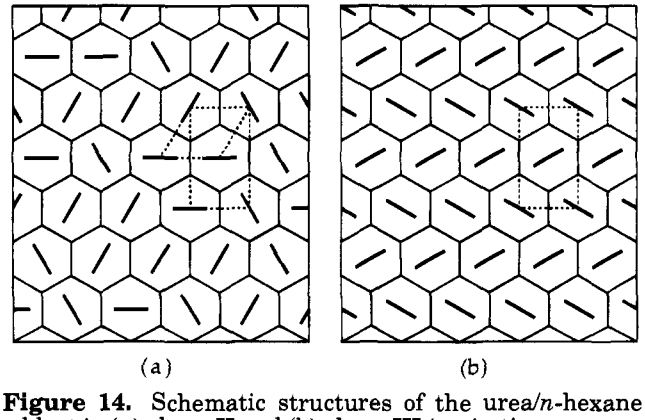

Figure 14. Schematic structures of the urea/*n*-hexane adduct in (a) phase II and (b) phase III (projections on $x-y$-plane) showing statistical and ordered arrangement of included paraffins (characterized by the plane of the C–C–C skeleton). Hexagonal and orthorhombic unit cells are indicated by dotted lines. (Reproduced from ref 156 with kind permission of Professor F. Frey. Copyright 1986 Elsevier.)

C_nH_{2n+2} provides perhaps the simplest examples,[6,156-158] but molecules with various side groups attached have also been studied,[158,159] and similar thiourea compounds are known,[160] although the thiourea channels are not always hexagonal.[161]

As well as the interactions between guest and host, which stabilize the framework, there are direct interactions between the chain molecules in both the longitudinal (parallel to **c**) and lateral (perpendicular to **c**) directions. These competing temperature-dependent interactions result in the occurrence of different phases and a variety of disorder phenomena which manifest themselves by more or less complicated diffraction patterns.[156,157]

To demonstrate the sorts of issue involved in this field we discuss briefly the hexadecane/urea system reported by Forst et al.[156,157] An example diffraction pattern is shown in Figure 15.

Several types of diffuse scattering are evident:

(1) Between the rows of Bragg peaks there are thin diffuse layers which have a spacing which is incommensurate with the spacing of the Bragg peaks. In the example shown (hexadecane) the first of these layers occurs at a position only slightly less than 0.5**c***, so that the incommensuration is only apparent at higher order levels. These incommensurate layers can be attributed to the chains of guest molecules which form a 1D chain within the urea channel with a repeat distance different from the urea repeat. The width (along **c***) of these layers is comparable to the width of the Bragg peaks, indicating that there is long-range order of the chains along **c***. Weissenberg photographs of the diffuse layers reveal that there is some fairly broad modulation of intensity within the layers, with maxima occurring at integral values of h and k. This indicates that the chains in neighboring channels are only very weakly correlated.

(2) A second type of diffuse layer of scattering (very broad), the first order of which can be seen near the top of Figure 15, corresponds to a real-space distance of 2.56 Å and can be attributed to the identity period of the nearly periodic alkane molecule.

(3) There is scattering within each Bragg layer, particularly around the Bragg peaks. On a Weissenberg photograph of a single layer, this scattering is seen to extend as a series of streaks linking the Bragg peaks.

(4) There is an overall continuous background scattering distributed nearly continuously in reciprocal space (monotonic Laue scattering), the origin of which is due to fluctuations in atomic position.

By studying these various features as a function of temperature (phase transitions are observed at ~365 K, ~148 K, and ~120 K) in addition to obtaining details of the average structures of the different phases, Forst et al. were able to obtain insights into the molecular behavior in each phase. They conclude that phase I (above 365 K) is hexagonal with a (longitudinal and orientational) random distribution of the included molecules. Phase II contains partial longitudinal ordering of the molecules. The transition from phase II to phase III involves the lateral orientational ordering of guest molecules in adjacent channels and a simultaneous orthorhombic deforma-

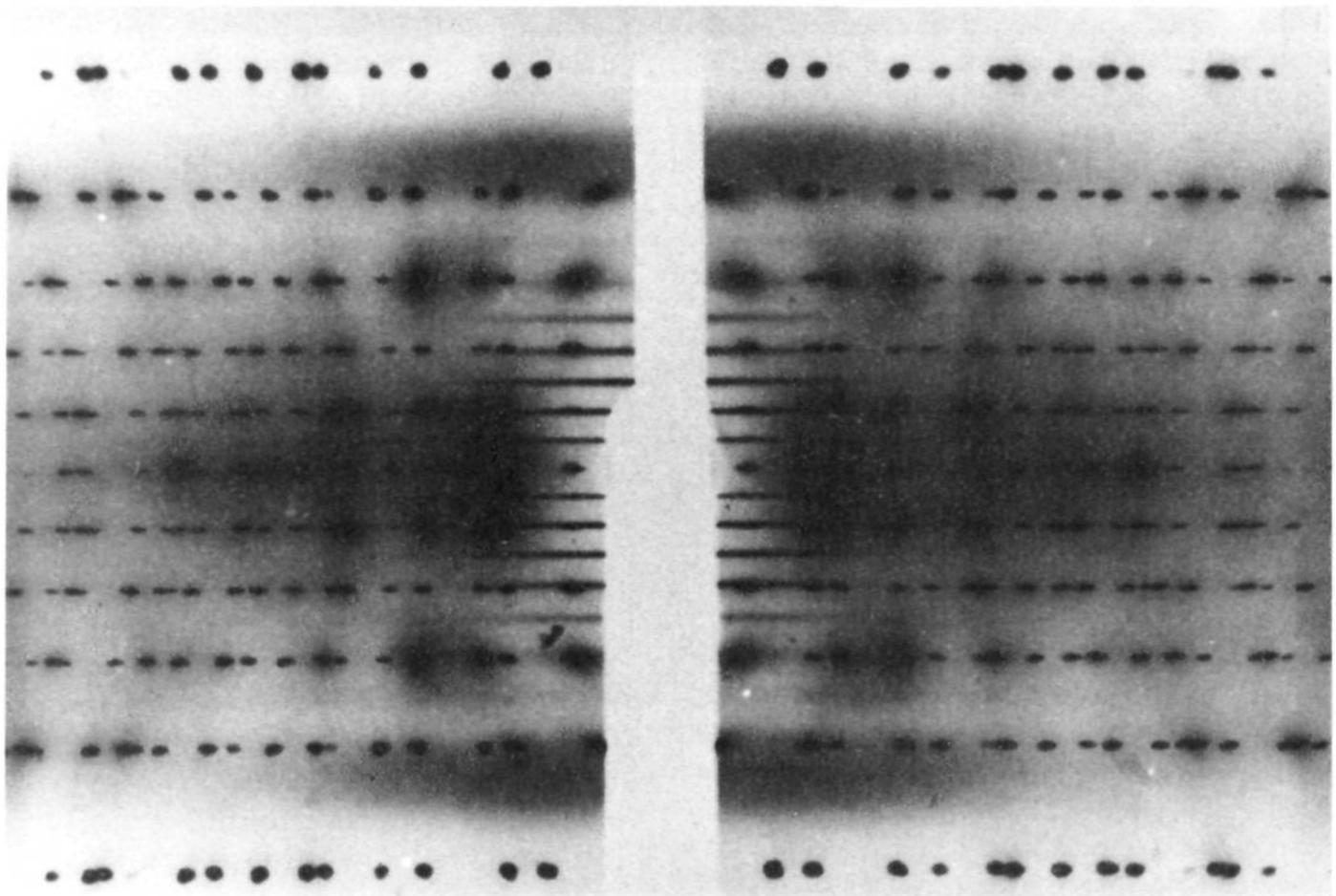

Figure 15. Oscillation photograph around the **c**-axis (±30°) of the hexadecane adduct; normal-beam technique; Cu Kα radiation; 5 h exposure time; ambient temperature. (Reproduced from ref 157 with kind permission of Professor F. Frey. Copyright 1987 Munksgaard.)

tion of the host. In phase IV a crystal-like ordering tendency of the paraffins plays the dominant role, while the host breaks into a heavily disordered domain structure. This study provides a good example of how careful observation of qualitative features of a diffraction pattern can provide a great deal of useful information about a system.

6.2. Triiodide Chain Compounds

There has been interest in a class of 1D conductors in which an organic matrix separates parallel channels filled with triiodide anions, I_3^-. Several of these compounds have been found to contain disordered chains of the triiodide anions contained in an otherwise crystalline organic matrix. In this respect there are strong similarities to the urea inclusion compounds. As for the guest alkanes in the urea compounds, the polyiodide chains here can be treated as essentially independent at ambient temperatures, but become increasingly interdependent at lower temperatures, leading to phase transitions. Studies of the complex diffraction patterns of these compounds, an example of which is shown in Figure 16, have been made by a number of workers over a long period of time.[6,141,162−164]

Although in many ways the diffraction patterns of these materials are similar to those of the urea inclusion compounds, there is one substantial difference. The diffuse planes of scattering, which can be attributed to the disordered polyiodide chains, become broader with increasing order of diffraction, indicating that there is no long-range order of the triiodide anions.

Attempts to understand the intensity distribution of the diffuse planes have used rather more quantitative approaches than has generally been the case for the urea compounds. Albouy et al. in work on the *compound tetraphenyldithiapyranylidene iodide* [DIPS$(C_6H_5)_4(I_3)_{0.76}$],[141] assumed that the distribution of triiodide anions along the **c**-direction followed that of a 1D harmonic liquid. They obtained expression for the intensity scattered by a chain in terms of only two parameters, the distance δ between two adjacent iodine atoms in an I_3^- unit, and the mean-squared fluctuation σ^2 of the distance between first neighbors

$$\mathbf{I}(\mathbf{q}) = |f_I(\mathbf{q})|^2[1 + 2\cos(q_z\delta)]^2\frac{\sinh(q_z^2\sigma^2/2)}{\cosh(q_z^2\sigma^2/2) - \cos(q_z\delta)} \quad (29)$$

Here, $f_I(q)$ is the atomic scattering factor for iodine and $1 + 2\cos(q_z\delta)$ is the geometric structure factor for the I_3^- unit. A good fit to the observed intensity distribution was obtained for value of $\sigma = 0.35$ Å and $\delta = 3.0$ Å.

In discussing 5,10-diethylphenazinium iodide [E_2-$PI_{1.6}$] Rosshirt et al.,[163] used an approach based on the Hosemann paracrystal method.[165−167] Here a distribution function $h_1(z)$ is assumed for the first neighbors of an arbitrary reference unit, and then the function describing the mth neighbor is obtained from this by an m-fold convolution. Three different models which differed in the form taken by $h_1(z)$ were tested. Of these, one, in which $h_1(z)$ was a Gaussian, was formally identical to the harmonic liquid distribution described in the previous paragraph but the other two models involved an asymmetric form for $h_1(z)$. The strongly asymmetric function used for the second model described a kind of "hard-sphere" model with a shortest distance of approach c_0 and had a characteristic width σ_1. The third model allowed some internal flexibility of the I_3^- unit and produced a first neighbor distribution with an intermediate

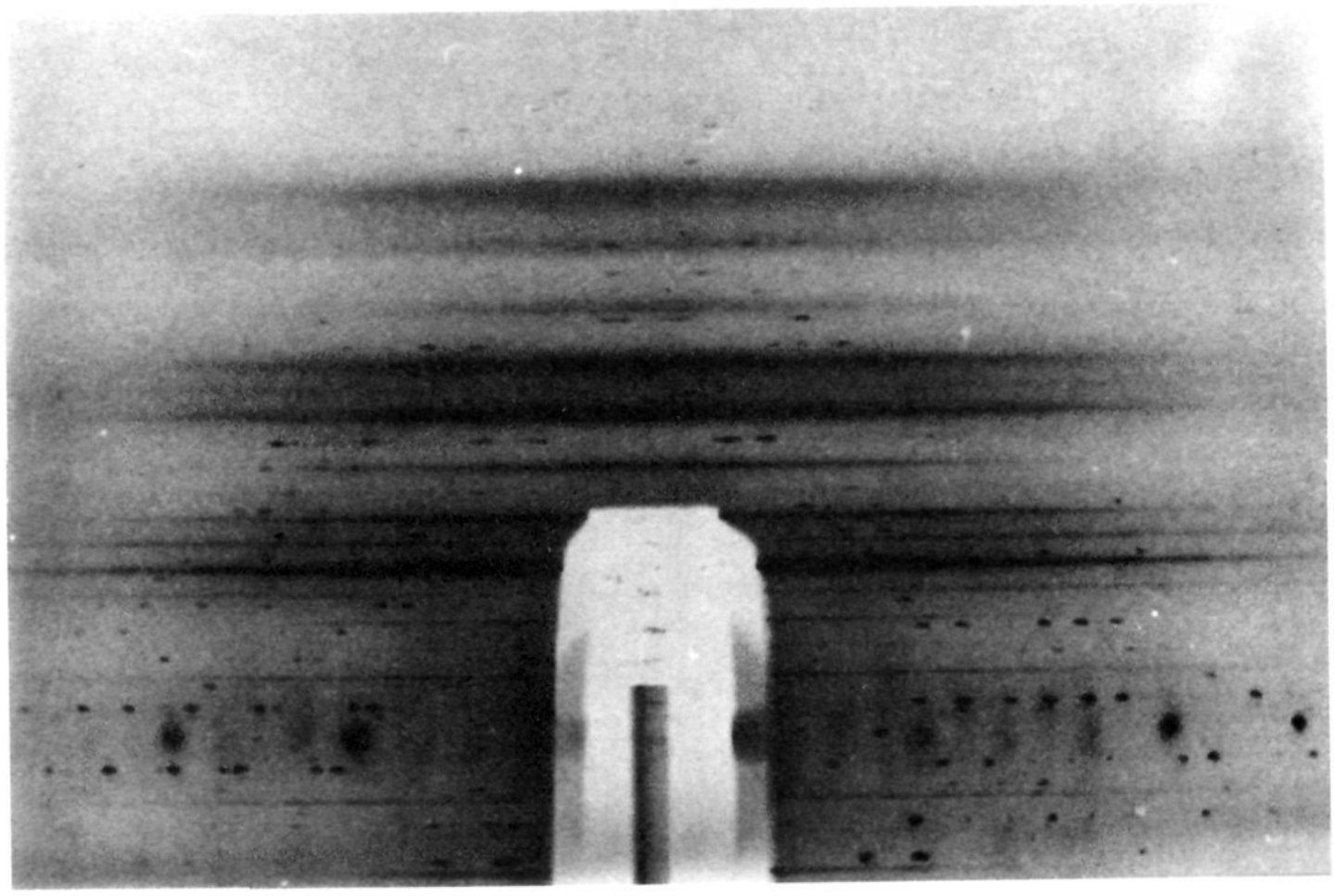

Figure 16. A stationary crystal stationary film monochromatic radiation diffraction pattern of the triiodide compound $E_2PI_{1.6}$ (5,10-diethylphenazinium iodide). (Reproduced with kind permission of Professor F. Frey.)

degree of asymmetry. Of the three models the authors found that this last fitted the observed distribution best, and they plotted the mean separation of the I_3^- units together with its mean square deviation, as a function of temperature.

In later studies on this system Frey[6] describes attempts to improve on the original analysis by including a more realistic I_3 molecular structure and including lateral dependence perpendicular to **c***. Analytical expressions as well as expansions in powers of Fourier–Bessel functions were used, but none of the models tested was able simultaneously to quantitatively fit the intensity distribution in all diffuse layers. It was concluded that it was necessary to allow all internal degrees of freedom of the iodine molecules to be treated as free parameters, and an analysis using such a model was attempted from pure diffuse data recorded at low temperatures (25–30 K) when the fluidlike character along **c** is lost. In all of this work Frey stresses the difficulty but also the importance of obtaining good-quality intensity data which have been corrected for background scattering and geometrical factors.

6.3. Hollandite

Another family of compounds that has attracted attention as an example of guest–host systems and because of its ionic conductivity properties is hollandite. A large number of hollandites both natural and synthetic are known and have the general formula $A_x^{u+}B_{8-y}^{v+}B'_y{}^{w+}O_{16}$, where $u = 1$ or 2, $v = 4$, and $w =$ 1, 2, or 3. Hollandites are constituted by a framework of $(B/B')O_6$ octahedra providing tunnels of square cross section running along c (see Figure 17). The tunnels can be viewed as a string of cavities large enough to accommodate the A cations. Diffraction patterns of hollandite-type structures generally display superstructure reflections or diffuse scattering,

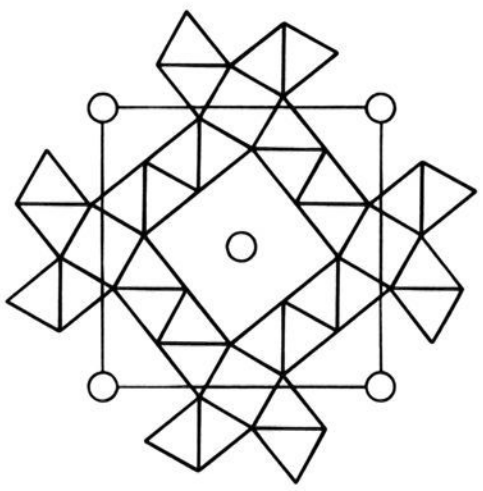

Figure 17. The hollandite structure viewed down **c** showing the network of $(B/B')O_6$ octahedra providing tunnels of square cross section which contain the cations (circles).

and it is well established that this is nearly always due to the arrangement of A cations in the host lattice.[168–169] Two extreme cases of superstructure can be distinguished: a 1D case in which the cations are ordered within tunnels but with no correlation between tunnels, and a 3D case in which there is both inter- and intratunnel ordering. Intermediate cases of the 3D ordering have been observed and can be characterized by a lateral correlation length. The 1D ordering may also be of a limited range and is characterized by an intratunnel correlation length. Another feature of the hollandite compounds is that the intratunnel order is often incommensurate with the period of the host lattice. The diffraction patterns of these incompletely ordered systems are characterized by the presence of diffuse layers of scattering perpendicular to **c***. These systems therefore have much in common with the urea inclusion compounds and the iodine chain compounds described above.

Terauchi et al.[170] discuss the case of the hollandite $K_{1.5}(Al_{1.5}Ti_{6.5})O_{16}$, in which the K^+ ions form a strongly

correlated commensurate structure along the tunnels but with relatively weak correlation between tunnels. The widths of the diffuse planes along the **c***-direction were found to correspond to a correlation length of ~100 Å while in the **a**−**b**-plane it was only ~40 Å.

The most comprehensive study of diffuse scattering in a hollandite has been reported in a number of papers by Rosshirt et al.[52,171−173] In this case the material studied had composition $K_{1.54}(Mg_{0.77}Ti_{7.23})O_{16}$ with the K^+ ions embedded in the tunnel cavities with an average occupancy of 0.77. This material had previously been studied by Beyeler[174] who reported the diffuse layer system perpendicular to **c*** indicating an incommensurate K ordering along the channels. Rosshirt et al. investigated both low (35 K) and high (875 K) temperature diffraction patterns as well as carrying out neutron diffraction and synchrotron radiation studies. Although qualitative explanations were given for most of the observed features of the diffraction pattern, a more quantitative analysis in terms of theoretical models was not given.

6.4. Graphite Intercalation Compounds

Graphite intercalation compounds may be considered to be a special case of guest−host systems and there is a considerable literature on them (see, e.g., ref 175). However, a relatively small number of studies on these systems has involved single-crystal X-ray diffraction, and most recent reports[175,176] reference the work of Rousseaux et al.,[177,178] who obtained diffuse X-ray diffraction photographs from RbC_{24} and KC_{24} single crystals as a function of temperature. At room temperature these showed modulated liquidlike rings of diffuse scattering around each graphite Bragg peak, while at lower temperatures the rings began to break up into discrete spots as the intercalated Rb or K tended to crystallize. More recently the same workers have reported more detailed studies using data recorded on a diffractometer.[179] Fan et al.[180] have performed molecular dynamics simulations to compare to the experimental patterns.

7. Diffuse Scattering from Molecular Crystals

Substitutional and/or orientational disorder occur frequently in organic molecular crystals, but when these effects are encountered they are all too frequently treated either solely as an average structure problem (with the use of increasingly sophisticated constraint/restraint algorithms to analyze the Bragg diffraction data) or ignored completely. Only relatively few attempts to utilize the diffuse scattering from these compounds have been made.

It is clear from the work described in earlier sections that applying the formalism used so successfully to analyze alloys becomes increasingly fraught with difficulties as disordered systems become more complex, so much so that for many systems only qualitative descriptions of effects seem possible. Many disordered organic molecular crystal systems represent a degree of complexity far greater than that of simple alloys. Not only are there many more atoms in the unit cell, but also each molecule often has independent interactions with a large number of surrounding molecules. Despite this, however, there is a large body of *a priori* chemical information available which is capable of defining the internal geometry of molecules using only a few parameters and, similarly, there are well-developed semiempirical theories of how molecules interact with each other, again only requiring relatively few defining parameters. When this is taken into account it is clear that quantitative descriptions of the diffuse scattering from molecular crystal systems should be feasible using only a small number of basic inter- and intramolecular interaction parameters.

Apart from the study of compounds which have interesting or useful properties directly linked to the disorder itself (e.g., the urea inclusion compounds or the charge-transfer complexes discussed in earlier sections), the study of disorder in molecular crystals generally can provide insights into problems which occur in disordered materials in other areas. The fact that organic synthesis can provide virtually limitless possibilities for varying molecular shapes, sizes, intramolecular degrees of freedom and even intermolecular interaction potentials allows tailor-made examples to be produced virtually at will. Added to this is the fact that, for many molecular solids, effects of interest are accessible at ambient (or close to ambient) temperatures and pressures, and crystals are generally easy to obtain and handle. With the recently increased interest in diffuse scattering from macromolecular crystals (see section 8) it is likely that a rigorous understanding of diffuse scattering from small molecule systems will provide a valuable adjunct to studies of macromolecules, in the same way that Bragg scattering studies of small molecules which mimic some aspect of macromolecular structure and function are currently considered valuable.

7.1. Substitutional Disorder in Anthracene and Benzene Derivatives

Extensive studies have been carried out on a number of aromatic systems in which disorder occurs because the disposition of methyl and halogen groups around the aromatic center allows the molecule to take up either one of two different orientations in a given molecular site[181−185] (see Figure 18). The possibility of disorder arises because of the similarity in size and shape of these constituent groups for

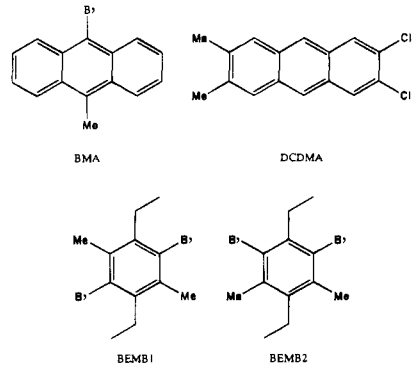

Figure 18. Some organic compounds that form disordered crystals in which the molecule can occupy a given site in the crystal in either one of two different orientations as a result of the similarity in size of the methyl and halogen substituents.

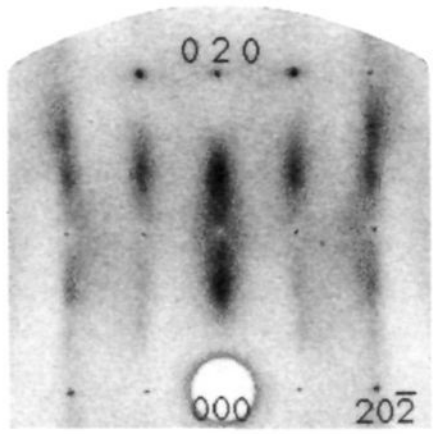

Figure 19. A portion of the ($hk\bar{h}$) section of the diffraction pattern of BEMB2 showing the "hole" in the diffuse scattering around the (010) reciprocal position.

crystal packing, and the large difference in X-ray scattering power between methyl and halogen makes these systems ideal examples for study of the resulting diffuse scattering distributions.

In early studies[181,182] the investigations yielded only qualitative descriptions of the short-range order which occurred between the orientation of molecules in neighboring sites. Later, a least-squares procedure in which correlation coefficients (or SRO parameters) were determined by fitting a series of calculated *distribution functions* to the observed patterns was developed.[183-185] Each distribution function consisted of those atom-pair terms in the SRO expression of eq 17 which corresponded to a given inter*molecular* vector and could be calculated from atom coordinates obtained from the average structure determination, leaving only the α^{ij}_{lmn} to be determined. Although this methodology was moderately successful for systems in which most of the diffuse scattering could be assumed to be of substitutional origin, it was still necessary to remove from the data regions of scattering near Bragg peaks, attributed to TDS. The methods were clearly inadequate for more general problems where displacements associated with the disorder might be important. Another limitation was the relatively small number of different distribution functions that could realistically be handled, a limitation that severely restricted the spatial resolution of the diffuse features that could be fitted.

The example of 1,3-dibromo-2,5-diethyl-4,6-dimethylbenzene (BEMB2)[185] displayed an interesting and unusual diffraction effect that has been the subject of further study.[186] In this material there is a broad region of diffuse scattering extending along the **b*** reciprocal axis which was well modeled by the earlier study. In the region of the (010) position, however, there is a distinct "*hole*" in the diffuse scattering (see Figure 19). This feature was not *modeled in the earlier study since the width of the* hole corresponds to a spatial frequency well in excess of any of the intermolecular vector distances that were incorporated in the analysis.

It was concluded that the SRO diffuse scattering is dominated by molecular dipole−dipole interactions which result in a tendency for molecules locally to try to pack in a configuration that results in a *c*-glide relationship between neighboring molecules. On a larger scale (the reciprocal of the hole diameter) the average structure is dominated by basic intermolecular repulsive forces which result in a preference for a packing with a 2_1-screw arrangement [which gives rise to the systematic absence close to (010)].

7.2. Disorder Involving Atomic Displacements

For systems in which significant displacements accompanying the substitutional disorder, terms in the diffraction equation other than the SRO term in eq 17 need to be considered. So far, however, no attempt has been made to analyze diffuse scattering from molecular crystals in this way. Instead computer simulations have been employed to model the disorder.

Detailed diffuse scattering patterns (see Figure 20a) have been recorded for *p*-chloro-*N*-(*p*-methylbenzylidene)aniline[5,187] (MECL see Figure 21). The observed scattering in this system has been interpreted by comparison with diffraction patterns of a model system obtained using Monte Carlo simulation

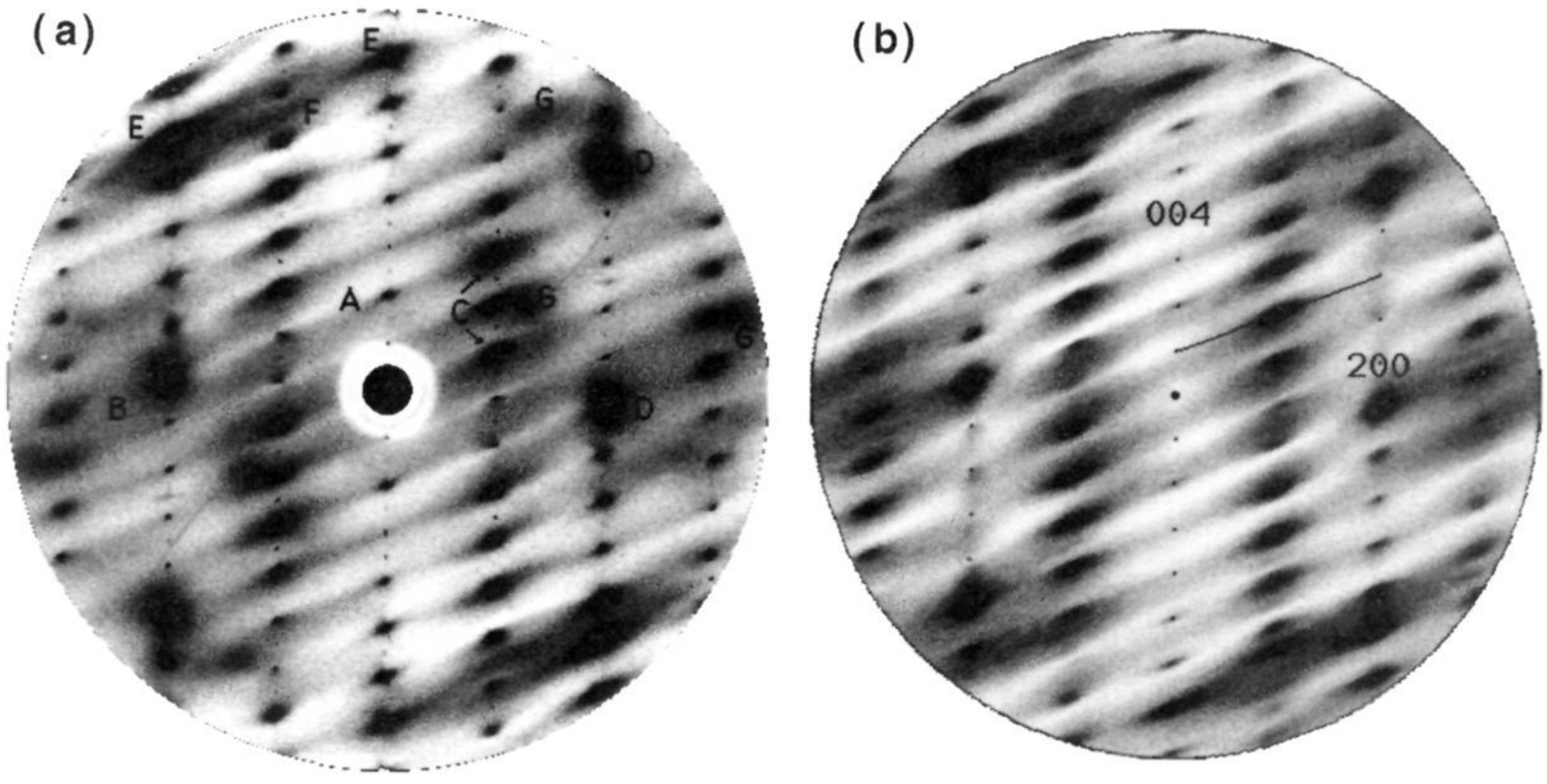

Figure 20. (a) Observed diffuse X-ray scattering in the ($h0l$) section of MECL and (b) diffraction pattern of the same section calculated from a Monte Carlo computer model.

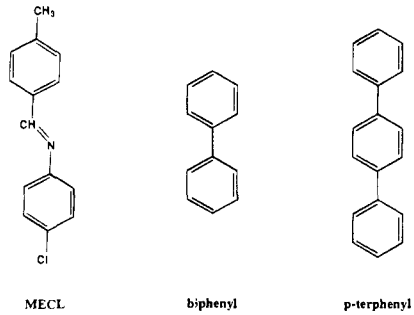

Figure 21. Some organic compounds that form disordered crystals in which atomic displacements make important contributions to the diffuse scattering.

(see Figure 20b). Strong diffuse scattering peaks (C) originate from a type of disorder in which the molecule is flipped *end-to-end* and indicate a tendency for the structure to form a superlattice with local symmetry $P2_1/n$ compared to the $P2_1/a$ symmetry of the average structure. A second type of disorder involving *side-to-side* flipping of the molecules appears to occur randomly with no evidence for short-range ordering, producing only broad regions of scattering (B). Accompanying these two effects there is also strong TDS-like diffuse scattering surrounding many of the Bragg peaks (D and E). This scattering remains strong on cooling to ~80 K and so must arise from static displacements resulting from the orientational disorder. This scattering was modeled reasonably satisfactorily by assuming rigid-body molecular displacements which were correlated from site to site, but which were assumed independent of the orientational SRO. This is clearly not a completely satisfactory description since some features (G) in the observed pattern are not reproduced, and further work is anticipated.

7.3. Disorder in Polyphenyls

There has been considerable interest over the last two decades in the crystalline states of *p*-polyphenyls. In such compounds (see Figure 21) phenyl rings are joined together by carbon–carbon σ-bonds. The conjugation favors a planar arrangement, but repulsion between the *o*-hydrogens induces a nonplanar conformation. In crystals the intermolecular forces are of a comparable magnitude to the torsion forces, and since these packing interactions prefer the molecules to assume flat configurations this competition gives rise to molecular conformation instability. At room temperature both biphenyl and *p*-terphenyl appear planar, but are evidently undergoing large torsional excursions. At lower temperatures phase transitions result as these torsional displacements are frozen in. Biphenyl forms incommensurately modulated low-temperature phases, and these have attracted experimental[188,189] as well as theoretical[190] interest. At low temperatures *p*-terphenyl forms a commensurate superstructure, involving a doubling of both the **a** and **b** cell dimensions, in which the phenyl rings are noncoplanar. The diffuse scattering which accompanies these changes has been observed by numerous workers, but no attempt has been made to quantitatively model the whole diffuse scattering distribution. Lechner et al.[191] made reciprocal space scans through a diffuse reflection at $^9/_2$ $^1/_2$ 0 at three temperatures just above the phase transitions. Subsequently Welberry and Mair[192] made a more extensive study of the variation of correlation length with temperature in each of three crystallographic directions. In this study these correlation lengths, ξ_1,. ξ_2, and ξ_3, were measured by fitting a Lorentzian form

$$I(\boldsymbol{q}) = AT/[(T - T_c)(1 + \xi_1^2 q_1^2 + \xi_2^2 q_2^2 + \xi_3^2 q_3^2)] \quad (30)$$

to 2D sections of diffuse data which extended over a reciprocal unit cell.

7.4. Orientational Disorder in Solid C_{60}

There has been considerable interest in recent times in the novel molecules, C_{60}, C_{70}, and higher analogue fullerenes.[193] Although these materials are intrinsically disordered and have been studied by a wide variety of techniques,[194] very little work has appeared involving diffuse X-ray scattering. At room temperature solid C_{60} forms a face-centered cubic (fcc) lattice where the nearly spherical C_{60} molecules are orientationally disordered. Below 259 K the crystals undergo an fcc to simple cubic (sc) orientational ordering phase transition, and a further transition at 225 K has also been reported.[195] Moret et al. carried out an investigation into this ordering process using diffuse X-ray scattering at temperatures ranging from ambient down to 20 K. Using fixed-crystal fixed-film diffuse scattering photographs, they observed three types of diffuse scattering. The authors report that two of these types of scattering are produced by fluctuations corresponding to the two structural transitions. They correspond to intermolecular correlations on a sc and a doubled-cell fcc lattice, respectively. The third type of scattering persists to low temperatures and it is presumed that this originates from a one-molecule disorder such as an orientational disorder of uncorrelated C_{60} molecules.

8. Diffuse Scattering from Macromolecular Crystals

Compared to the study of diffuse scattering in small molecule and other simple structures the study of diffuse scattering in macromolecules is still very much in its infancy. It is not difficult to understand why this should be so, since determination of the average structure from the Bragg reflections is itself far from routine for these massive structures. The simplified view of a crystal in which each unit cell contains the same identical arrangement of atoms is no longer completely tenable. Owing to their large size and weakly coupled atomic interactions, protein molecules can assume many different, although closely related, conformational substates at room temperature. In addition, protein crystals are often only about half protein; the other half of the crystal volume being occupied by solvent molecules.[196]

Given the multiplicity of different ways in which diffuse scattering can arise even in simple systems together with the large number of atoms or larger structural component that may be present in a protein crystal, it might appear that the problem of

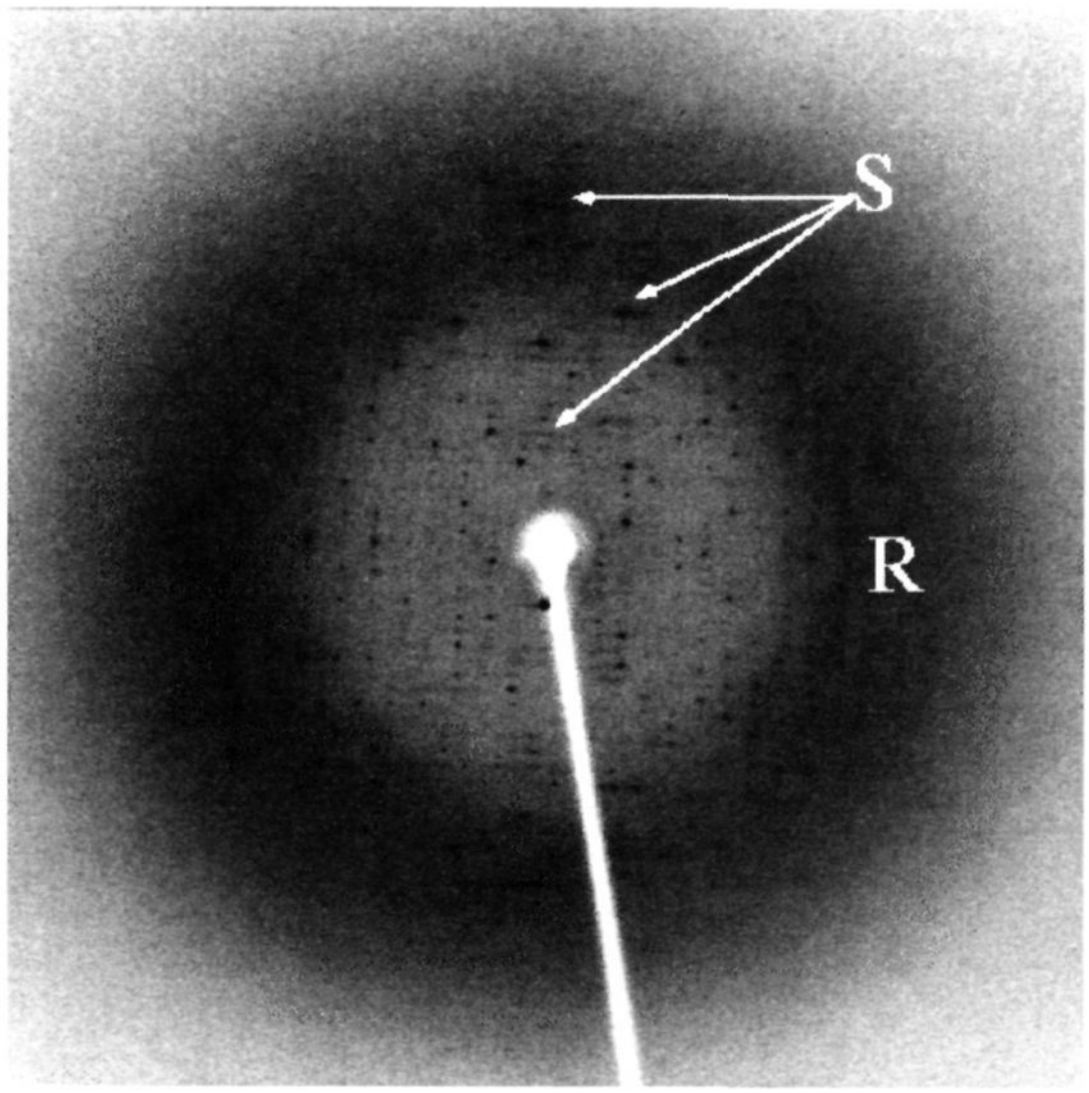

Figure 22. Diffuse scattering observed in single-stranded DNA binding protein from *E. coli*[206] A 4° oscillation with the oscillation axis vertical. Note the broad diffuse ring "R" and the diffuse streaks "S". (Reproduced by kind permission of Dr. Paul Carr. Copyright 1994 Academic.)

obtaining useful information from the diffuse scattering presents an intractable problem. On the other hand, it is well established that the biological activity of proteins is related not only to their mean molecular structure, but also to their intramolecular mobility.[197-200] Consequently any information that might be obtained from the diffuse scattering, which originates directly from such motions, offers potentially rich rewards over and above the information that is obtained from the average structure analysis. In this section we explore the progress which has been made so far in this difficult field.

Interest in diffuse scattering from proteins has undoubtedly greatly benefited from the advent of synchrotron X-ray sources[201] with their high intensity, high beam collimation, wavelength tunability, and ability to produce less beam damage than conventional sources. Using such sources Glover et al.[202] have explored the different types of diffuse scattering effects that can be observed in a variety of different macromolecular systems. The examples presented by these authors exhibit a whole range of different diffuse scattering effects. These range from avian pancreatic polypeptide[203] (aPP) which, for a macromolecular crystal, has an unusually small amount of diffuse scattering, through ones such as bovine ribonuclease A (RNAse),[204] which shows distinct acoustic thermal diffuse-scattering halos around the Bragg peaks. A rabbit serum transferrin[205] crystal exhibited considerable diffuse scattering consisting of a broad ring with a distinct diamond shape to its inner (low-resolution) edge but also contained a series of streaks running at approximately 45° to the Bragg layer lines. In addition, there are other features apparently not associated with the Bragg peaks.

Such scattering can also be recorded on more conventional sources. In Figure 22 we show a typical diffuse scattering pattern recorded using an R-axis image−plate system.

Although some investigations have been carried out on systems in which there is clearly disorder involving different species within the lattice,[207] the majority of studies have concentrated on modeling the atomic displacement patterns in crystals where it is assumed that a single molecular species is present. There is strong evidence of the dynamic nature of the disorder in the majority of macromolecular crystals.[208-212]

A common feature of most diffuse patterns is the presence of an anisotropic ring of inhomogeneous diffuse intensity in the regions between ~4.5 Å and 2.8 Å resolution[202] (see also Figure 22). Although solvent scattering (both within and surrounding the crystal) and scattering from the glass capillary may account for some of this, the intensity and marked anisotropy of the ring clearly indicates that much of the scattering originates from, and is characteristic of, the sample. Attempts to model this scattering in terms of atomic displacement patterns may be taken in several stages.

The intensities of Bragg reflections at the reciprocal lattice points (hkl) correspond to the squared Fourier transform of the average structure, $F^2(hkl) = |\boldsymbol{FT}\langle\varrho(\mathbf{r})\rangle|^2$, whereas the total intensity $F^2(\mathbf{S})$ scattered by the crystal as a function of the continuous reciprocal space coordinate $S = |\mathbf{S}| = 2\sin(\theta/\lambda)$ is defined by the average of the squared Fourier transforms of the

instantaneous structures $\langle|\boldsymbol{FT}\varrho(\mathbf{r})|^2\rangle$. The diffuse part of the scattering pattern, or what is referred to as variational scattering in the protein literature, corresponds to the difference between these two (i.e., the difference between the average of the square and the square of the average transform, or the variance of the transformed density):

$$I_{\text{diffuse}}(\mathbf{S}) = \langle|\boldsymbol{FT}\varrho(\mathbf{r})|^2\rangle - |\boldsymbol{FT}\langle\varrho(\mathbf{r})\rangle|^2 \quad (31)$$

For an Einstein crystal in which it is assumed that each atom is vibrating as an independent harmonic oscillator with the same mean-square displacement δ^2, the form of this intensity is[202,213]

$$I = \sum_j f_j^2[1 - \exp\{-(2\pi S\delta)^2\}] \quad (32)$$

where $S = 2\sin(\theta/\lambda)$. This intensity corresponds to that lost from the Bragg reflections which are damped by the normal Debye–Waller temperature factor, $\exp(-2\pi S\delta)^2 \exp(-1/2BS^2)$. The ratio of the spherically averaged diffuse intensity to the intensity of the Bragg peaks thus goes as $[\exp(2\pi S\delta)^2 - 1]$ where δ^2 is the mean-squared displacement of the atomic movements. Clarage et al.[196] point out that for a mean temperature factor $B \approx 20$ Å^2, which is typical for many protein crystals, the integrated diffuse intensity will exceed that of the Bragg peaks beyond a resolution of $1/\mathbf{S} = 3.8$ Å and, at the resolution required to locate atoms in protein crystals, more X-rays are diffusely scattered than are diffracted into Bragg reflections.

In contrast to the Einstein crystal, if it is assumed that the motions of the atoms within a molecule are all perfectly correlated, i.e., the molecules are undergoing independent rigid-body vibrations, then the diffuse intensity assumes the form of the difference Fourier transform (DFT)[8]

$$I_{\text{DFT}} = \mathscr{F}^2[1 - \exp\{-(2\pi S\delta)^2\}] \quad (33)$$

where $\mathscr{F}$ is now the molecular transform,

$$\mathscr{F}(\mathbf{S}) = \sum_j f_j \exp\{2\pi i\mathbf{r}_j\cdot\mathbf{S}\} \quad (34)$$

and the summation is over all of the atoms in the molecule. The diffuse diffraction patterns of crystals of many small rigid molecules were shown to be well approximated by this DFT function.[8] The change from independent atoms to independent molecules does not affect the overall envelope of the diffuse intensity but simply adds structure to it.

For macromolecules containing many internal degrees of freedom, however, the DFT is clearly not satisfactory. While the motions of neighboring atoms may be highly correlated (because they are bonded to each other) the motions of atoms at opposite ends of the molecule may be quite uncorrelated. Caspar et al.[213] in trying to model the diffuse scattering from insulin have attempted to give expression to this by assuming the variational intensity can be modeled by an expression of the form

$$I_{\text{V}}(\mathbf{S}) = [1 - \exp\{-(2\pi S\delta_{\text{s}})^2\}] \times \boldsymbol{FT}[P_0(\mathbf{r})\exp\{-(1/2)(r/\gamma_{\text{s}})^2\}] \quad (35)$$

Here $P_0(\mathbf{r})$ is the Patterson or autocorrelation function of the ideally ordered unit-cell structure, $\boldsymbol{FT}$ stands for "Fourier transform", and $\exp\{-(1/2)(r/\gamma_{\text{s}})^2\}$ is a monotonically decreasing function that smoothly truncates the Patterson function. As an alternative to this Gaussian function, a simple exponential, $\exp\{-(r/\gamma_{\text{s}})\}$, was also used. γ_{s} is a parameter specifying a range over which short-range coupling of the atomic motions occurs (hence the subscript s) and together with the root mean-squared displacement δ_{s} represent short-range coupling parameters that may be adjusted to obtain the best fit to the observations. For insulin the value of γ_{s} that gave best agreement was ~6 Å and of δ_{s} 0.4–0.45 Å.

In addition to these short-range couplings which act over a range much shorter than the unit-cell dimensions, it is also necessary to consider the coupling of motions over distances comparable to and greater than the unit cell dimensions. These may largely be attributed to low-frequency lattice modes or acoustic phonons but these may couple with intramolecular modes involving the movement of large fragments of the molecule. These motions, involving long-range correlations, result in diffuse halos around the Bragg peak positions. For a harmonic lattice wave description of a crystal, the acoustic phonon scattering intensity of the halo is predicted to diminish as $1/q^2$, where q is the distance from the Bragg peak position.[202] Glover et al. showed that the observed acoustic diffuse scattering around a 6 Å reflection from ribonuclease agreed well with this $1/q^2$ fall-off although additional structure could be seen in the scattering. In contrast Caspar et al.[213] found that for insulin the fall-off was more gradual than this and chose to model the diffuse halos in terms of a similar function to that used for the short-range couplings (eq 35) but with a much larger coupling range, γ_{L} and a different independent contribution to the displacement amplitudes δ_{L}. For this second longer range type of coupling they found a value of γ_{L} = ~20–30 Å appropriate for rms displacement amplitudes ~0.25 Å, and concluded that the short-range coupling motions accounted for most of the disorder in the structure with the longer range couplings being relatively less important.

A similar analysis has also been applied to the diffuse scattering from two different crystal forms (triclinic and tetragonal) of lysozyme.[214] Again the predominant component of the scattering came from short-range (~6 Å) coupled motions. Lattice-coupled movements, with a correlation distance ~50 Å, accounted for only about 5–10% of the total mean square displacements in the protein crystal. These results are at odds with surmises based on normal mode calculations[215] and rigid-body movements,[216] as well as inferences from measurements of Young's modulus[217] and the speed of sound in protein crystals,[218] all of which implicate long-range coupled displacements as the major contribution to temperature factors.

A third form of lysosyme (orthorhombic) in which diffuse streaks are observed along planes perpen-

dicular to the **a*** and **b*** reciprocal axes has also been studied.[219,220] Here the authors find that a model in which entire rows of molecules are assumed to undergo rigid-body translations parallel to the **a**- and **c**-axes produces good agreement with the observed diffuse streaking, while a model which assumes oscillations of dimers gives poor agreement.

The global ~6 Å coupling range used in the studies of insulin and the triclinic and tetragonal forms of lysozyme above presents a picture of the disorder in which the motions within the protein are *liquid-like* in the sense that correlations decay rapidly and are homogeneous. Clearly, since thermal parameters vary enormously for different parts of a protein structure, such a global coupling range is often likely to be inappropriate. However recent studies of yeast initiator tRNA demonstrate that models can be developed[221] which incorporate features specific to particular regions of the protein. The total scattering in this example was attributed to six different components: Bragg intensity, bulk water diffraction, independent atom motion, long-range lattice-coupled motion along the **c**-axis, long-range lattice-coupled motion perpendicular to the **c**-axis, and short-range motion local to the anticodon arm of the molecule.

In summary, methods to try and extract useful information from the diffuse scattering in many protein and nucleic acid diffraction patterns are developing. While the diffuse scattering intensities cannot be Fourier inverted to produce directly a description of the atomic motions, diffuse scattering can be calculated from models and compared with experimental results to yield insights about macromolecular motions. A number of assumptions and approximations are made in the models currently used, and there is some difference between results obtained from these models with calculations based on normal-mode analysis of protein structures and various measurements of physical properties which depend on elastic constants of crystals. One hopes that as the methods of analysis are further developed and more experience is gained on different examples that these differences can be reconciled.

9. Diffuse Scattering from Quasi-Crystals

It was discovered only 10 years ago or so[222] that certain materials form phases which, although appearing crystalline and having diffraction patterns consisting of sharp Bragg-like diffraction peaks, possess a symmetry not conforming to any of the permissible Bravais lattices known in classical crystallography. The number of systems exhibiting such *quasi-crystalline* phases possessing 8-, 10-, or 12-fold axes of symmetry has grown rapidly since that time,[223] so the phenomenon can no longer be considered merely a curiosity. As a result of this there has been considerable interest in models which can give rise to such noncrystallographic symmetries. Understanding the diffraction patterns of perfect quasi-crystals and their relationship to conventional crystalline phases itself presents a not insignificant challenge to the classical crystallographer but the concept of a perfect quasi-crystal is only a model and, as for conventional crystallography, real examples depart from this ideal in various ways. This gives rise to diffuse scattering.

Most early examples of quasi-crystallinity were obtained from rapidly quenched alloys, and the samples often were quasi-crystalline on a scale up to only a few hundred angstroms. More recently, however, examples have been found which possess icosohedral or decagonal symmetry in macroscopic samples on the scale of millimeters.[224,225]

9.1. Penrose Tiling

As a model for the explanation of quasi-crystal diffraction patterns, interest has centered on Penrose tiling and its generalizations.[226−229] Such tiling, in which "*the unit cell*" of classical crystallography is replaced by two differently shaped "tiles", completely fills space without defects and possesses long-range orientational order, but does not possess translational symmetry. In Figure 23 we show a small section of

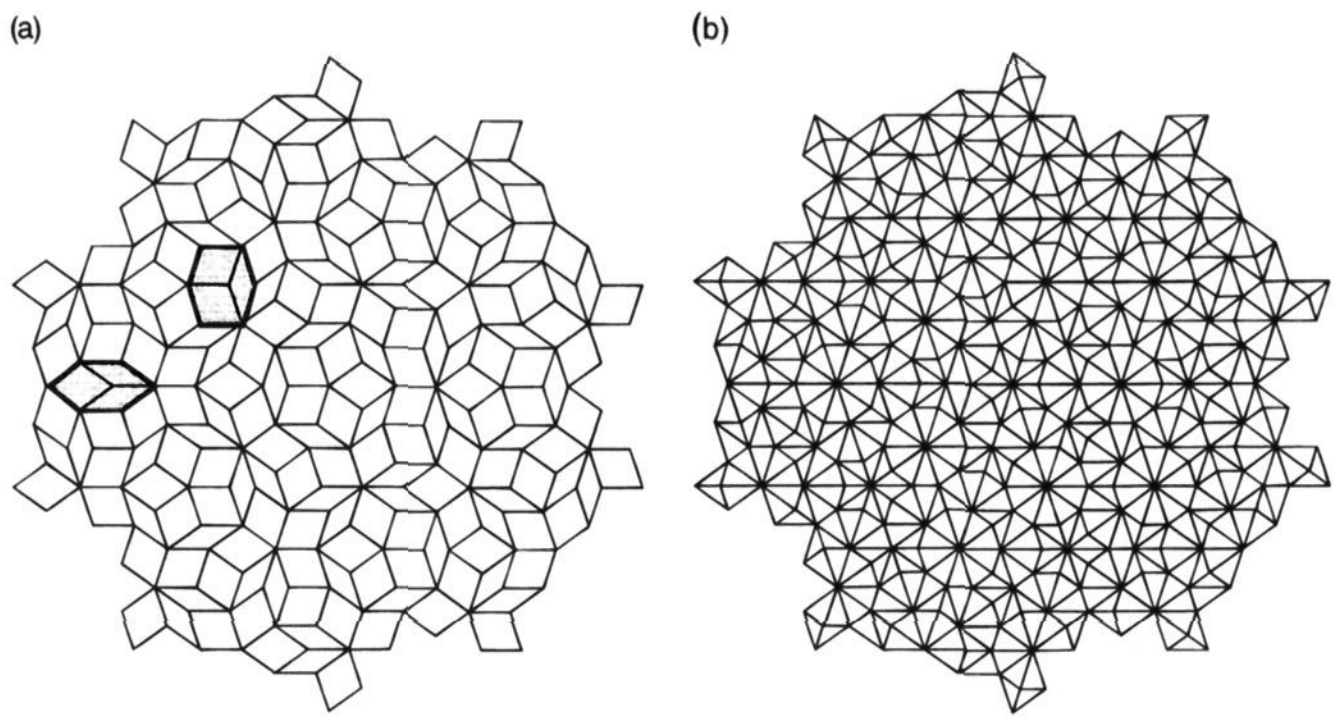

Figure 23. Two different types of 2D Penrose tiling: (a) using the *fat* and *thin* rhombs and (b) using the small and large Robinson triangles. The shaded areas in part a show the two types of tile combination which may be *flipped* to obtain disordered structures.

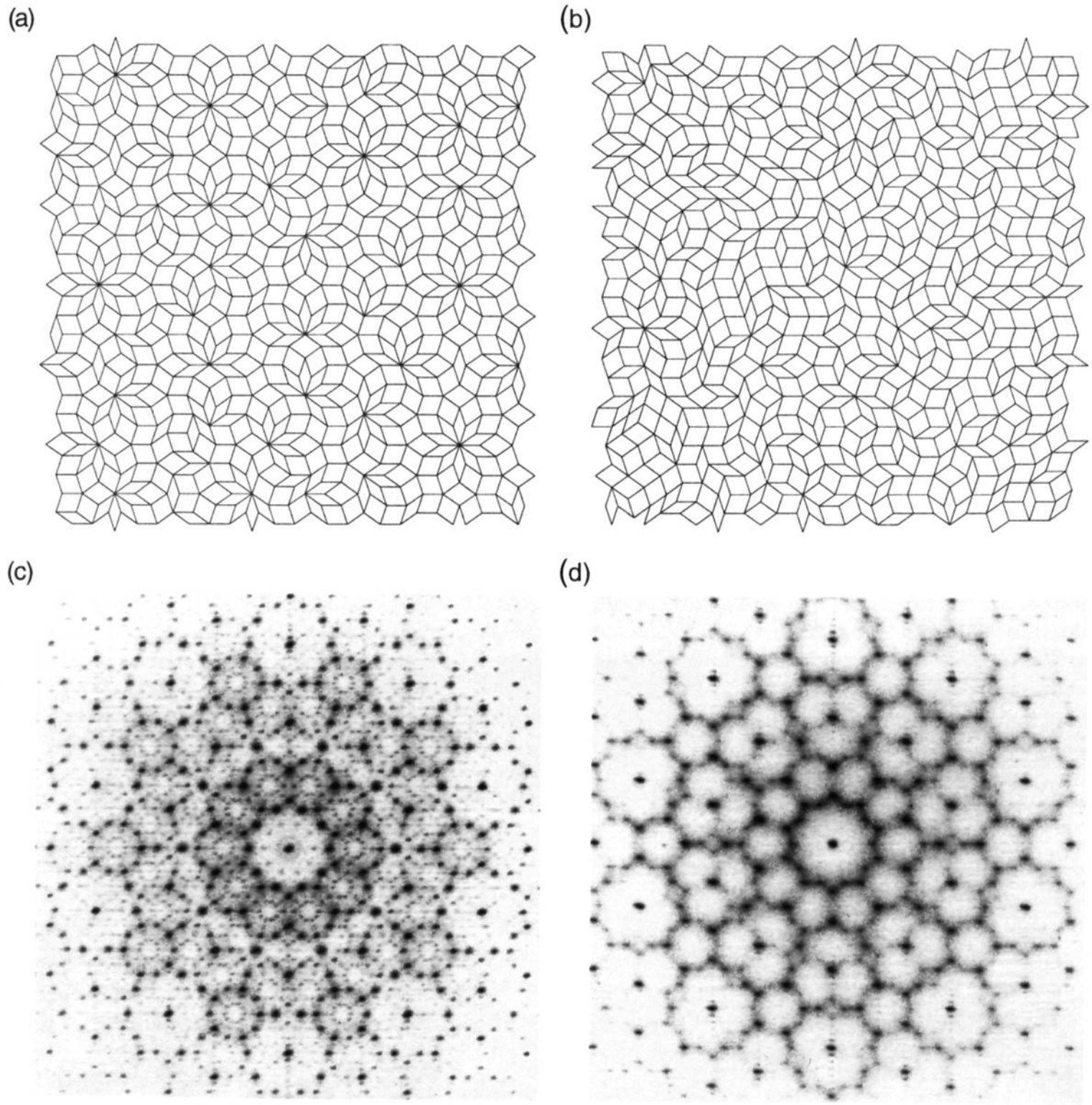

Figure 24. Disordered 2D structures produced by a succession of phason flips from an initial perfect Penrose tiling pattern. In a nearest-neighbor tile configurations consisting of a pair of thin rhombs is energetically preferred, while b corresponds to random tiling where no preference is made for any particular tile combination. Panels c and d show respectively the optical diffraction patterns obtained from these structures. The structures shown are small regions taken from much larger samples (each of ~20 000 tiles) that were used to obtain the diffraction patterns. The optical diffraction patterns were obtained by placing a single scattering point at the corners of each rhomb.

2D Penrose tiling using two different tile combinations. In Figure 23a the two types of tile are a "fat rhomb" and a "thin rhomb", while in Figure 23b the two types of tile are the small and large Robinson triangle. Comparison of the two figures reveals the relationship between the two types of tiling.

A characteristic of the diffraction pattern of perfect Penrose tiling is the presence of a large number of high order diffraction peaks. Although some examples (see Figure 3 of He et al.[230]) show a large number of higher order diffraction peaks, other examples do not.[231] In these examples, produced by rapid quenching, a model such as that shown in Figure 23a may be appropriate, but, for examples which appear to be thermodynamically stable, an alternative approach has been sought to explain the way in which the quasi-crystalline order might be formed. Consequently there has been interest in "random tiling" models. In these, the perfect quasi-periodicity of the Penrose pattern is destroyed by the successive application of local rearrangements of groups of tiles (phason fluctuations).

Much recent discussion in the literature[232−235] has centered on these phason fluctuations. The view is held that the near-degeneracy of all possible tilings, whether periodic, quasi-periodic, or random, and interconversion between these, may be achieved by a succession of low-energy phason flips. In this way it is feasible that an initially fairly random structure could be annealed to obtain long-range order approaching that of the Penrose pattern. Examples of diffraction patterns of some 2D random tiling models have been given by Welberry,[236] and two of these are reproduced in Figure 24. These examples reveal that a whole variety of different tilings are accessible from the perfect Penrose pattern via phason fluctuations, but the work stops short of being able to reverse the procedure to obtain a well-ordered Penrose pattern from an initially disordered arrangement.

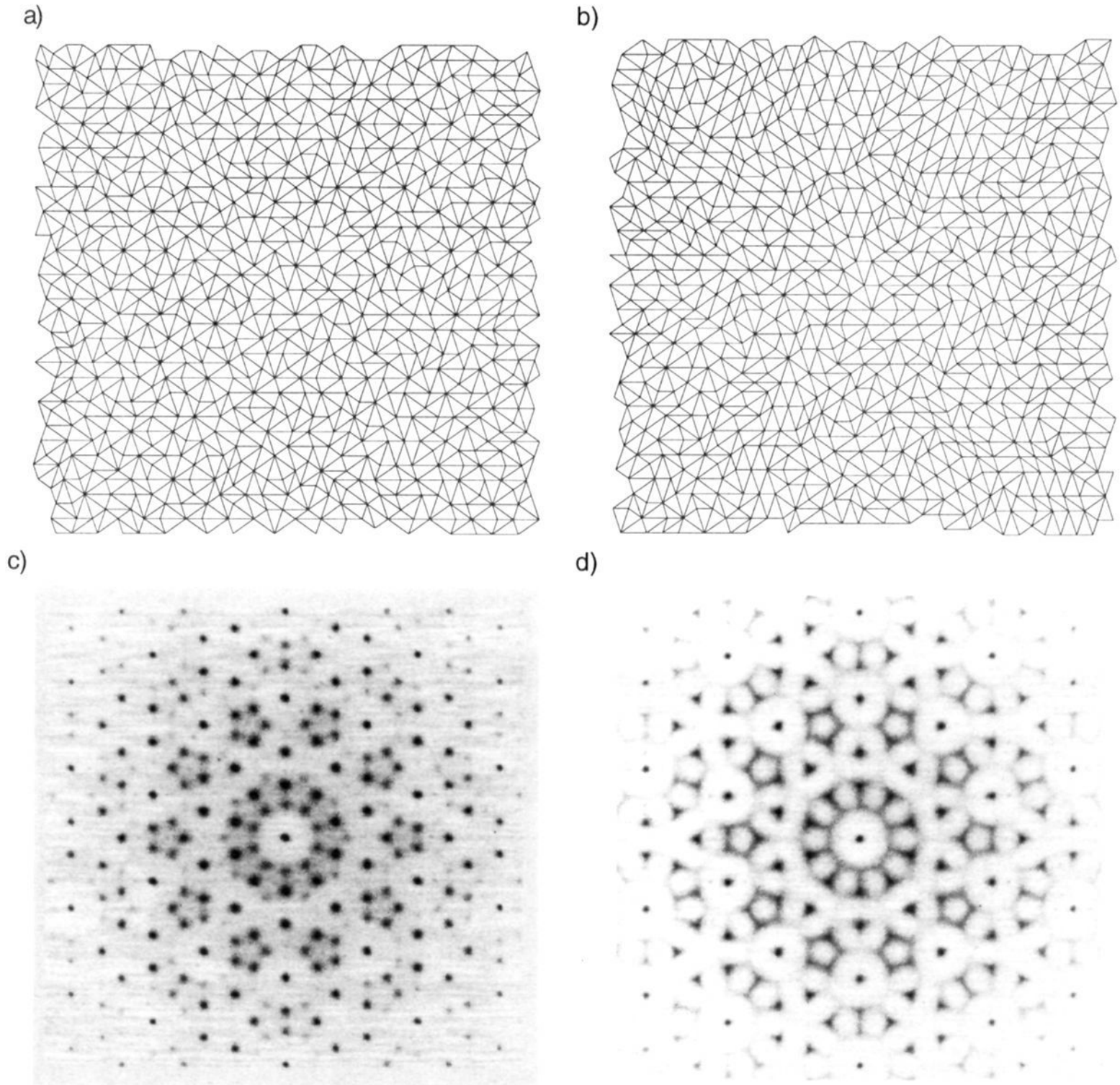

Figure 25. Disordered 2D structures constructed using Robinson triangles. The structures were generated by a growth algorithm in which tiles were added sequentially to a central seed. In a there is a preference for nearest-neighbor pairs of tiles to adopt configurations found in the Penrose tiling pattern, while in b neighboring tiles are selected more randomly. Parts c and d show, respectively, the optical diffraction patterns obtained from these structures. The structures shown are the central region of much larger samples (each of ~20 000 tiles) that were used to obtain the diffraction patterns. The optical diffraction patterns were obtained by placing a single scattering point at the corners of each triangle.

9.2. Disordered Growth Tiling

In contrast to the Penrose type of model, Pauling[237,238] proposed an alternative explanation in terms of crystal twinning. Subsequently Budai et al.[239] showed that the Pauling twinning mechanism could not explain the phason strain in icosahedral Al–Mn. In an attempt to reconcile the quasi-crystal versus the Pauling twinning model points of view, Wolny and his co-workers[240] discussed a number of different structures, all built with the same two types of tile called Robinson triangles,[241] and which all tile the 2D plane without defects. Welberry[242] extended these ideas to produce, via a growth algorithm, structures with varying degrees of order ranging from ones which were *Penrose*-like to ones which were *twinned-crystal*-like and obtained model diffraction patterns using optical diffraction. Two examples of these patterns are shown in Figure 25. In Figure 25a there is a tendency for nearest-neighbor tiles to adopt configurations found in the Penrose tiling pattern, whereas in Figure 25b neighboring tile combinations are selected more randomly. Corresponding optical diffraction patterns are shown in Figure 25, parts c and d, respectively.

9.3. Examples of Real Quasi-Crystals Exhibiting Disorder

Decagonal quasi-crystals are *quasi-crystalline* in two dimensions and *crystalline* in the third direction, parallel to the unique axis. In a sense the decagonal quasi-crystals may be considered as intermediate between translationally ordered crystals and true quasi-crystals. Among the decagonal phase alloys identified so far there are only a few thermodynamically stable phases which have been studied by scattering methods in detail. In all of these, diffuse scattering effects are evident, revealing the presence of disorder of various kinds.

Frey and Steuer[243] have compared the isotypical decagonal phases $Al_{70}Ni_{15}Co_{15}$ (ANC) and $Al_{65}Cu_{20}$-

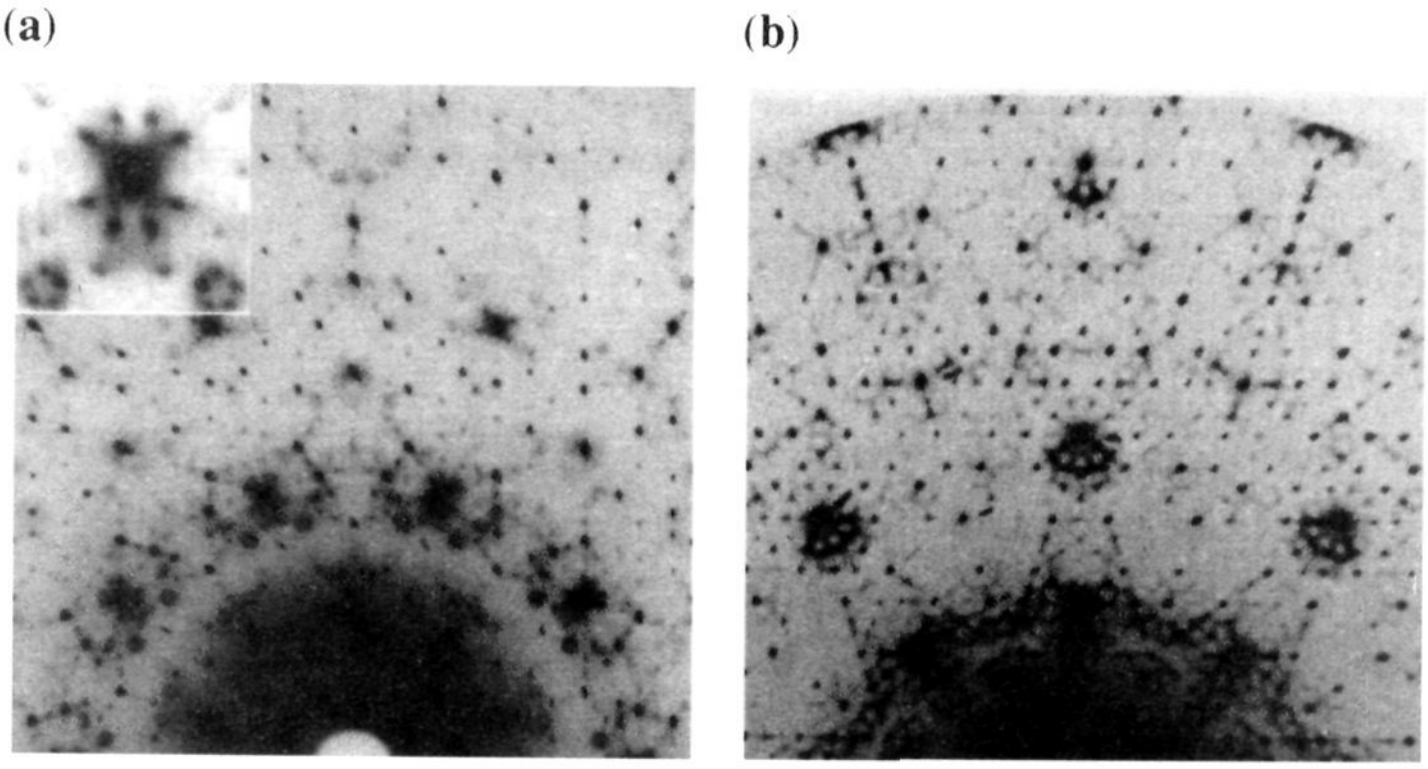

Figure 26. (a) Portion of the zero-level X-ray diffraction pattern of $Al_{70}Ni_{15}Co_{15}$ (ANC) with an enlarged region (inset) showing the diffuse streaking from a strong Bragg peak toward a ring of satellite peaks and the nearby pentagons of five diffuse spots. (b) Portion of the zero-level X-ray diffraction pattern of $Al_{70.5}Mn_{16.5}Pd_{13}$ (AMP). Note the ring of diffuse pentagons encircling some strong Bragg peaks. (Reproduced with kind permission of Professor W. Steurer.)

Co_{15} (ACC) with $Al_{70.5}Mn_{16.5}Pd_{13}$ (AMP). ANC and ACC show remarkable diffuse scattering of various kinds. Most prominent are "modulated" diffuse layers which occur between the integral reciprocal layers which contain the Bragg peaks. These diffuse layers are attributed to a doubling of the repeat within columnar structural units caused by chemical ordering of the Ni and Co atoms along the unique direction and the fact that the layer thickness is small indicates that this ordering is relatively long range. The distribution of diffuse scattering within the diffuse layers and also within the Bragg layers is attributed to orientational disorder of the columns and to positional disorder arising as a consequence of the longitudinal ordering process.

A portion of the zeroth-layer diffraction pattern of ANC is shown in Figure 26a. Two features are of particular note. There are diffuse streaks emanating from the strong Bragg peaks and ending in a ring of satellite reflections. These correspond to modulation waves of approximately 60 Å wavelength. Similar modulations have been observed[244] in the icosohedral phase of an Al−Fe−Cu alloy and found to vary as a function of annealing conditions. The second interesting feature of the pattern is the presence of a ring of small pentagons surrounding some strong Bragg peaks; each pentagon consists of five diffuse spots superimposed on a broader diffuse maximum. Neither the centers of the pentagons nor the spots can be identified as being due to the same quasi-lattice as the Bragg peaks.

In marked contrast to ANC and ACC the diffraction patterns of AMP reveal disorder related only to the quasi-periodic ordering. Reciprocal layers normal to the unique axis are characterized by the presence of sharp reflections and diffuse scattering. Unlike ANC/ACC there are no additional diffuse layers. A dominant feature of all layers is a dense array of diffuse pentagons (see Figure 26b). These features show a great resemblance to the optical diffraction patterns of the random Robinson triangle tilings shown in Figure 25b. Similar features have also been observed in electron diffraction patterns of AMP.[245] Steuer et al.[246] conclude that the basic building blocks of the structure are columnar clusters (~20 Å) with cross sections corresponding to parts of a decorated Penrose tiling. The clusters themselves are packed in a way that results in a disordered Robinson-triangle tiling.

10. Conclusion

In this review we have attempted to give a broad overview of the many different areas whereas diffuse X-ray scattering has played and continues to play an important role in the development of our understanding of the structure and function of crystalline materials. These have been presented under specific section headings, but there are many interconnections between these various categories, and each distinct field draws on the experience gained in others.

While the range of materials covered is extremely broad, ranging from simple alloys to large macromolecules, in order to keep the subject matter within reasonable bounds there have inevitably had to be omissions. For example some of the earliest studies of diffuse X-ray scattering were concerned with stacking faults in close-packed or layered materials,[247−250] and an extensive literature in this area has existed for many years. Good summaries of the historical development of the treatment of stacking disorder are given in recent papers by Sebastian and Krishna[251] and Nikolin and Babkevich.[252] Included in this general area is the large body of work that exists on clay minerals[253,254] and on polytypism.[255,256] Despite its long history, however, interest in layer-stacking disorder has by no means been exhausted and numerous examples are to be found in the recent literature.[257−267] We have also made no attempt to seek out the many isolated examples where diffuse scattering has been reported, possibly as a result of

a chance encounter during the course of an unrelated study.

The examples presented in this paper, which range from the quantitative determination of short-range order and atomic displacements in metallic alloys, to the coupled molecular motions in protein crystals, demonstrate the range of materials in which diffuse scattering has proven to be a valuable tool. With the continued development of experimental procedures for recording diffuse scattering, and more particularly, of methods to analyze and model disordered structures by including as much *a prior* chemical information as possible to the analysis, the opportunity exists for more quantitative approaches to be applied where only more qualitative treatments have been used previously.

References

(1) Warren, B. E. *X-ray Diffraction*; Addison-Wessley: Reading, MA, 1969; reprinted Dover: New York, 1990.
(2) Welberry, T. R. *Rep. Prog. Phys.* **1985**, *48*, 1543.
(3) Jagodzinski, H. *Prog. Cryst. Growth Charact.* **1987**, *14*, 47.
(4) Epperson, J. E.; Anderson, J. P.; Chen, H. *Metall. Mater. Trans. A* **1994**, *25*, 17.
(5) Welberry, T. R.; Butler, B. D. *J. Appl. Crystallogr.* **1994**, *27*, 205.
(6) Frey, F. Proceedings of the IUCr Symposium: New trends in Small Moiety Crystallography. *Acta Crystallogr.*, submitted for publication.
(7) Schwartz, L. H.; Cohen, J. B. *Diffraction from Materials*; Springer-Verlag: Berlin, 1987.
(8) Amoros, J. L.; Amoros, M. *Molecular Crystals—their Transforms and Diffuse Scattering*; Wiley: New York, 1968.
(9) Guinier, A. *X-ray Diffraction in Crystals, Imperfect Crystals and Amorphous Bodies*; W. H. Freeman: San Francisco, 1963.
(10) Hukins, D. W. L. *X-ray Diffraction by Disordered and Ordered Systems*; Pergamon Press: Oxford, 1981.
(11) Jagodzinski, H.; Frey, F. Disorder diffuse scattering of X-rays and neutrons. *International Tables for Crystallography*; Shmueli, U., Ed.; A. J. C. Kluwer Academic Publishers: Dordrecht, 1993; Vol. B, pp 392–433.
(12) Willis, B. T. M. Thermal diffuse scattering of X-rays and neutrons. *International Tables for Crystallography*; Shmueli, U., Ed.; A. J. C. Kluwer Academic Publishers: Dordrecht, 1993; Vol. B, pp 384–391.
(13) Krivoglaz, M. A. *The Theory of X-ray and Thermal Neutron Scattering by Real Crystals*; New York: Plenum Press, 1969.
(14) Fontaine, D. de *J. Phys. Chem. Solids* **1972**, *33*, 297.
(15) Fontaine, D. de *J. Phys. Chem. Solids* **1973**, *34*, 1285.
(16) Perez-Mato, J. M.; Madariaga, G.; Tello, M. J. *J. Phys. C* **1986**, *19*, 2613.
(17) Schweika, W. *Statics and Dynamics of Alloy Phase Transformations (NATO ASI Series B. Physics v. 319)*; Turchi, P. E. A., Gonis, A., Eds.; Plenum Press: New York, 1994; pp 103–126.
(18) Borie, B. *Acta Crystallogr.* **1957**, *10*, 89.
(19) Borie, B. *Acta Crystallogr.* **1959**, *12*, 280.
(20) Borie, B. *Acta Crystallogr.* **1961**, *14*, 472.
(21) Borie, B.; Sparks, C. J. *Acta Crystallogr.* **1971**, *A27*, 198.
(22) Tibballs, J. E. *J. Appl. Crystallogr.* **1975**, *8*, 111.
(23) Hayakawa, M.; Cohen, J. B. *Acta Crystallogr.* **1975**, *A31*, 635.
(24) Georgopoulos, P.; Cohen, J. B. *J. Phys. (Paris) Colloq.* **1977**, *38* (7), 191.
(25) Dietrich, S.; Fenzl, W. *Phys. Rev.* **1989**, *B39*, 8873.
(26) Warren, B. E. *X-ray Diffraction*; Dover: New York, 1990; pp 35–38.
(27) Cowley, J. M. *J. Appl. Phys.* **1950**, *21*, 24.
(28) Cowley, J. M. *Phys. Rev.* **1950**, *77*, 669.
(29) Clapp, P. C.; Moss, S. C. *Phys. Rev.* **1966**, *142*, 418.
(30) Clapp, P. C.; Moss, S. C. *Phys. Rev.* **1968**, *171*, 754.
(31) Clapp, P. C.; Moss, S. C. *Phys. Rev.* **1968**, *171*, 764.
(32) Warren, B. E.; Averbach, B. L.; Roberts, B. W. *J. Appl. Phys.* **1951**, *22*, 1493.
(33) James, R. W. *The Optical Principles of the Diffraction of X-rays*; G. Bell and Sons Ltd.: London, 1948.
(34) Wu, T. B.; Matsubara, E.; Cohen, J. B. *J. Appl. Crystallogr.* **1983**, *16*, 407.
(35) Matsubara, E.; Cohen, J. B. *Acta Metall.* **1983**, *31*, 2129.
(36) Matsubara, E.; Cohen, J. B. *Acta Metall.* **1985**, *33*, 1945.
(37) Matsubara, E.; Cohen, J. B. *Acta Metall.* **1985**, *33*, 1957.
(38) Gehlen, P. C.; Cohen, J. B. *Phys. Rev.* **1965**, *A139*, 844.
(39) Gragg, J. E.; Bardhan, P.; Cohen, J. B. *Critical Phenomena in Alloys, Magnets and Superconductors*; Mills, R. E., Ascher, E., Jaffee, R. I., Eds.; McGraw-Hill: New York, 1971; p 309.
(40) Cenedese, P.; Bley, F.; Lefebvre, S. *Acta Crystallogr.* **1975**, *A31*, 635.
(41) Haeffner, D. R.; Cohen, J. B. *Acta Metall. Mater.* **1992**, *40*, 831.
(42) Quintana, J. P.; Cohen, J. B. *J. Mater. Res.* **1993**, *8*, 855.
(43) Butler, B. D.; Cohen, J. B. *Acta Metall. Mater.* **1993**, *41*, 41.
(44) Reinhard, L.; Robertson, J. L.; Moss, S. C.; Ice, G. E.; Zschack, P.; Sparks, C. J. *Phys. Rev.* **1992**, *B45*, 2662.
(45) Ohshima, K.; Harada, J.; Morinaga, M.; Georgopuolos, P.; Cohen, J. B. *Acta Crystallogr. A* **1988**, *44*, 167.
(46) Butler, B. D.; Withers, R. L.; Welberry, T. R. *Acta Crystallogr.* **1992**, *A48*, 737.
(47) Butler, B. D.; Welberry, T. R. *Acta Crystallogr.* **1993**, *A49*, 736.
(48) Ramesh, T. G.; Rameseshan, S. *Acta Crystallogr.* **1971**, *A27*, 569.
(49) Ice, G. E.; Sparks, C. J.; Shaffer, L. B. In *Resonant Anomalous X-ray Scattering, Theory and Applications*; Materlik, G., Sparks, C. J., Fischer, K., Eds.; Elsevier Science: Amsterdam, 1994.
(50) Ice, G. E.; Sparks, C. J.; Habenschuss, A.; Shaffer, L. B. *Phys. Rev. Lett.* **1992**, *68*, 863.
(51) Schönfeld, B.; Ice, G. E.; Sparks, C. J.; Haubold, H.-G.; Schweika, W.; Shaffer, L. B. *Phys. Status Solidi* **1994**, *183*, 79.
(52) Rosshirt, E.; Frey, F.; Kupcik, V.; Miehe, V. *J. Appl. Crystallogr.* **1990**, *23*, 21.
(53) See, for example: *Physics Today* May **1981** (Special Issue: Synchrotron Radiation).
(54) Baruchel, J., Hodeau, J. L., Lehmann, M. S., Regnard, J. R., Schlenker, C., Eds. *Neutron and Synchrotron Radiation for Condensed Matter Studies, Vol. 1: Theory Instruments and Methods*; Springer-Verlag: Berlin, 1993.
(55) Bacon, G. E. *Neutron Diffraction*; Oxford University Press: London, 1962.
(56) Heath, R. L. *Adv. X-ray Anal.* **1972**, *15*, 1.
(57) Gasiot, J.; Bräunlich, P.; Fillard, J. P. *Appl. Phys. Lett.* **1982**, *40*, 376.
(58) Templer, R. H.; Warrender, N. A.; Seddon, J. M.; Davis, J. M. *Nucl. Instrum. Methods* **1991**, *A310*, 232.
(59) Clark, R.; Rodricks, B.; Smither, R. *Rev. Sci. Instrum.* **1989**, *60*, 2280.
(60) James, M. Ph.D. Thesis, Northwestern University, 1984.
(61) Sparks, C. J. *Phys. Rev. Lett.* **1974**, *33*, 262.
(62) Ice, G. E.; Sparks, C. J. *Nucl. Instrum. Methods* **1990**, *A291*, 110.
(63) Guinier, A. *X-ray Diffraction in Crystals, Imperfect Crystals, and Amorphous Bodies*; W. H. Freeman and Company: San Francisco, 1963; p 15.
(64) *International Tables for X-ray Crystallography*; Londsdale, K., Ed.; Kynoch Press: Birmingham, 1962; Vol. III, pp 250–252.
(65) *International Tables for Crystallography*; Wilson, A. J. C., Ed.; Kluwer Academic Publishers: Dordrecht, 1992; Vol. C, pp 574–578.
(66) Quintana, J. P. *J. Appl. Crystallogr.* **1991**, *24*, 261.
(67) Osborn, J. C.; Welberry, T. R. *J. Appl. Crystallogr.* **1990**, *23*, 476.
(68) Buerger, M. J. *X-ray Crystallography*; Wiley: New York, 1942.
(69) Reid, J. S.; Clackson, S. G. *J. Appl. Crystallogr.* **1992**, *25*, 244.
(70) He, Y.; Hu, R.; Egami, T.; Poon, S. J.; Shiflet, G. J. *Phys. Rev. Lett.* **1993**, *70*, 2411.
(71) Terauchi, H.; Cohen, J. B. *Acta Crystallogr. A* **1979**, *35*, 646.
(72) Morinaga, M.; Cohen, J. B. *Acta Crystallogr. A* **1979**, *35*, 975.
(73) Steel, D.; Fender, B. E. F. *J. Phys. C* **1974**, *7*, 1.
(74) Allpress, J. G.; Rossell, H. J. *J. Solid State Chem.* **1975**, *15*, 68.
(75) Hudson, B.; Moseley, P. T. *J. Solid State Chem.* **1976**, *19*, 383.
(76) Faber, J.; Mueller, M. H.; Cooper, B. R. *Phys. Rev. B* **1978**, *17*, 4884.
(77) Morinaga, M.; Cohen, J. B.; Faber, J. *Acta Crystallogr. A* **1979**, *35*, 789.
(78) Morinaga, M.; Cohen, J. B.; Faber, J. *Acta Crystallogr. A* **1980**, *36*, 520.
(79) Horiuchi, H.; Schultz, A. J.; Leung, C. W.; Williams, J. M. *Acta Crystallogr. B* **1984**, *40*, 367.
(80) Suzuki, S.; Tanaka, M.; Ishigame, M. *Jpn. J. Appl. Phys.* **1985**, *24*, 401.
(81) Andersen, N. H.; Clausen, K.; Hackett, M. A.; Hayes, W.; Hutchings, M. T.; Macdonald, J. E.; Osborn, R. *Physica (Utrecht)* **1986**, *136B*, 315.
(82) Neder, R. B.; Frey, F.; Schultz, H. *Acta Crystallogr. A* **1990**, *46*, 799.
(83) Rossell, H. J.; Scott, H. G. *J. Phys. (Paris), Colloq.* **1977**, *38* (C7), 28.
(84) Allpress, J. G.; Rossell, H. J.; Scott, H. G. *J. Solid State Chem.* **1975**, *14*, 264.
(85) Neder, R. B.; Frey, F.; Schultz, H. *Acta Crystallogr. A* **1990**, *46*, 792.
(86) Proffen, Th.; Neder, R. B.; Frey, F.; Assmus, W. *Acta Crystallogr. B* **1993**, *49*, 599.
(87) Proffen, Th.; Neder, R. B.; Frey, F.; Keen, D. A.; Zeyen, C. M. E. *Acta Crystallogr. B* **1993**, *49*, 605.
(88) Hashimoto, S. *Acta Crystallogr. A* **1974**, *30*, 792.
(89) Welberry, T. R.; Withers, R. L.; Thompson, J. G.; Butler, B. D. *J. Solid State Chem.* **1992**, *100*, 71.

(90) Welberry, T. R.; Butler, B. D.; Thompson, J. G.; Withers, R. L. *J. Solid State Chem.* **1993**, *106*, 461.
(91) Welberry, T. R.; Withers, R. L.; Mayo, S. C. *J. Solid State Chem.* **1995**, *115*, 43.
(92) Manenc, J.; Herai, T.; Thomas, B.; Benard, J. *C. R. Acad. Sci. Paris* **1964**, *258*, 4528.
(93) Hazen, R. M.; Jeanloz, R. *Rev. Geophys. Space Phys.* **1984**, *22*, 37.
(94) Koch, F.; Cohen, J. B. *Acta Crystallogr. B* **1969**, *25*, 275.
(95) Yamamoto, A. *Acta Crystallogr. B* **1982**, *38*, 1451.
(96) Radler, M. J.; Cohen, J. B.; Faber, J., Jr. *J. Phys. Chem. Solids* **1990**, *51*, 217.
(97) Hayakawa, M.; Morinaga, M.; Cohen, J. B. *Defects and Transport in Oxides*; Seltzer, M. S., Jaffee, R. I., Eds.; Plenum Press: New York, 1990; pp 177–199.
(98) Garstein, E.; Mason, T. O.; Cohen, J. B. *J. Phys. Chem. Solids* **1986**, *47*, 759.
(99) Garstein, E.; Cohen, J. B.; Mason, T. O. *J. Phys. Chem. Solids* **1986**, *47*, 775.
(100) Garstein, E.; Mason, T. O.; Cohen, J. B. *Adv. Ceram.* **1987**, *23*, 699.
(101) Welberry, T. R.; Christy, A. G. *J. Solid State Chem.* **1995**, *117*, 398.
(102) Agrell, S. O.; Smith, J. V. *J. Am. Ceram. Soc.* **1960**, *43*, 69.
(103) Cameron, W. E. *Am. Ceram. Soc. Bull.* **1977**, *56*, 1003.
(104) Saalfeld, H. *Neues Jahrb. Mineral. Abh.* **1979**, *134*, 305.
(105) Tokanami, M.; Nakajima, Y.; Morimoto, N. *Acta Crystallogr. A* **1980**, *36*, 270.
(106) Nakajima, Y.; Ribbe, P. H. *Am. Mineral.* **1981**, *66*, 142.
(107) McConnell, J. D. C.; Heine, V. *Phys. Rev. B* **1985**, *31*, 6140.
(108) Angel, R. J.; Prewitt, C. T. *Am. Mineral.* **1986**, *71*, 1476.
(109) Angel, R. J.; Prewitt, C. T. *Acta Crystallogr. B* **1987**, *62*, 116.
(110) Welberry, T. R.; Withers, R. L. *Phys. Chem. Miner.* **1990**, *17*, 117.
(111) Butler, B. D.; Welberry, T. R.; Withers, R. L. *Phys. Chem. Miner.* **1993**, *20*, 323.
(112) Butler, B. D.; Welberry, T. R. *J. Appl. Crystallogr.* **1994**, *27*, 742.
(113) Hull, S.; Wilson, C. C. *J. Solid State Chem.* **1992**, *100*, 101.
(114) Moret, R.; Gougeon, P.; Potel, M.; Levet, J.-C.; Noel, H. *Physica C* **1990**, *168*, 315.
(115) Jiang, X.; Wochner, P.; Moss, S. C.; Zschack, P. *Phys. Rev. Lett.* **1991**, *67*, 2167.
(116) Cai, Z.-X.; Zhu, Y.; Welch, D. O. *Phys. Rev. B* **1992**, *46*, 11014.
(117) Isaacs, E. D.; Aeppli, G.; Zschack, P.; Cheong, S.-W.; Williams, H.; Buttrey, D. J. *Phys. Rev. Lett.* **1994**, *72*, 3421.
(118) Collin, G.; Boilot, J. P.; Colomban, Ph.; Comes, R. *Phys. Rev. B* **1986**, *34*, 5838.
(119) Collin, G.; Boilot, J. P.; Comes, R. *Phys. Rev. B* **1986**, *34*, 5850.
(120) Sakuma, T. *J. Phys. Soc. Jpn.* **1992**, *61*, 4041.
(121) O'Sullivan, K.; Chiarotti, G.; Madden, P. A. *Phys. Rev. B* **1991**, *43*, 13526.
(122) Cava, R. J.; Fleming, R. M.; Reitman, E. A. *Solid State Ionics* **1983**, *9–10*, 1347.
(123) Keen, D. A.; Nield, V. M.; McGreevy, R. L. *J. Appl. Crystallogr.* **1994**, *27*, 393.
(124) McGreevy, R. L.; Pusztai, L. *Mol. Simul.* **1988**, *1*, 359.
(125) Comés, R. *Phys. Scr.* **1982**, *T1*, 46.
(126) Peierls, R. E. *Quantum Theory of Solids*; OUP: Oxford, 1955; p 108.
(127) Kittel, C. *Introduction to Solid State Physics*, 5th ed.; John Wiley: New York, 1976; p 315.
(128) Withers, R. L.; Wilson, J. A. *J. Phys. C: Solid State Phys.* **1986**, *19*, 4809.
(129) Comés, R.; Lambert, M.; Launois, H.; Zeller, H. R. *Phys. Rev.* **1973**, *B8*, 571.
(130) Comés, R.; Lambert, M.; Zeller, H. R. *Phys. Status Solidi* **1973**, *58*, 587.
(131) Ferraris, J.; Cowan, D. O.; Walatka, V., Jr.; Perlstein, J. H. *J. Am. Chem. Soc.* **1973**, *95*, 948.
(132) Monceau, P.; Ong, N. P.; Portis, A. M.; Merchaut, A.; Rouxel, J. *Phys. Rev. Lett.* **1976**, *37*, 602.
(133) Mutka, H.; Zuppiroli, L.; Molinie, P.; Bourgoin, J. C. *Phys. Rev.* **1980**, *B23*, 5030.
(134) Bouffard, S.; Chipaux, R.; Jérome, D.; Bechgaard, K. *Solid State Commun.* **1980**, *37*, 405.
(135) Forro, L.; Zuppiroli, L.; Pouget, J. P.; Bechgaard, K. *Phys. Rev.* **1983**, *B27*, 7600.
(136) Tomic, S.; Pouget, J. P.; Jérome, D.; Bechgaard, K. *J. Phys.* **1983**, *44*, 375.
(137) Liu, Q.; Ravy, S.; Pouget, J. P.; Johannsen, I.; Bechgaard, K. *J. Phys. I Fr.* **1993**, *3*, 803.
(138) Ilakovac, V.; Lui, Q.; Ravy, S.; Albouy, P. A.; Pouget, J. P.; Lenoir, C.; Batail, P.; Johannsen, I.; Bechgaard, K. *Synth. Met.* **1993**, *55–57*, 2372.
(139) Pouget, J. P.; Ravy, S.; Hennion, B. *Phase Transitions* **1991**, *30*, 5.
(140) Ravy, S.; Pouget, J. P.; Comés, R. *J. Phys. I Fr.* **1992**, *2*, 1173.
(141) Albouy, P. A.; Pouget, J. P.; Strzelecka, H. *Phys. Rev.* **1987**, *B35*, 173.
(142) Varma, C. M.; Simons, A. L. *Phys. Rev. Lett.* **1983**, *51*, 138.
(143) Doran, N. J.; Ricco, B.; Schreiber, M.; Titterington, D.; Wexler, G. *J. Phys. C: Solid State Phys.* **1978**, *11*, 699.
(144) Inglesfield, J. E. *J. Phys. C: Solid State Phys.* **1980**, *13*, 17.
(145) Van Landuyt, J.; Van Tenderloo, G.; Amelinckx, S. *Phys. Status Solidi A* **1974**, *26*, 359.
(146) Scruby, C. B.; Williams, P. M.; Parry, G. S. *Philos. Mag.* **1975**, *31*, 255.
(147) Wilson, J. A.; Di Salvo, F. J.; Mahajan, S. *Adv. Phys.* **1975**, *24*, 117.
(148) Schlenker, C., Ed. *Low Dimensional Properties of Molybdenum Bronzes and Oxides*; Kluwer Academic Publishers: New York, 1989.
(149) Foury, P.; Pouget, J. P. *Synth. Met.* **1993**, *55–57*, 2605.
(150) Foury, P.; Pouget, J. P.; Wang, E.; Greenblatt, M. *Europhys. Lett.* **1991**, *16*, 485.
(151) Whangbo, M. H.; Canadell, E.; Foury, P.; Pouget, J. P. *Science* **1991**, *252*, 96.
(152) Canadell, E.; Whangbo, M. H. *Chem. Rev.* **1991**, *91*, 965.
(153) Lenné, H.-U. *Z. Kristallography* **1963**, *118*, 439.
(154) Harris, K. D. M.; George, A. R.; Thomas, J. M. *J. Chem. Soc., Faraday Trans.* **1993**, *89*, 2017.
(155) Shannon, I. J.; Harris, K. D. M.; Rennie, A. J.; Webster, M. B. *J. Chem. Soc., Faraday Trans.* **1993**, *89*, 2023.
(156) Forst, R.; Boysen, H.; Frey, F.; Jagodzinski, H.; Zeyen, C. *J. Phys. Chem. Solids* **1986**, *47*, 1089.
(157) Forst, R.; Jagodzinski, H.; Boysen, H.; Frey, F. *Acta Crystallogr.* **1987**, *B43*, 187.
(158) Harris, K. D. M.; Thomas, J. M. *J. Chem. Soc., Faraday Trans.* **1990**, *86*, 2985.
(159) Harris, K. D. M.; Smart, S. P.; Hollingsworth, M. D. *J. Chem. Soc., Faraday Trans.* **1991**, *87*, 3423.
(160) Aliev, A. E.; Harris, K. D. M. *J. Am. Chem. Soc.* **1993**, *115*, 6369.
(161) Garneau, I.; Raymond, S.; Brisse, F. *Acta Crystallogr.* **1995**, *C51*, 538.
(162) Lowe-Ma, C.; Williams, R.; Samson, S. *J. Chem. Phys.* **1981**, *74*, 1966.
(163) Rosshirt, E.; Frey, F.; Boysen, H.; Jagodzinski, H. *Acta Crystallogr.* **1985**, *B41*, 66.
(164) Endres, H.; Pouget, J. P.; Comés, R. *J. Phys. Chem. Solids* **1982**, *43*, 739.
(165) Hosemann, R. *Z. Phys.* **1950**, *128*, 1.
(166) Hosemann, R. *Z. Phys.* **1950**, *128*, 46.
(167) Hosemann, R. *Z. Phys.* **1950**, *128*, 465.
(168) Vicat, J.; Fanchon, E.; Strobel, P.; Qui, D. T. *Acta Crystallogr.* **1986**, *B42*, 162.
(169) Fanchon, E.; Hodeau, J. L.; Vicat, J.; Watts, J. A. *J. Solid State Chem.* **1991**, *92*, 88.
(170) Terauchi, H.; Futamura, T.; Ishii, T.; Fujiki, Y. *J. Phys. Soc. Jpn.* **1984**, *53*, 2311.
(171) Rosshirt, E.; Frey, F.; Boysen, H. *Neues Jahrb. Mineral. Abh.* **1991**, *163*, 101.
(172) Rosshirt, E.; Frey, F.; Boysen, H. *Physica B* **1989**, *156–157*, 109.
(173) Rosshirt, E.; Frey, F.; Boysen, H.; Eckold, G.; Steigenberger, U. *Mater. Sci. Forum* **1988**, *27/28*, 129.
(174) Beyeler, H. U. *Phys. Rev. Lett.* **1976**, *37*, 1557.
(175) Moss, S. C.; Moret, R. *Graphite Intercalation Compounds I–Structure and Dynamics*; Zabel, H., Solin, S. A., Eds.; Springer-Verlag: Berlin, 1990; pp 5–58.
(176) Ravy, S.; Albouy, P. A.; Megtert, S.; Moret, R.; Pouget, J. P.; Comés, R. *Phase Transitions* **1989**, *16/17*, 193.
(177) Rousseaux, F.; Moret, R.; Guérard, D.; Lagrange, P.; Lelaurain, M. *J. Phys. Lett.* **1984**, *45*, L-1111.
(178) Rousseaux, F.; Moret, R.; Guérard, D.; Lagrange, P.; Lelaurain, M. *Synth. Met.* **1985**, *12*, 45.
(179) Rousseaux, F.; Moret, R.; Guérard, D.; Lagrange, P. *Phys. Rev. B* **1990**, *42*, 725.
(180) Fan, J. D.; Karim, O. A.; Reiter, G.; Moss, S. C. *Phys. Rev. B* **1989**, *39*, 6111.
(181) Epstein, J.; Welberry, T. R.; Jones, R. D. G. *Acta Crystallogr. Sect. A* **1982**, *38*, 611.
(182) Welberry, T. R.; Jones, R. D. G.; Epstein, J. *Acta Crystallogr. Sect. B* **1982**, *38*, 1518.
(183) Epstein, J.; Welberry, T. R. *Acta Crystallogr. Sect. A* **1983**, *39*, 882.
(184) Welberry, T. R.; Siripitayananon, J. *Acta Crystallogr. Sect. B* **1982**, *42*, 262.
(185) Welberry, T. R.; Siripitayananon, J. *Acta Crystallogr. Sect. B* **1982**, *43*, 97.
(186) Welberry, T. R.; Withers, R. L.; Osborn, J. C. *Acta Crystallogr. Sect. B* **1990**, *46*, 267.
(187) Welberry, T. R.; Butler, B. D.; Heerdegen, A. P. *Acta Chim. Hung.* **1993**, *130*, 327.
(188) Cailleau, H.; Moussa, F.; Mons, J. *Solid State Commun.* **1979**, *32*, 521.
(189) Cailleau, H.; Messager, J. C.; Moussa, F.; Bugaut, F.; Zeyen, C. M. E.; Vettier, C. *Ferroelectrics* **1986**, *67*, 3.
(190) Benkert, C.; Heine, V.; Simmons, E. H. *J. Phys. C: Solid State Phys.* **1987**, *20*, 3337.
(191) Lechner, R. E.; Toudic, B.; Cailleau, H. *J. Phys. C: Solid State Phys.* **1984**, *17*, 405.

(192) Welberry, T. R.; Mair, S. L. *J. Phys. C: Solid State Phys.* **1987**, *20*, 4773.
(193) Billups, W. E., Ciufolini, M. A., Eds. *Buckminsterfullerenes*; VCH Publishers, Inc.: New York, 1993.
(194) Kroto, H. W., Fischer, J. E., Cox, D. E., Eds. *The Fullerenes*; Pergamon: Oxford, 1993.
(195) Moret, R.; Ravy, S.; Godard, J.-M. *J. Phys. I Fr.* **1992**, *2*, 1699.
(196) Clarage, J. B.; Phillips, G. N., Jr. *Acta Crystallogr.* **1994**, *D50*, 24.
(197) Huber, R.; Bennett, W. S. *Biopolymers* **1983**, *22*, 261.
(198) Westhof, E.; Altschuh, D.; Moras, D.; Bloomer, A. C.; Mondragon, A.; Klug, A.; Van Regenmortel, M. H. V. *Nature* **1984**, *311*, 123.
(199) Tainer, J. A.; Getzoff, E. D.; Alexander, H.; Houghten, R. A.; Olson, A. J.; Lerner, R. A.; Hendrickson, W. A. *Nature* **1984**, *312*, 127.
(200) Bennett, W. S.; Huber, R. *Crit. Rev. Biochem.* **1984**, *15*, 291.
(201) Helliwell, J. R. *Macromolecular Crystallography with Synchrotron Radiation*; Cambridge University Press: Cambridge, 1992.
(202) Glover, I. D.; Harris, G. W.; Helliwell, J. R.; Moss, D. S. *Acta Crystallogr.* **1991**, *B47*, 960.
(203) Wood, S. P.; Pitts, J. E.; Blundell, T. L.; Jenkins, J. A. *Eur. J. Biochem.* **1977**, *78*, 119.
(204) Carlisle, C. H.; Palmer, R. A.; Mazumdar, S. I.; Gorinsky, B. A.; Yeates, D. G. R. *J. Mol. Biol.* **1974**, *85*, 1.
(205) Al-Hilal, D.; Baker, E.; Carlisle, C. H.; Gorinsky, B. A.; Horsburgh, R. C.; Lindley, P. F.; Moss, D. S.; Schneider, H.; Stimpson, R. *J. Mol. Biol.* **1976**, *108*, 255.
(206) Thorn, J. M.; Carr, P. D.; Chase, J. W.; Dixon, N. E.; Ollis, D. *J. Mol. Biol.* **1994**, *240*, 396.
(207) Doucet, J.; Benoit, J.-P.; Cruse, W. B. T.; Prange, T.; Kennard, O. *Nature* **1989**, *337*, 190.
(208) Frauenfelder, H.; Petsko, G. A.; Tsernoglou, D. *Nature* **1979**, *280*, 558.
(209) Nienhaus, G. U.; Heinzl, J.; Huenges, E.; Parak, F. *Nature* **1989**, *338*, 665.
(210) Phillips, G.; Fillers, J.; Cohen, C. *Biophys. J.* **1980**, *10*, 485.
(211) Parak, F.; Hartmann, H.; Auman, K.; Reuscher, H.; Rennekamp, G.; Bartunik, H. *Eur. Biophys. J.* **1987**, *15*, 237.
(212) Petsko, G.; Ringe, D. *Annu. Rev. Biophys. Bioeng.* **1983**, *12*, 475.
(213) Caspar, D. L. D.; Clarage, J.; Salunka, D. M.; Clarage, M. *Nature* **1988**, *332*, 659.
(214) Clarage, J. B.; Clarage, M. S.; Phillips, W. C.; Sweet, R. M.; Caspar, D. L. D. *Proteins: Struct., Funct. Genet.* **1992**, *12*, 145.
(215) Diamond, R. *Acta Crystallogr.* **1990**, *A46*, 425.
(216) Kuriyan, J.; Weis, W. I. *Proc. Nat. Acad. Sci. U.S.A.* **1991**, *88*, 2773.
(217) Morozov, V. N.; Morozova, T. Y. A. *J. Theor. Biol.* **1986**, *121*, 73.
(218) Edwards, C.; Palmer, S. B.; Emsley, P.; Helliwell, J. R.; Glover, I. D.; Harris, G. W.; Moss, D. S. *Acta Crystallogr.* **1990**, *A46*, 315.
(219) Doucet, J.; Benoit, J.-P. *Nature* **1987**, *325*, 643.
(220) Doucet, J.; Benoit, J.-P.; Faure, P.; Durand, D. *J. Phys. I* **1989**, *2*, 981.
(221) Kolatkar, A. R.; Clarage, J. B.; Phillips, G. N., Jr. *Acta Crystallogr.* **1994**, *D50*, 210.
(222) Schechtman, D.; Blech, I.; Gratias, D.; Cahn, J. W. *Phys. Rev. Lett.* **1984**, *53*, 1951.
(223) Steurer, W. *Z. Kristallogr.* **1990**, *190*, 179.
(224) Elswijk, H. B.; de Hosson, J. T. M.; van Smaalens, S.; de Boer, J. L. *Phys. Rev. B* **1988**, *38*, 1681.
(225) Steurer, W.; Mayer, J. *Acta Crystallogr.* **1989**, *B45*, 355.
(226) Penrose, R. *Bull. Inst. Math. Appl.* **1974**, *10*, 255.
(227) Mackay, A. L. *Sov. Phys. Crystallogr.* **1981**, *26*, 517.
(228) Mackay, A. L. *Physica (Utrecht)* **1982**, *A114*, 609.
(229) Gardner, M. *Sci. Am.* **1977**, *236*, 110.
(230) He, L. X.; Wu, Y. K.; Kuo, K. H. *J. Mater. Sci. Lett.* **1988**, *7*, 1284.
(231) Zhang, Z.; Ye, H. Q.; Kuo, K. H. *Philos. Mag.* **1985**, *A52*, L49.
(232) Strandburg, K. J.; Tang, L.-H.; Jaric, M. V. *Phys. Rev. Lett.* **1989**, *63*, 314.
(233) Tang, L.-H.; Jaric, M. V. *Phys. Rev. B* **1990**, *41*, 4524.
(234) Tang, L.-H. *Phys. Rev. Lett.* **1990**, *64*, 2390.
(235) Zhang, Z.; Li, H. L.; Kuo, K. H. *Phys. Rev. B* **1993**, *48*, 6949.
(236) Welberry, T. R. *J. Appl. Crystallogr.* **1991**, *24*, 203.
(237) Pauling, L. *Nature (London)* **1985**, *317*, 512.
(238) Pauling, L. *Phys. Rev. Lett.* **1987**, *58*, 365.
(239) Budai, J. D.; Tischler, J. Z.; Habenschuss, A.; Ice, G. E.; Elser, V. *Phys. Rev. Lett.* **1987**, *58*, 2304.
(240) Wolny, J.; Pytlik, L.; Lebech, B. *J. Phys. C* **1988**, *21*, 2267.
(241) Robinson, R. M. Unpublished 1975, University of California.
(242) Welberry, T. R. *J. Appl. Crystallogr.* **1989**, *22*, 308.
(243) Frey, F.; Steurer, W. *J. Non-Cryst. Solids* **1993**, *153*, *154*, 600.
(244) Menguy, N.; Audier, M. *Methods of Structural Analysis of Modulated Structures and Quasicrystals*; World Scientific: Singapore, 1991; p 572.
(245) Hiraga, K.; Lincoln, F. J.; Sun, W. *Mater. Trans.* **1991**, *32*, 308.
(246) Steurer, W.; Haibach, T.; Zhang, B.; Beeli, C.; Nissen, H.-U. *J. Phys. Condens. Matter.* **1994**, *6*, 613.
(247) Wilson, A. J. C. *Proc. R. Soc. Lond. A* **1942**, *180*, 277.
(248) Wilson, A. J. C. *Proc. R. Soc. Lond. A* **1943**, *181*, 360.
(249) Hendricks, S. B. *Phys. Rev.* **1940**, *57*, 448.
(250) Hendricks, S. B.; Teller, E. *J. Chem. Phys.* **1942**, *10*, 147.
(251) Sebastian, M. T.; Krishna, P. *Acta Crystallogr.* **1987**, *B43*, 409.
(252) Nikolin, B. I.; Babkevich, A. Y. *Acta Crystallogr.* **1989**, *A45*, 797.
(253) Brindley, G. W.; Brown, G. *Crystal Structures of Clay Minerals and their X-ray Identification*; Mineralogical Society: London, 1980.
(254) Wood, I. G.; Brown, G. *J. Appl. Crystallogr.* **1988**, *21*, 154.
(255) Guinier, A. Report of the International Union of Crystallography Ad-Hoc Committee on the Nomenclature of Disordered, Modulated and Polytype Structures. *Acta Crystallogr.* **1984**, *A40*, 399 (A. Guinier, Chairman).
(256) Durovic, S. *Phase Transitions* **1993**, *43*, 81.
(257) Chaudhary, S. K. *Acta Crystallogr.* **1993**, *B49*, 454.
(258) Kumar, B.; Trigunayat, G. C. *Acta Crystallogr.* **1992**, *A48*, 733.
(259) Kumar, B.; Trigunayat, G. C. *J. Appl. Crystallogr.* **1993**, *26*, 41.
(260) Pandey, D.; Lele, S. *Acta Metall.* **1986**, *34*, 405.
(261) Pandey, D.; Lele, S. *Acta Metall.* **1986**, *34*, 415.
(262) Sebastian, M. R.; Narayanan; Krishna, P. *Phys. Status Solidi A* **1987**, *102*, 241.
(263) Tjoetta, S.; Samuelsen, E. J.; Jagner, S. *J. Phys.: Condens. Matter* **1991**, *3*, 3411.
(264) Samuelsen, E. J.; Tjoetta, S.; Jagner, S. *J. Phys.: Condens. Matter* **1991**, *3*, 3421.
(265) Samuelsen, E. J.; Jagner, S. *Phase Transitions* **1993**, *43*, 89.
(266) Gosk, J.; Kozielski, M. J. *Cryst. Res. Technol.* **1994**, *29*, 509.
(267) Farkas-Jahnke, M. *Phase Transitions* **1993**, *43*, 5.

CR940444B